Institut für Entwicklungsgenetik
GSF Forschungszentrum für Umwelt und Gesundheit

Fibroblast growth factor and Wnt signaling in the development of the vertebrate central nervous system

Thomas Fischer

Vollständiger Abdruck der von der Fakultät Wissenschaftszentrum Weihenstephan für Ernährung, Landnutzung und Umwelt der Technischen Universität München zur Erlangung des akademischen Grades eines

Doktors der Naturwissenschaften

genehmigten Dissertation.

Vorsitzender:	Univ.-Prof. Dr. S. Scherer
Prüfer der Dissertation:	1. Univ.-Prof. Dr. W. Wurst
	2. Univ.-Prof. Dr. M. Hrabe de Angelis
	3. Univ.-Prof. Dr. K. H. Schneitz

Die Dissertation wurde am 8. März 2006 bei der Technischen Universität München eingereicht und durch die Fakultät Wissenschaftszentrum Weihenstephan für Ernährung, Landnutzung und Umwelt am 30. Mai 2006 angenommen.

Danksagung

Ich danke Herrn Prof. Dr. Wolfgang Wurst für die Möglichkeit, meine Promotionsarbeit an seinem Institut durchzuführen. Sein Interesse an meiner Arbeit, sein Ideenreichtum und seine konstruktive Kritik in zahlreichen Diskussionen haben meine Begeisterung an der Wissenschaft gefördert und wesentlich zu meiner Motivation beigetragen. Frau Dr. Nilima Prakash danke ich für ihre hervorragende Betreuung in allen wissenschaftlichen Fragen während meiner Promotion. Sowohl praktisch wie auch theoretisch konnte ich viel von ihr lernen, wobei vor allem ihre kritische, analytische Denkweise und ihr fundiertes Wissen mein wissenschaftliches Verständnis und meine Argumentationsfähigkeit geschärft haben. Ich danke Herrn Prof. Dr. Scherer, Herrn Prof. Dr. Hrabé De Angelis und Herrn Prof. Dr. Schneitz für ihre Bereitschaft, meine Dissertation zu beurteilen und die Promotionsprüfung durchzuführen. Weiterhin danke ich Frau Dr. Daniela Vogt Weisenhorn für ihre exzellente Beratung in histologischen und morphologischen Analysen, und Herrn Dr. Jan Deussing für seine Hilfestellung bei molekularbiologischen Fragen. Herrn Dr. Chichung Lie danke ich für die Bereitstellung der verwendeten Zelllinien und seine Beratung in Fragen der Zellkultur. Ich danke Prof. Dr. Magdalena Götz für ihre Bereitschaft, mich in ihrem Institut die Primärkultur-Experimente durchführen zu lassen, und Andrea Steiner für ihre tatkräftige Unterstützung bei diesen Arbeiten. Ruth Klafke und Thorsten Naserke danke ich für zahlreiche anregende Diskussionen und ihre Unterstützung im Labor. Ruth Klafke, Michael Barkley sowie Markus und Karin Fischer bin ich zu großem Dank verpflichtet für ihr gewissenhaftes und kritisches Korrekturlesen des Manuskripts. Den technischen Angestellten des Instituts, allen voran Annerose Kurz-Drexler, Susanne Laaß, Katja Mayer, Claudia Kühne und Miriam Homburg danke ich für ihre Unterstützung und Hilfsbereitschaft bei zahlreichen Experimenten im Labor. Mein besonderer Dank gilt auch allen Tierpflegerinnen, vor allem Resi, Rosi, Monika und Claudia, ohne deren Engagement und Hilfsbereitschaft diese Arbeit nicht möglich gewesen wäre. Ich danke außerdem allen Mitgliedern unseres Instituts für die kollegiale und freundschaftliche Atmosphäre, die den Arbeitsalltag wesentlich erleichtert hat. Meiner Familie und meinen Freunden danke ich für ihre Unterstützung, ihren Zuspruch und ihre Geduld während meines Studiums und meiner Promotion, die mir geholfen haben, diesen Weg zu beschreiten.

Contents

1. Abstract

The development of the central nervous system (CNS) of vertebrates is a complex process, controlled by an intricate network of extrinsic and intrinsic determinative factors. Fibroblast growth factors (Fgfs) and Wnts (wingless-related MMTV integration sites) constitute two important families of secreted signaling molecules with diverse functions in numerous developmental, physiological and disease-related processes. Although the functions of many Fgfs and Wnts have been characterized in neural development, the role of several members of these protein families in this process is still unclear. Furthermore, new functions of individual Fgfs or Wnts are frequently discovered that are distinct from already known properties.

Fgf15 is expressed in the developing CNS of vertebrates, yet its function during neural development is not known. Here, it is shown that Fgf15 is involved in the regulation of cell cycle exit of neuroepithelial cells, as embryos deficient for *Fgf15* show an increased number of neural cells that remain in the cell cycle at E11.5. This failure to exit the cell cycle results in perturbed neurogenesis, reflected by an apparent increase in neural progenitor cells and a decrease in early postmitotic neurons in the neuroepithelium of mutant embryos. Moreover, the expression of genes encoding neurogenic basic helix-loop-helix (bHLH) transcription factors and Inhibitor of differentiation (Id) proteins is up-regulated, whereas the expression of genes encoding proneural bHLH transcription factors is down-regulated in the neuroepithelium of $Fgf15^{-/-}$ embryos.

The role of Wnt1 as an important factor in CNS development has been addressed extensively in the past, where it has been implicated in various processes such as proliferation, differentiation and cell survival. However, a recent study has revealed a pivotal role of Wnt1 in the development of mesencephalic dopaminergic (mesDA) neurons. While it has been demonstrated that Wnt1 is involved in the regulation of the identity and fate of these neurons, the downstream signaling cascade, including receptors and target genes, that is activated in mesDA progenitors upon Wnt1 binding has not been determined. In the present work, three Frizzled (Fzd) receptors are identified as candidates to transduce the Wnt1 signal in mesDA neuron development. Of these, *Fzd6* shows a highly restricted expression specifically in the caudal cephalic flexure where mesDA neurons arise. Co-expression analyses of *Fzd6*, *Wnt1* and markers for mesDA progenitors and neurons, respectively, reveal that Fzd6 may transduce the Wnt1 signal necessary for the establishment of the mesDA progenitor domain, as well as the Wnt1-mediated terminal differentiation of mesDA neurons.

2. Introduction

The vertebrate brain represents perhaps the most complex of tissues that have evolved in biological systems. The number of different cell types found in neural tissue exceeds by far any other organ in vertebrates (Stevens, 1998), and this complexity is further multiplied by an extensive network of connections that is established between these cells. The great diversity of neuronal cell types, the large number of neurons and their intricate connectivity underlie the remarkable information processing capacity of the CNS. The development of the CNS therefore requires the elaborate coordination of events that will lead to the correct numbers, types, locations and interconnections of neural cells. Brain development in vertebrates begins with the induction of neural cells in the ectoderm of the early embryo (around embryonic day 7 (E7) in mouse). These neuroectodermal cells form the neural plate. The neural plate subsequently folds up and the lateral edges of the neural plate fuse at the dorsal side of the embryo to form the neural tube. The rostral neural tube is initially subdivided in the anterior-posterior (A/P) axis into 3 primary brain vesicles, the prosencephalon, the mesencephalon and the rhombencephalon. Later in development, the prosencephalon gives rise to the telencephalon and diencephalon and the rhombencephalon to the metencephalon and myelencephalon (Fig. 1A). In the dorso-ventral (D/V) axis, the neural tube is divided from ventral to dorsal into the floor plate (FP), the basal plate (BP), the alar plate (AP) and the roof plate (RP) (Fig. 1B). The cortex and the basal ganglia of the adult brain develop from the telencephalon, the thalamus and hypothalamus arise from the diencephalon, the midbrain derives from the mesencephalon, the cerebellum develops from the metencephalon and the brain stem from the myelencephalon. The initially uniform neuroepithelial cells of the neural tube proliferate and generate the different cell types of the brain in a defined order. First, neurons are generated in a process termed neurogenesis (mostly between E10 and E14 in mouse), followed by the production of the two types of glial cells, astrocytes (mostly between E14 and E18 in mouse) and oligodendrocytes (mostly postnatally in mouse). During neurogenesis, extracellular signals along the A/P and D/V axes of the neural tube provide positional cues that confer different regional identities to developing neuronal precursors, resulting in the specification of distinct subtypes of neurons in different areas of the developing brain. The number of neurons that are produced and the type of neurons that are generated are therefore determined by two processes, proliferation of neuronal progenitors and differentiation of neuronal precursors, that are tightly linked in neurogenesis.

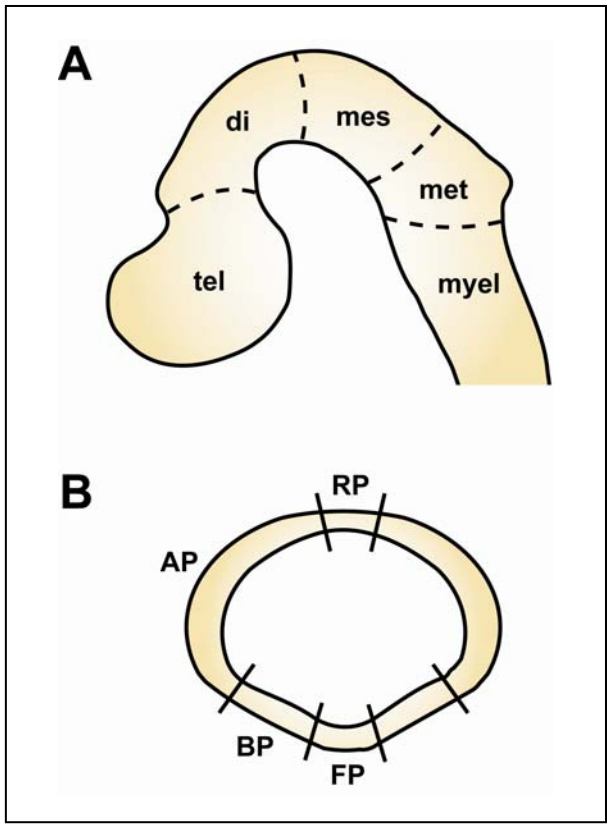

Figure 1 Schematic drawing of the subdivision of the neural tube along the A/P (A) and D/V axes (B) at early stages of neural development. (A) Sagittal view of the anterior neural tube of an E9.5 mouse embryo, anterior is to the left. The neural tube is divided from rostral to caudal into the telencephalon, diencephalon, mesencephalon, metencephalon and myelencephalon. (B) Cross-section through the anterior neural tube, dorsal is at the top, ventral at the bottom. Along the D/V axis, the neural tube is divided from ventral to dorsal into the floor plate, basal plate, alar plate and roof plate. Boundaries between adjacent domains are depicted as broken and solid lines, respectively. tel telencephalon; di diencephalon; mes mesencephalon; met metencephalon; myel myelencephalon; FP floor plate; BP basal plate; AP alar plate; RP roof plate.

2.1 The intracellular control of proliferation

During proliferation, a cell traverses through the cell cycle and gives rise to two daughter cells. The cell cycle is divided into distinct phases, and the progression from one phase to the next is controlled by a characteristic set of regulators, which together constitute the so-called cell cycle machinery (Murray, 1994; Sherr, 1994; Hunter, 1993). The phases of the cell cycle are termed G1-phase (G for gap), S-phase (S for synthesis), G2-phase and M-phase (M for mitosis). During the S-phase, the DNA of the cell is replicated and histones are synthesized. In M-phase the actual division of the cell into two daughter cells takes place. The M-phase involves the condensation of chromatin, the disintegration of the nuclear envelope, the

segregation of the condensed sister chromatids and their translocation to opposite poles of the mitotic spindle, and finally the division of the cytoplasm, or cytokinesis. G1-phase, between M- and S-phase, and G2-phase, between S- and M-phase, represent control phases in which intra- and extracellular cues influencing the cell cycle are integrated and the progress of the cell cycle is monitored, to ensure that S-phase and M-phase are entered correctly and only under suitable conditions (Alberts et al., 2002).

Key molecules in the control of cell cycle progression are a family of protein kinases termed cyclin-dependent kinases (Cdks). The activity of Cdks rises and falls as the cell progresses through the cycle. These oscillations lead directly to cyclical changes in the phosphorylation of intracellular proteins that initiate or regulate major events of the cell cycle. Cyclical changes in Cdk activity are controlled in turn by a complex array of proteins, the most important of which are the cyclins. Cdks are dependent on cyclins for their activity and exert their kinase activity only if they are bound to a cyclin. Cyclins undergo degradation and synthesis during each cell cycle, whereas the level of Cdks remains largely constant, resulting in the cyclic assembly and activation of cyclin-Cdk complexes. There are four classes of cyclins, each defined by the stage of the cell cycle at which they bind Cdks.

1. G1-cyclins: bind Cdks in mid-G1 and promote passage through G1
2. G1/S-cyclins: bind Cdks in late G1 and commit the cell to DNA replication
3. S-cyclins: bind Cdks during S-phase and are required for the initiation of DNA replication
4. M-cyclins: bind Cdks during M-phase and promote the events of mitosis

(Alberts et al., 2002).

In addition to the formation of a functional complex with cyclins, Cdk activity depends on the phosphorylation of specific amino acids of the Cdk proteins. Phosphorylation of these sites by the protein kinase Wee1 inhibits Cdk activity, while dephosphorylation of these sites by the phosphatase Cdc25 increases Cdk activity (Alberts et al., 2002). The transition from G1- to S-phase is a key step for cell cycle progression. It is controlled by cyclin D/Cdk4 and cyclin D/Cdk6 complexes, which act in mid-G1-phase, and by cyclin E/Cdk2, which operates in late G1. An important substrate of these cyclin/Cdk complexes are the retinoblastoma proteins Rb (or p110), Rb2 (or p130) and p107. In their hypophosphorylated (active) form these proteins bind to and inactivate members of the E2F family of transcription factors. The E2F proteins in turn are required for the transcription of genes that encode proteins necessary for S-phase

entry, including G1/S-cyclins and S-cyclins. When the above mentioned cyclin/Cdk complexes are activated, they phosphorylate the retinoblastoma proteins. The hyperphosphorylation, i.e. inactivation, of the retinoblastoma proteins results in the liberation of E2F proteins and subsequently in the transcription of cell cycle progression genes (Fig. 2; Galderisi et al., 2003). Therefore, retinoblastoma proteins represent key regulators of the cell cycle by inhibiting progression through the cell cycle in their activated form and allowing cell cycle progression when inactivated. This is in line with the tumor suppressor properties ascribed to Rb, and the occurrence of an inherited form of eye cancer in children, known as retinoblastoma, associated with mutations in the *Rb* gene (Lee et al., 1987; Goodrich and Lee, 1990).

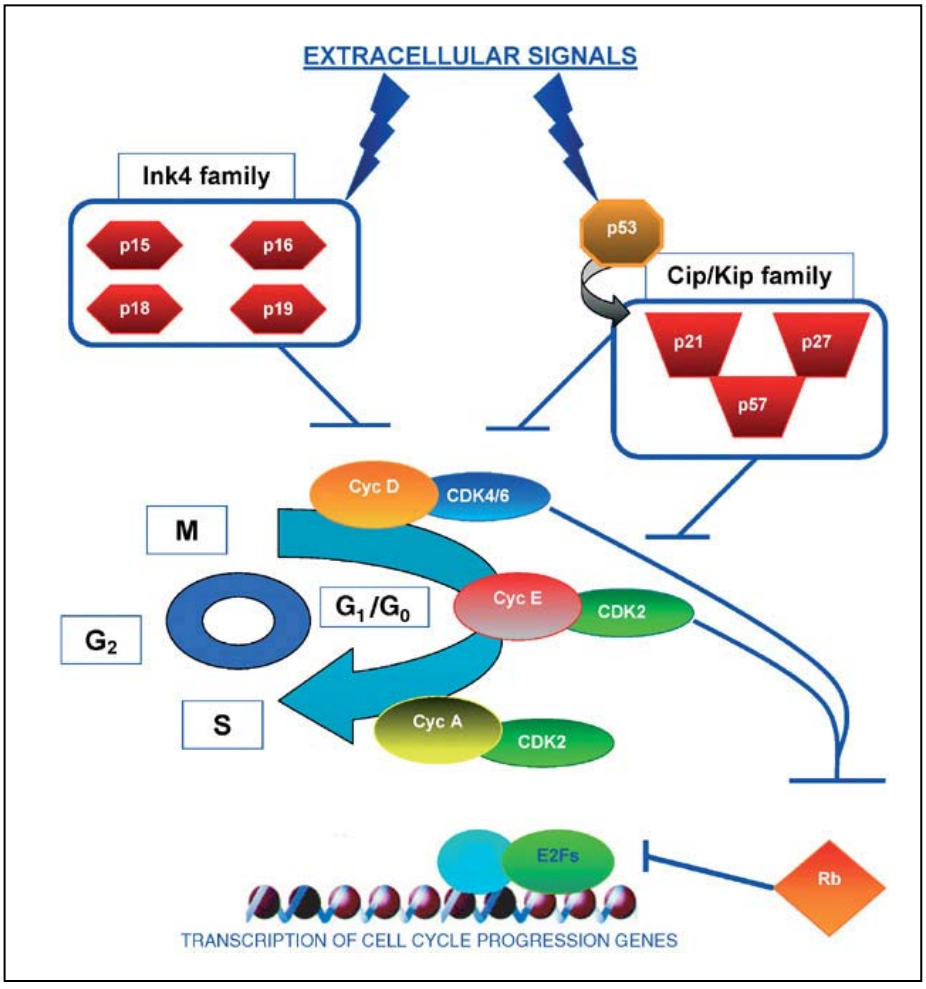

Figure 2 Schematic overview of cell cycle control. Cdkis of the Ink4 and Cip/Kip family inhibit the activity of cyclin/Cdk complexes. Active cyclin/Cdk complexes are required to phosphorylate (i.e. inactivate) retinoblastoma proteins. In their active form these proteins inhibit E2F-mediated transcription of cell cycle progression genes and at the same time relieve Id inhibition of bHLH factors that are required for the transcription of differentiating genes. M M-phase; G1/G2/G0 G1-/G2-/G0-phase; S S-phase; Cyc cyclin. Adapted from Galderisi et al., 2003.

Inhibitors of Cdk activity (Cdkis) consequently act as cell cycle inhibitors, arresting cells in G1-phase through the activation of retinoblastoma proteins. Cdkis are divided into two classes of molecules, dependent on the mechanism underlying Cdk inhibition. The Ink4 class includes $p16^{INK4a}$, $p15^{INK4b}$, $p18^{INK4c}$ and $p19^{INK4d}$. They interact specifically with Cdk4 and Cdk6 and impair their interaction with cyclin D. The Cip/Kip class of Cdks includes $p21^{Cip1}$, $p27^{Kip1}$ and $p57^{Kip2}$. The Cip/Kip molecules act on assembled cyclin/Cdk complexes and inhibit their activity by forming ternary complexes (Fig. 2; Galderisi et al., 2003).

2.2 Proliferation and differentiation are tightly linked during neurogenesis

Proliferation and differentiation are tightly connected during neurogenesis by the molecular coordination between cell cycle exit and neuronal cell fate specification, in which determination factors influence the cell cycle, and cell cycle regulators influence determination (Ohnuma and Harris, 2003). A fundamental signaling pathway controlling the acquisition of a neuronal fate by a neural precursor cell is the Notch pathway. Originally discovered in *Drosophila*, the Notch pathway has been demonstrated to be highly conserved also in vertebrates (Beatus and Lendahl, 1998). Notch signaling controls the differentiation of neuronal (and other) cells by a mechanism termed 'lateral inhibition'. This process ensures the generation of two distinct cell types in the correct numbers from an initially homogenous cell population. In this model, all cells of the initial population express the single pass transmembrane proteins Notch and Delta, which function as receptor and corresponding ligand, respectively. The interaction between Delta ligands and Notch receptors mutually represses each others expression in neighboring cells via bHLH transcription factors. Notch activation up-regulates the expression of transcriptional repressors (called Enhancer of Split (E(spl)) in *Drosophila* and Hes in mammals) which in turn down-regulate the expression of a transcriptional activator (termed achaete-scute (asc) in *Drosophila* and Mash in mammals). Asc/Mash is a positive regulator of Delta expression. A minimal stochastic difference in the expression levels of Delta in a cell of the initially homogenous cell population, for example, will induce stronger E(spl)/Hes expression in neighboring cells via the Notch receptor. Increased levels of E(spl)/Hes will repress the expression of asc/Mash and subsequently of Delta in these cells. The decreased levels of Delta ligands in the environment of the cell which initially expressed Delta at slightly higher levels will down-regulate Notch signaling in this cell. This leads to lower levels of E(spl)/Hes expression, which further increases asc/Mash

activity and Delta expression (Lewis, 1996). By this feedback mechanism, small changes in the expression of Notch and Delta in adjacent cells are rapidly amplified and ultimately result in different cell fates adopted by initially homogenous cells. While in *Drosophila* and *Xenopus* the principal function of Notch is the discrimination between two alternative cell types, i.e. epidermal versus neuronal cells, in mammalian CNS development it rather appears to be the maintenance of undifferentiated progenitor cells in the neuroepithelium (Beatus and Lendahl, 1998).

A number of bHLH transcriptional activators and repressors regulate proliferation and differentiation upon Notch signaling (Fig. 3). bHLH repressors maintain neuronal progenitors and inhibit neurogenesis and are classified as neurogenic proteins. In mammals this class of bHLH factors includes Hes1, Hes3 and Hes5, which are direct effectors of Notch signaling (Jarriault et al., 1998; Ohtsuka et al., 1999; Ishibashi et al., 1995; Nakamura et al., 2000; Ohtsuka et al., 2001; Kageyama et al., 2005). The somewhat misleading term 'neurogenic' for factors that actually inhibit neurogenesis originates from loss-of-function (LOF) experiments in which the inactivation of *Hes* genes results in the depletion of the neuronal progenitor pool due to premature neurogenesis and consequently to a reduced number of neurons. bHLH activators that promote neuronal differentiation are termed proneural factors. In mammals this group includes Mash, Math (mammalian homolog of *Drosophila* athonal (ath)), Neurogenin (Ngn) and NeuroD (Bertrand et al., 2002; Ross et al., 2003). Hes factors function in the maintenance of neuronal progenitors through two distinct mechanisms. First, Hes factors form homo- and heterodimers with closely related family members and bind to DNA elements called N boxes. This binding represses the expression of target genes, e.g. *Mash1*, that are required for neuronal differentiation (Fig. 3A). Second, Hes factors interact physically with proneural bHLH proteins, and this interaction functionally antagonizes the activity of proneural bHLH factors. In addition to Hes repressors, another class of HLH factors, the Id proteins, contribute to the maintenance of an undifferentiated progenitor state in neural development. While Hes factors act predominantly during neurogenesis, Id proteins are ubiquitously expressed and inhibit differentiation in many tissues (Jen et al., 1996; Jen et al., 1997). Id factors form heterodimers with E2A proteins, which are required by proneural bHLH factors for the activation of target gene transcription. Therefore, Ids inhibit proneural bHLH activity by sequestering E2A proteins from bHLH factors that consequently cannot activate the transcription of target genes necessary for neuronal differentiation (Norton, 2000). In addition to the negative regulation of differentiation, Id proteins play a direct role in promoting cell proliferation. Ids stimulate progression through the cell cycle by inhibiting the

ability of retinoblastoma proteins to bind to E2F factors, which leads to the transcription of cell cycle progression genes (Iavarone et al., 1994).

In cells that are specified towards a neuronal fate, the transition from proliferation to differentiation involves a coordinate increase in proneural activity and a decrease in neurogenic and Id activity. Progression in the differentiation process is mediated by successive waves of expression of proneural bHLH factors. In neural progenitors, expression levels of Mash and Ngns are low. A transient increase in expression levels of these factors initiates neuronal differentiation, concomitant with a down-regulation of *Hes* and *Id* genes. As neuronal differentiation proceeds, another set of bHLH factors start to be expressed in neuronal precursor cells, e.g. NeuroDs, which are involved in mediating terminal differentiation (Fig. 3B; Ross et al., 2003; Bertrand et al., 2002). In addition to specifying a generic neuronal fate, several members of early and late proneural bHLH factors are involved in the acquisition of distinct neuronal subtypes (Bertrand et al., 2002).

While the transcriptional control of the factors which regulate neurogenesis is far from being fully understood, epistatic relationships between several components have been determined. As already mentioned, *Hes* genes are direct targets of Notch signaling and in turn repress the expression of *Mash1*. *Mash1* acts upstream of *Ngn1* and *NeuroD*, and *Ngn1* and *Ngn2* are required for the expression of *Math3* and *NeuroD* (Fig. 3; Cau et al., 2002; Fode et al., 1998; Ma et al., 1998). These examples indicate that the specification towards a neuronal fate is initiated by a down-regulation of Notch signaling. The further commitment to the neuronal fate is then mediated, at least in part, by the activation of a cascade of proneural bHLH factors that promote successive steps in the acquisition of a neuronal phenotype (Bertrand et al., 2002).

Cell cycle withdrawal appears to be a necessary prerequisite for a cell to differentiate. Blocking cells in the *Xenopus* retina in the G1-phase by the overexpression of p27, for example, potentiates the activity of proneural bHLH factors. Overexpression of cyclin E, in contrast, reduces the activity of proneural bHLH factors (Ohnuma et al., 2002). Similar results have been obtained in mammalian cell culture experiments in which cyclin D1 has been demonstrated to down-regulate the transcriptional activity of the proneural factor NeuroD (Ratineau et al., 2002). While these examples demonstrate that cell cycle regulators affect neuronal differentiation, the reverse is also true, i.e. that many determination factors affect the cell cycle. Loss of the proneural factor ath5 in the developing retina of zebrafish, for instance, inhibits cell cycle withdrawal of neuronal progenitors (Kay et al., 2001). Overexpression of NeuroD, Mash1 or Ngn1 in P19 embryonic carcinoma cells induces the expression of p27 and

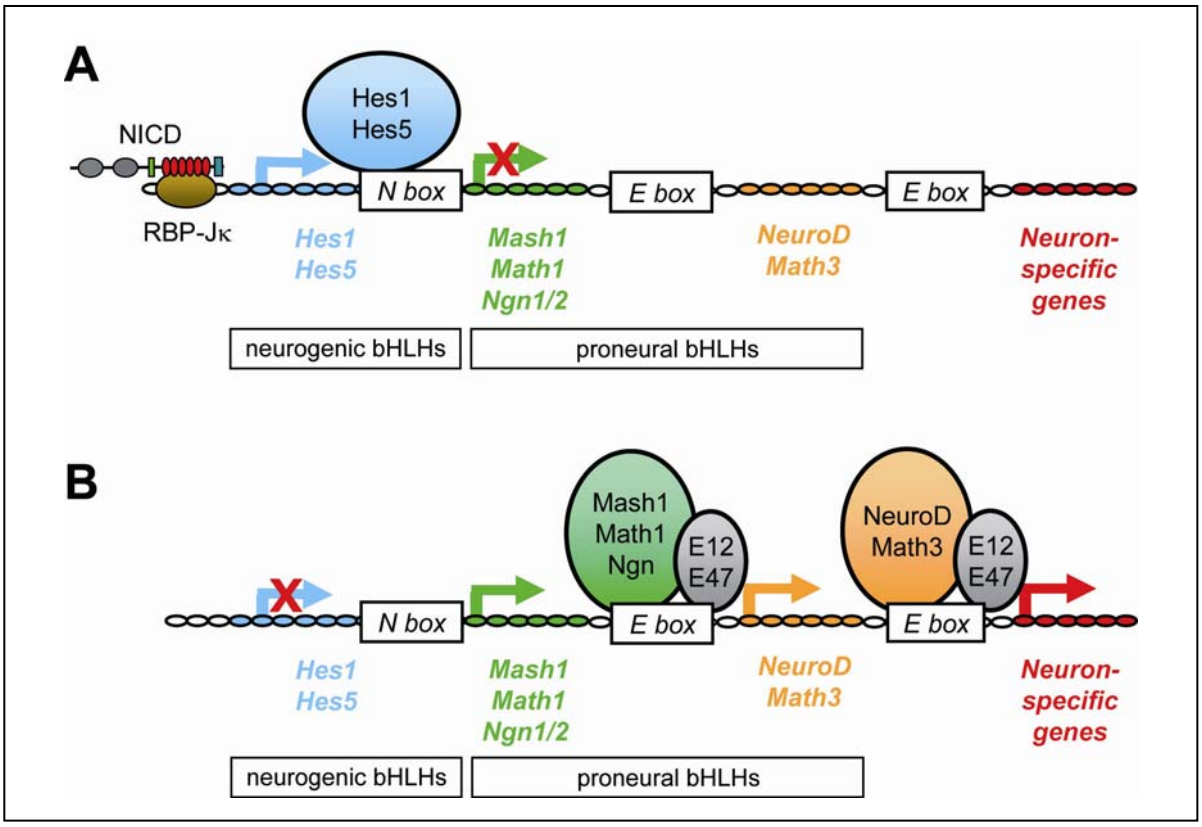

Figure 3 Schematic overview of the epigenetic relationship between neurogenic and proneural genes during neurogenesis. (A) Upon activation of the Notch receptor by binding to its ligand Delta, the intracellular domain of Notch (NICD) is cleaved from the receptor and translocated to the nucleus. Here, it interacts with RBP-Jκ (termed suppressor of hairy in *Drosophila*) to activate the transcription of *Hes* genes (blue). Hes factors then bind to N boxes and thus inhibit the transcription of proneural bHLH genes. (B) In the absence of Notch signaling, *Hes* genes become down-regulated, which allows the transcription of early proneural genes such as *Mash1*, *Math1* and *Ngns* (green). The bHLH factors encoded by these genes bind, together with E2A factors (grey), to E boxes and initiate the transcription of later proneural genes like *NeuroD* and *Math3* (orange). These factors in turn dimerize with E2A proteins and promote the transcription of genes necessary for the differentiation of a neuronal phenotype (red). Courtesy of N. Prakash.

causes cell cycle arrest in G1 (Farah et al., 2000). Conversely, the neurogenic factor Hes1 has been demonstrated to inhibit differentiation of PC12 cells and overexpression of *Hes1* strongly represses the transcription of the Cdki $p21^{CIP}$ (Castella et al., 2000). In line with this finding, suppression of Hes1 activity in human neural stem cells has been shown to stimulate the expression of $p21^{CIP}$ and to initiate differentiation (Kabos et al., 2002).

Considerable progress has been made in the understanding of the intracellular control of cell cycle progression, cell cycle withdrawal and differentiation and the cross-talk between them. However, the extracellular cues regulating these processes and the integration of such signals within a cell are still not well understood. Among the extracellular signals implicated in the regulation of proliferation and differentiation during neurogenesis (in addition to the

already discussed membrane-bound factors Notch and Delta) are secreted glycoproteins like Sonic hedgehog (Shh) and Wnts and various growth factors such as epidermal growth factor (Egf), transforming growth factors (Tgfs), bone morphogenic proteins (Bmps), platelet-derived growth factor (Pdgf) and fibroblast growth factors (Fgfs) (reviewed in Edlund and Jessell, 1999; Ferguson and Slack, 2003).

2.3 Fibroblast growth factors in neurogenesis

The family of Fgfs comprises 22 members in mouse and human, numbered Fgf1-23 (note that human FGF19 is the ortholog of mouse Fgf15, so there is no human FGF15 and no mouse Fgf19) (Itoh and Ornitz, 2004). Most Fgfs are secreted from cells and act as extracellular signaling molecules. Fgf11-14 remain intracellular and seem to share a structural, but not a functional homology with other Fgfs. For this reason, they are alternatively termed Fgf homologous factors (Fhfs) (Schoorlemmer and Goldfarb, 2001). The majority of secreted Fgfs contain an amino-terminal signal peptide (Fgf3-8, 10, 15, 17-18, 21 and 23). Fgf9, 16 and 20 do not contain a classical signal peptide but are nevertheless secreted from cells. Fgf1 and 2 also lack a signal peptide, but unlike Fgf9, 16 and 20, they are not secreted from cells. Extracellular Fgf1 and 2 are either released from damaged cells or by an exocytotic mechanism that is independent from the endoplasmic reticulum-Golgi pathway (Ornitz and Itoh, 2001). Fgf22, with a putative amino-terminal signal peptide, remains attached to the cell surface rather than being secreted (Itoh and Ornitz, 2004). Secreted Fgfs signal via a family of receptor tyrosine kinases, the Fgf receptors (Fgfrs), with 4 members in mouse and human. Each Fgfr is bound and activated by a unique subset of Fgfs, the specificity of which is further regulated by alternative splicing of the genes encoding the Fgfrs (Ibrahimi et al., 2004; Harmer et al., 2004; Fujita et al., 1991). The effective binding of Fgfs to Fgfrs requires the interaction with heparin or heparan sulfates, which stabilizes Fgfs and prevents proteolysis (Ornitz, 2000). Fgfrs and heparin or heparan sulfate are bound by distinct domains within the conserved core region of the Fgf proteins, which consists of 12 antiparallel β-strands arranged in a triangular array (Ornitz and Itoh, 2001). Fgf signaling is transduced within the cell by several pathways, of which the best understood are the RAS-MAP kinase pathway, the PI-3 kinase/AKT pathway and the PLCγ pathway (Dailey et al., 2005; Schlessinger, 2000). Activation of these signaling cascades leads to alterations in the phosphorylation status of different proteins and ultimately to changes in gene activity. Fgfs and their receptors are

widely expressed in developing and adult tissues and have various biological functions, including roles in angiogenesis, mitogenesis, cellular differentiation, cell migration and tissue-injury repair. In the development of the CNS, a major function of Fgfs is the patterning of the neural tube. A key molecule in this process is Fgf8, which is expressed at two important signaling centers in the neural tube, the anterior neural ridge (ANR) in the most rostral part of the telencephalon, and in the mid-/hindbrain boundary (MHB) region at the junction of the midbrain and the hindbrain (Maruoka et al., 1998). In the forebrain, it has been shown that Fgf8 soaked beads can rescue the expression of the forebrain-specific factor *Bf1* in mouse explants lacking the ANR. Further support for a role of Fgf signaling in patterning of the forebrain has been derived from LOF experiments, in which reduced Fgf activity resulted in proliferation and apoptosis defects, midline defects and perturbed morphogenesis of the olfactory bulbs (Wilson and Houart, 2004). The organizer activity of the MHB has been identified through a series of transplantation experiments in chicken embryos. In these experiments, tissue grafts derived from MHB territory induced mesencephalic and metencephalic fates in ectopic positions, i.e. the diencephalon and rhombomeres 2-5, in the recipient (Martinez et al., 1991; Marin and Puelles, 1994; Martinez et al., 1995), and Fgf8 has been demonstrated to be a key molecule in mediating this patterning activity (reviewed in Sato et al., 2004; Prakash and Wurst, 2004). Besides this prominent role of Fgf signaling in patterning of the neural tube, Fgfs are also involved in various aspects of neurogenesis (reviewed in Dono, 2003; Ford-Perriss et al., 2001; Reuss and von Bohlen und Halbach, 2003). For example, Fgf2 has been identified as a potent mitogenic and survival factor of neural cells both *in vivo* and *in vitro*. In line with this observation, it is expressed in proliferative regions of the developing CNS, as are Fgfr1, 2 and 3, and becomes down-regulated by the end of neurogenesis. Other Fgfs are implicated in the generation of specific neuronal populations. Fgf8, for instance, is an important factor for the development of midbrain dopaminergic neurons, and Fgf4, together with Fgf8, appears to play a role in the generation of serotonergic cell populations (Ye et al., 1998). Like in the case of Fgf2, these functions are consistent with an expression of Fgf8 in the MHB region adjacent to the region where dopaminergic neurons develop (see below) and of Fgf4 in the mesenchyme underlying the FP of the neural tube.

Fgf15 has been identified as a downstream target of the chimeric homeodomain oncoprotein Pbx1-E2A (McWhirter et al., 1997). *Fgf15* mRNA is expressed strongly in the developing CNS of the mouse (McWhirter et al., 1997; Gimeno et al., 2002; Gimeno et al., 2003). LOF and gain-of-function (GOF) experiments in mouse and chicken, however, have

not provided any evidence for a role of this factor in neural development. Fgf15 is generally required for viability, as mice deficient for *Fgf15* (*Fgf15*$^{-/-}$) die during development between E12.5 and postnatal day 21 (P21) (Wright et al., 2004; Vincentz et al., 2005). The variability in the developmental stage at which lethality occurs, as well as the finding that about 3% of homozygous mutant animals survive into adulthood (which will be referred to as 'escapers'), suggest that genetic modifiers may exist in these mouse lines that in part suppress the *Fgf15* phenotype responsible for embryonic lethality. Results of GOF experiments in chicken embryos have suggested a function of Fgf15 in inner ear development, since overexpression of *Fgf15* in rostral ectoderm explants of chicken embryos induces the expression of early otic markers *Pax2* and *Nkx5-1*. However, the development of the otic system appears to be unaffected in *Fgf15*$^{-/-}$ embryos and adult escapers (Wright et al., 2004). This indicates that either redundant factors can compensate for the loss of Fgf15, or that the *in vitro* experiments did not recapitulate the *in vivo* situation correctly. In addition to the expression in the developing CNS, *Fgf15* is also expressed in the pharyngeal arches early in development. Consistent with this expression domain, *Fgf15*$^{-/-}$ embryos display morphological defects of the cardiac outflow tract, which result from alterations in the remodeling of neural crest cells migrating into the pharyngeal arches (Vincentz et al., 2005). The analysis of a *Shh*$^{-/-}$ mutant mouse line provided evidence that Fgf15 may be involved in a Shh-dependent signaling relay that regulates the growth of the diencephalon and mesencephalon (Ishibashi and McMahon, 2002). In the absence of Shh, the expression of the Wnt target gene *cyclin D1* (*Ccnd1*) as well as the T-cell specific factor *Tcf7l2*, a mediator of Wnt signaling (see below), are down-regulated in the dorsal parts of the diencephalon and midbrain of *Shh*$^{-/-}$ embryos at early somite stages, which subsequently leads to reduced proliferation in these regions. Since Shh is expressed only in the FP and BP, but not in dorsal domains of the diencephalon and mesencephalon, a relay mechanism has been proposed to explain the dorsal phenotype of *Shh*$^{-/-}$ embryos. In this signaling relay, a Shh-dependent factor is thought to control the dorsal expression of *Ccnd1* and *Tcf7l2*. Fgf15 was identified as a candidate for this mechanism, as 1) it is expressed in close vicinity to the *Shh* domain ventrally as well as overlapping with *Ccnd1* and *Tcf7l2* dorsally, 2) its expression is strongly reduced in the dorsal diencephalon and mesencephalon in *Shh*$^{-/-}$ embryos, and 3) electroporation of an *Fgf15* expression vector in mouse embryonic brain explants increases the expression of *Tcf7l2* (Ishibashi and McMahon, 2002). Furthermore, it has been demonstrated that Gli2, a transcription factor mediating Shh signaling, activates a 3.6kb fragment of the *Fgf15* promoter region in the diencephalon and mesencephalon of transgenic mouse embryos that carry a lacZ gene under this promoter

fragment (Saitsu et al., 2005). In zebrafish, the role of Fgf19, the ortholog of mouse Fgf15 in fish, has been addressed in LOF and GOF experiments (Miyake et al., 2005). Fgf19 was shown to be required for cell proliferation and survival, as well as for patterning of the forebrain. Furthermore, it was shown that in the absence of Fgf19 signaling, GABAergic neurons and oligodendrocytes in the forebrain do not develop properly (Miyake et al., 2005).

The obvious discrepancy between the prominent expression of *Fgf15* in the developing CNS of the mouse and the absence of a neural phenotype in *Fgf15* deficient mice, together with the neural Fgf19 phenotype reported in zebrafish, prompted me to analyze the mouse line described in Wright et al. (2004) more closely in respect to CNS development. The present work reports for the first time a function of Fgf15 in neural development *in vivo*. In the absence of Fgf15, neural progenitors fail to exit the cell cycle at E11.5, resulting in an increased progenitor pool in the neuroepithelium. The failure in cell cycle withdrawal is accompanied by perturbed neurogenesis, as assessed by the increased expression of *Hes* and *Id* genes, and the down-regulation of proneural bHLH genes in the neural tube of *Fgf15*$^{-/-}$ embryos. It is further demonstrated that the described phenotype depends on the genetic background, as it occurs only in the outbred CD1 strain and not in the inbred C57Bl/6 strain.

2.4 Secreted factors in the development of mesDA neurons

As mentioned before, secreted factors play an important role in the specification and differentiation of neuronal subpopulations within the neural tube. In the developing midbrain a pivotal population of neurons arise, which are characterized by the synthesis and release of the neurotransmitter dopamine (Dahlstrom and Fuxe, 1964). Based on this neurotransmitter phenotype and their localization in the mesencephalon, they are classified as mesencephalic dopaminergic (mesDA) neurons. The progenitor domain of mesDA neurons is established in close vicinity of two important signaling centers of the embryonic neural tube. These are the ventral midline or FP and the boundary between the presumptive mid- and hindbrain, the MHB. The FP comprises cells that secrete the glycoprotein Shh, a key signaling molecule in the specification of different neuronal subpopulations along the D/V axis of the neural tube (Fig. 4; Jessell, 2000). The MHB has been identified as an important secondary organizer that controls patterning events in the developing mid- and hindbrain (Wurst and Bally-Cuif, 2001; Prakash and Wurst, 2004; Liu and Joyner, 2001), and several secreted factors expressed in the MHB region have been implicated in mesDA neurogenesis, among them Fgf8, Tgf-α and –β

and Wnt1 (Fig. 4A). Besides these secreted molecules, intracellular factors involved in mesDA neuron development include the nuclear receptor Nr4a2 and transcription factors like Lmx1b, Pitx3, En1 and 2 (reviewed in Prakash and Wurst, 2006). More recent studies have shown that also the proneural bHLH factor Ngn2 and the homeobox transcription factors Lmx1a and Msx1 are involved in mesDA neurogenesis (Andersson et al., 2006a; Kele et al., 2006; Andersson et al., 2006b).

The mesDA system of the human brain is involved in the modulation of various brain functions, including movement, cognition and reward. The degeneration or dysfunction of these neurons underlies severe neurological and psychiatric disorders, e.g. Parkinson's disease, schizophrenia and addiction (Lang and Lozano, 1998; Nieoullon, 2002; Maldonado, 2003). Considerable progress has been made in recent years in the identification of extracellular and intracellular factors involved in the induction, maturation and maintenance of mesDA neurons. However, the exact relationships and interactions of these factors and the mechanisms by which they exert their function in mesDA neuron development are still not fully understood (reviewed in Prakash and Wurst, 2006).

Since the rate-limiting enzyme in the biochemical pathway of dopamine synthesis is tyrosine hydroxylase (Th), the expression of Th identifies a neuron as capable of producing dopamine. In the ventral mesencephalon the first Th-positive neurons appear at E11.5, and mesDA neurogenesis proceeds until around E14 in the mouse (Bayer et al., 1995). The progenitor population of mesDA neurons has not been identified unequivocally, but there is evidence that these progenitors express the enzyme retinaldehyde dehydrogenase 1 (Aldh1a1) (Wallen et al., 1999). Expression of *Aldh1a1* first appears at E9.5 in the cephalic flexure and persists throughout development into postnatal stages. Although a function of Aldh1a1 in mesDA neuron development has not been demonstrated *in vivo*, its expression represents the only presently available marker for the putative mesDA progenitor population. One day later, at E10.5, as mesDA precursors become postmitotic, they begin to express the orphan nuclear receptor Nr4a2 (Perlmann and Wallen-Mackenzie, 2004). Unlike Aldh1a1, Nr4a2 has been shown to be required for the proper development of mesDA neurons. In *Nr4a2*$^{-/-}$ mutant mice, mesDA progenitors are induced, but lost later during embryonic development. Furthermore, expression of genes encoding proteins that are necessary for dopamine synthesis and neurotransmission like *Th*, the vesicular monoamine transporter 2 (*Slc18a2*) and the dopamine transporter (*Slc6a3*), is not initiated (Zetterstrom et al., 1997; Saucedo-Cardenas et al., 1998; Wallen et al., 1999; Smits et al., 2003). While *Nr4a2* is also expressed in other brain regions beside the ventral mesencephalon, the gene encoding the transcription factor Pitx3 is

expressed in a highly restricted fashion in the developing and adult CNS specifically in mesDA precursors and mature neurons (Smidt et al., 1997). At E12.5, expression of *Pitx3* and *Th* are partially segregated, but these differences disappear as development proceeds, so that a complete overlap is observed at adult stages (Maxwell et al., 2005). These findings have been interpreted in the way that two ontogenetically different subpopulations of precursors may exist early in development that together constitute the mesDA neuron population in the adult. The analyses of a naturally occurring *Pitx3* mutant, the aphakia (*ak*) mouse, and of a genetically engineered mouse line in which the *Pitx3* coding sequence is replaced by an eGFP reporter sequence, revealed that Pitx3 is an essential factor for proper mesDA development (Smidt et al., 2004; van den Munckhof et al., 2003; Zhao et al., 2004; Maxwell et al., 2005). It appears to be required for the terminal differentiation of a subpopulation of mesDA neurons (the population that expresses Pitx3 early in development) by regulating the expression of *Th* in these cells, but it is not necessary for the generation and maintenance of their progenitors (Maxwell et al., 2005).

2.5 Wnt signaling in mesDA neuron development

The role of Wnt1 in mesDA neuron development *in vivo* has been addressed in a recent study by the analysis of several transgenic mouse lines that display different mesDA neuron phenotypes (Prakash et al., 2006). *Wnt1* is expressed in a ring encircling the neural tube at the MHB, in the RP of the midbrain and posterior diencephalon, and in the cephalic flexure where mesDA neurons arise (Fig. 4A; Parr et al., 1993; Panhuysen et al., 2004). Wnt1 has been shown to exert two different functions in mesDA neuron generation *in vivo*. Early in this process, it is necessary for the establishment of a characteristic genetic network in the caudal ventral midbrain. Wnt1 has been demonstrated to be required for the maintenance of the expression of the transcriptional repressor Otx2 in this region. Otx2 in turn is essential for the repression of the transcription factor Nkx2-2 in the FP/ BP. In this Nkx2-2 negative territory, under the influence of Shh emanating from the FP and Fgf8 derived from the MHB, mesDA neurons are generated (Fig. 4B; Prakash et al., 2006). Later in development, Wnt1 is required for the complete differentiation of mesDA neurons. Two independent pathways have been implicated in the terminal differentiation of these neurons: an Nr4a2-controlled pathway required for the initiation of *Th* and *Slc6a3* transcription (Kim et al., 2003; Saucedo-Cardenas et al., 1998; Smits et al., 2003; Zetterstrom et al., 1997), and an Lmx1b-controlled pathway

necessary for the expression of *Pitx3* (Smidt et al., 2000). It has been suggested that Wnt1 is acting downstream of Lmx1b in the regulation of *Pitx3* expression in the second pathway (Fig. 4C; Prakash et al., 2006).

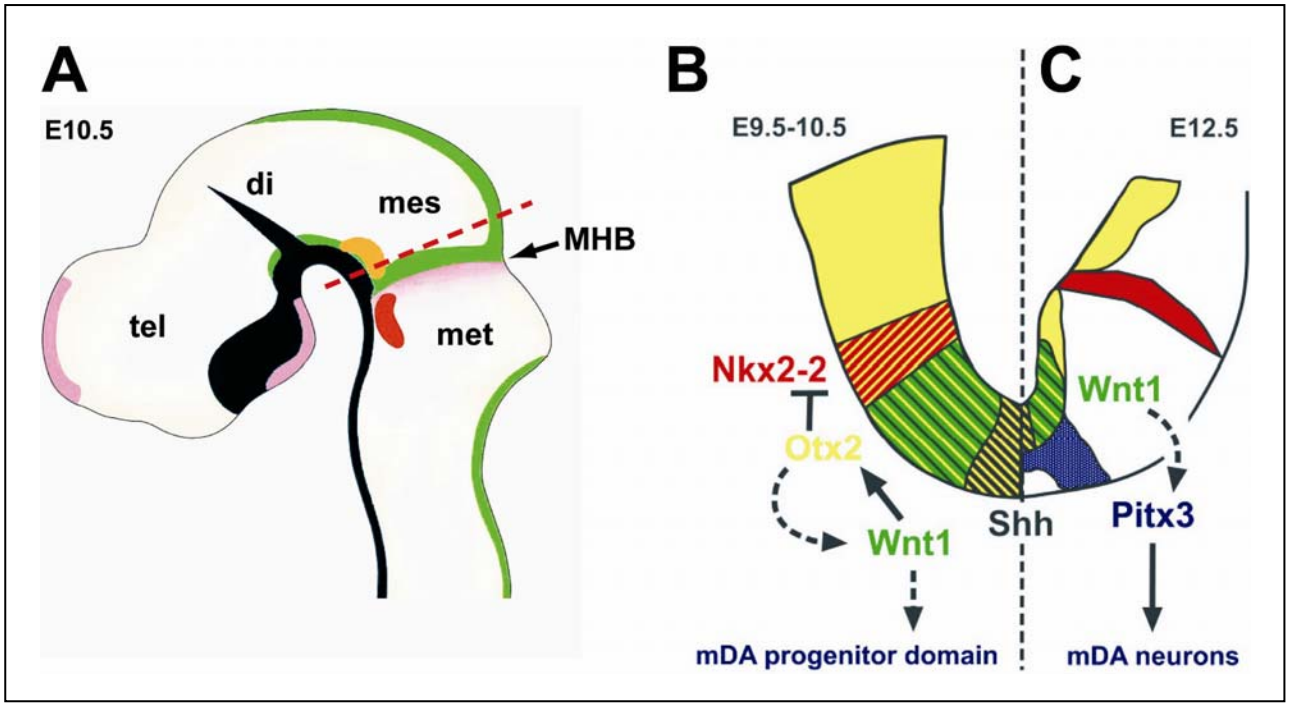

Figure 4 (A) Schematic drawing of the anterior neural tube of an E10.5 mouse embryo viewed from the side. Anterior is to the left. The expression domains of Fgf8 (purple), Shh (black) and Wnt1 (green) are depicted. The positions of the progenitor domains of mesDA neurons (orange) and rostral serotonergic neurons (red) are also indicated. The position of the MHB is marked by an arrow. (B, C) Schematic drawing of a cross-section through the mouse ventral midbrain close to the MHB at E9.5-10.5 (B) and E12.5 (C). The plane of section is depicted as a broken red line in (A). The expression domains of Wnt1 (green), Otx2 (yellow), Nkx2-2 (red), Shh (black) and Pitx3 (blue) are depicted. (B) At E9.5-10.5, Wnt1 maintains the expression of *Otx2* in the ventral neural tube (and vice versa). Otx2 represses the expression of *Nkx2-2*. The mesDA progenitor domain is established under the influence of Shh in this Nkx2-2-negative territory. (C) At E12.5, Wnt1 may be required for the terminal differentiation of mesDA neurons by inducing the expression of *Pitx3*. Hypothetical interactions are depicted as broken arrows. Abbreviations as in Fig. 1. Adapted from Prakash and Wurst, 2004 and Prakash et al., 2006.

Wnt signals are transduced through at least three distinct intracellular signaling pathways, the canonical Wnt/β-catenin pathway, the Wnt/Ca^{2+} pathway and the planar cell polarity (PCP) pathway (Wodarz and Nusse, 1998). In all three pathways, Fzd proteins have been identified as receptors for Wnt ligands (Huang and Klein 2004). Wnt1 signals via the canonical Wnt/β-

catenin pathway (Wodarz and Nusse, 1998; Huang and Klein, 2004), and *in vitro* experiments indicate that Wnt signaling in mesDA neuron development is also transduced via the β-catenin pathway (Castelo-Branco et al., 2004). In this signaling cascade, the extracellular glycoprotein Wnt1 binds to and activates a receptor complex consisting of a Fzd protein and a low density lipoprotein receptor-related protein (LRP). In the absence of Wnt signaling, the activity of an intracellular protein complex is responsible for the constitutive phosphorylation and degradation of β-catenin in the proteasome of the cell. The activation of Wnt receptors leads to the inactivation of this protein complex and consequently to the accumulation of β-catenin in the cytosol and to its translocation into the nucleus. Here, it transactivates T-cell specific transcription factors (Tcfs) and lymphoid enhancer binding factor 1 (Lef1) and initiates the transcription of Wnt target genes (for a recent review see Logan and Nusse, 2004).

In mammals, 10 genes encoding Fzd receptors have been identified. The Fzd proteins share a common structure with an amino-terminal signal peptide, a cysteine-rich domain (CRD) and seven hydrophobic transmembrane domains (Bhanot et al., 1996; Dann et al., 2001). The CRD consists of 120-125 amino acids with ten conserved cysteines, all of which form disulfide bonds, and is necessary and sufficient for ligand binding. A conserved motif of 6 amino acids (KTXXXW) located two amino acids after the seventh transmembrane domain is essential for the activation of the canonical Wnt/β-catenin pathway (Umbhauer et al., 2000). The mechanism by which Fzd proteins transduce signals upon ligand binding is still not well understood. The multi-module protein dishevelled (Dsh) is recruited to the plasma membrane if Fzds are overexpressed (Boutros et al., 2000), and it has been proposed that Dsh interacts directly with the carboxyl terminus of Fzds (Wong et al., 2003), but the physiological significance of membrane recruitment of Dsh is not clear. The specific functions of Fzd receptors in mammals have been addressed by a number of LOF experiments in the mouse. The phenotypes associated with LOF of different *Fzd* genes are briefly summarized in Table 1. The phenotypes reported for *Fzd* mutants appear to be relatively mild, given the prominent and essential functions that have been ascribed to many of the Wnt ligands. Furthermore, the inactivation of a specific Fzd receptor does not recapitulate the inactivation of a specific Wnt ligand. These findings suggest that functional redundancies may exist between several Fzd receptors, and that loss of a given Fzd receptor may therefore be compensated by another member of the family.

Gene	Phenotype	References
Fzd1	n/a	
Fzd2	n/a	
Fzd3	defects in axon guidance and loss of major fibre tracts in the rostral CNS	Wang et al., 2002 Wang et al., 2006 Lyuksyotova et al., 2003
Fzd4	cerebellar, auditory, and esophageal defects and impaired corpora lutea formation	Wang et al., 2001 Hsieh et al., 2005
Fzd5	defects in placental and yolk sac angiogenesis	Ishikawa et al., 2001
Fzd6	defects in macroscopic hair patterning	Guo et al., 2004
Fzd7	n/a	
Fzd8	n/a	
Fzd9	defects in hippocampal development and B cell maturation	Zhao et al., 2005 Ranheim et al., 2005
Fzd10	n/a	

Table 1 Phenotypes of LOF experiments of *Fzd* genes in the mouse. n/a: no data available.

In the present study, I wanted to identify candidate receptors of the Fzd family that may transduce the Wnt1 signal specifically in the development of mesDA neurons. To this end, probes for all 10 *Fzd* genes were cloned and a detailed expression analysis of these genes during the crucial mesDA neurogenic period was performed. Based on these expression patterns, only Fzd3, Fzd6 and Fzd9 were identified as possible Wnt1 receptors in this process. While *Fzd3* and *Fzd9* transcripts were expressed widely in the developing CNS, *Fzd6* displayed a highly restricted expression in the cephalic flexure and may therefore play a specific role in the development of mesDA neurons.

3. Results

3.1 The role of Fgf15 in neurogenesis

During CNS development, the number and different types of cells that are produced are determined by two tightly controlled and interconnected processes, proliferation and differentiation. A number of extracellular and intracellular factors have been demonstrated to play a role in the regulation of neurogenesis. Here, I examined the function of Fgf15 in the control of neurogenesis during vertebrate CNS development by analyzing an *Fgf15* deficient mouse line.

3.1.1 *Fgf15* gene expression during midgestational stages of mouse embryonic development

In order to examine a putative role of *Fgf15* in CNS development, an important issue was to determine the exact temporal and spatial expression pattern of this gene during early neural development. Several studies have addressed this issue using non-radioactive whole mount *in situ* hybridization at midgestational stages of mouse embryonic development, i.e. from E8.5 to E12.5 (McWhirter et al., 1997; Gimeno et al., 2002; Gimeno et al., 2003). Although this method is suitable to obtain an overview of gene expression, it is often difficult to determine the precise extent and boundaries of expression. Furthermore, very faint expression domains might be missed due to the limited sensitivity of detection. To obtain a more accurate picture of *Fgf15* mRNA distribution and to increase the sensitivity of the analysis, radioactive *in situ* hybridization on sections of E9.5 to E12.5 wild type embryos was performed in the present study.

In the rostral neural tube of E9.5 embryos, *Fgf15* was expressed at the anterior end of the telencephalon, in the dorsal diencephalon and in the dorsal midbrain, while no expression was detected in ventral domains of the anterior neural tube. In the dorsal midbrain, the caudal boundary of the *Fgf15* expression domain coincided with the MHB, abutting the *Fgf8* expression domain in the anterior dorsal hindbrain (Fig. 5A-C). The expression pattern of *Fgf15* mRNA in the telencephalon and diencephalon did not change between E9.5 and E12.5 (Fig. 5E, H, K). In the dorsal midbrain of E10.5 embryos, a caudal to rostral gradient became evident, with strongest expression anterior to the isthmic *Fgf8* expression domain (Fig. 5D-F).

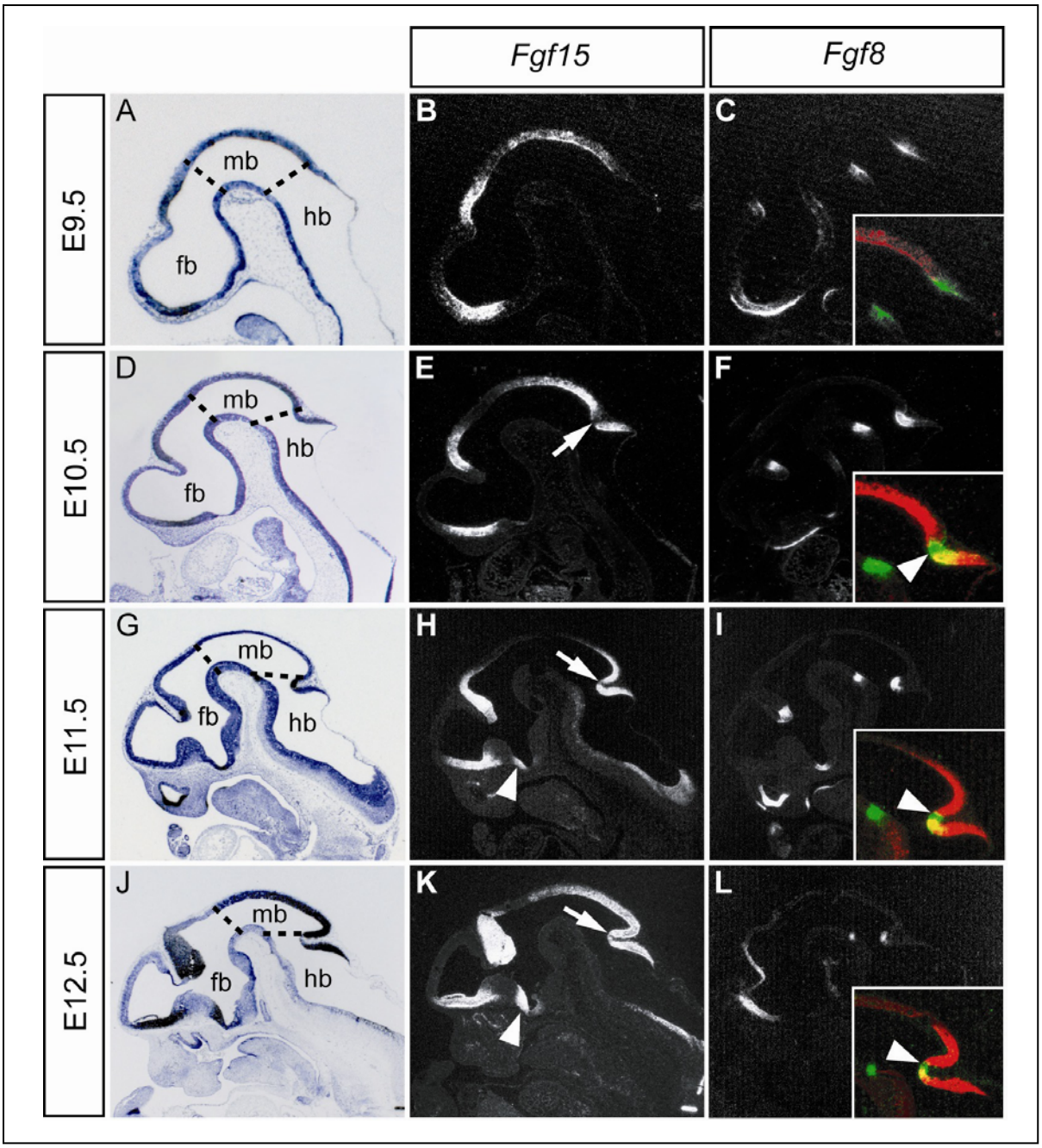

Figure 5 Expression of *Fgf15* in wild type embryos from E9.5 to E12.5 on sagittal sections. Anterior is to the left. (A, D, G, J) Brightfield images of (B, F, I, K). (B, C, E, F, H, I, K, L) Darkfield images of corresponding sections. Insets in (C, F, I, L): pseudocolor overlay images of consecutive sections hybridized with probes for *Fgf15* (red) and *Fgf8* (green). (A-C) At E9.5, *Fgf15* was expressed in the anterior telencephalon, in the dorsal diencephalon, and in the dorsal midbrain (B). *Fgf8* expression was complementary to *Fgf15* at the MHB (C). (D-E) At E10.5, *Fgf15* was additionally expressed in the dorsal anterior hindbrain (rhombic lip), resulting in a gap at the MHB (arrow in E). The gap at the MHB corresponded to the anterior part of the *Fgf8* expression domain (arrowhead in F, inset). (G-L) At E11.5 and E12.5, *Fgf15* was expressed in the commissural plate, the dorsal thalamus and at the entrance of the optic stalk (arrowheads in H, K). *Fgf15* was expressed in a caudal to rostral gradient in the dorsal midbrain, and in the dorsal anterior hindbrain (H, K). The gap at the MHB narrowed substantially (arrows in H, K), following a narrowing of the *Fgf8* expression domain at the MHB (arrowheads in insets in I, L). fb forebrain; mb midbrain; hb hindbrain; approximate boundaries between fb and mb and between mb and hb are indicated by broken lines in (A, D, G, J).

In addition, *Fgf15* transcripts were detected in the dorsal anterior hindbrain (rhombic lip), with a gap at the MHB (Fig. 5E). A pseudocolor overlay revealed that the *Fgf15* negative territory corresponded to the anterior part of the *Fgf8* expression domain, while *Fgf15* expression overlapped with the *Fgf8* domain posteriorly (Fig. 5F). At E11.5 and E12.5, the expression of *Fgf15* in the brain was similar to the expression at E10.5 (Fig. 5H, K). An additional expression domain of *Fgf15* appeared in the ventral telencephalon, corresponding to the entrance of the optic stalk (Fig. 5H, K). The gap in the *Fgf15* expression at the dorsal MHB at these stages narrowed, still sparing the anterior part of the *Fgf8* expression domain and overlapping with *Fgf8* mRNA posteriorly (Fig. 5I, L). Notably, the narrowing of the gap in *Fgf15* expression followed the narrowing of the *Fgf8* domain.

Coronal sections were hybridized with a probe for *Fgf15* to examine the expression pattern of *Fgf15* in the D/V axis. The plane of sections in this analysis was chosen in a way to cut the mid-/hindbrain region perpendicular to the A/P axis of the neural tube, resulting at forebrain levels in a plane of section between horizontal and coronal, termed ‘oblique’ in the following paragraphs. For better orientation, the plane of coronal/oblique sections is indicated in Fig. 6D, H, L. Between E9.5 and E11.5, *Fgf15* expression was detected in the ventral telencephalon, with a narrow *Fgf15* negative domain in the ventral midline, presumably corresponding to the *Fgf8* expression domain at the ANR (Fig. 6A′, E′, I′). The same sections show expression of *Fgf15* in the AP of the anterior diencephalon, while *Fgf15* was not expressed in the RP of the diencephalon (Fig. 6A′, E′, I′). In the midbrain of E9.5, E10.5 and E11.5 embryos, *Fgf15* expression was detected in the AP of the neural tube, with the RP and BP/FP showing no *Fgf15* expression (Fig. 6B′, F′, J′). Between E9.5 and E11.5, *Fgf15* in the midbrain showed a dynamic expression: initially, *Fgf15* was expressed uniformly in the AP of the neural tube, whereas later distinct domains appeared in the lateral walls of the neural tube that expressed different levels of *Fgf15* (Fig. 6B′, F′, J′). At E10.5 and E11.5, *Fgf15* transcripts were also detected in the retina as well as in the neuroepithelium of the optic stalk (Fig. 6F′, J′). In the anterior hindbrain of E9.5 and E10.5 embryos, the *Fgf15* expression domain comprised the dorsal part of the neural tube. In the RP of the anterior hindbrain, *Fgf15* expression displayed a narrow gap at these stages (Fig. 6C′, G′). In the anterior hindbrain of E11.5 embryos, *Fgf15* transcripts were detected in the AP of the neural tube, as well as in the BP, but sparing the FP (Fig. 6K′). In contrast to the expression at E9.5 and E10.5, at E11.5 *Fgf15* mRNA was also expressed in the RP of the anterior hindbrain (Fig. 6K′).

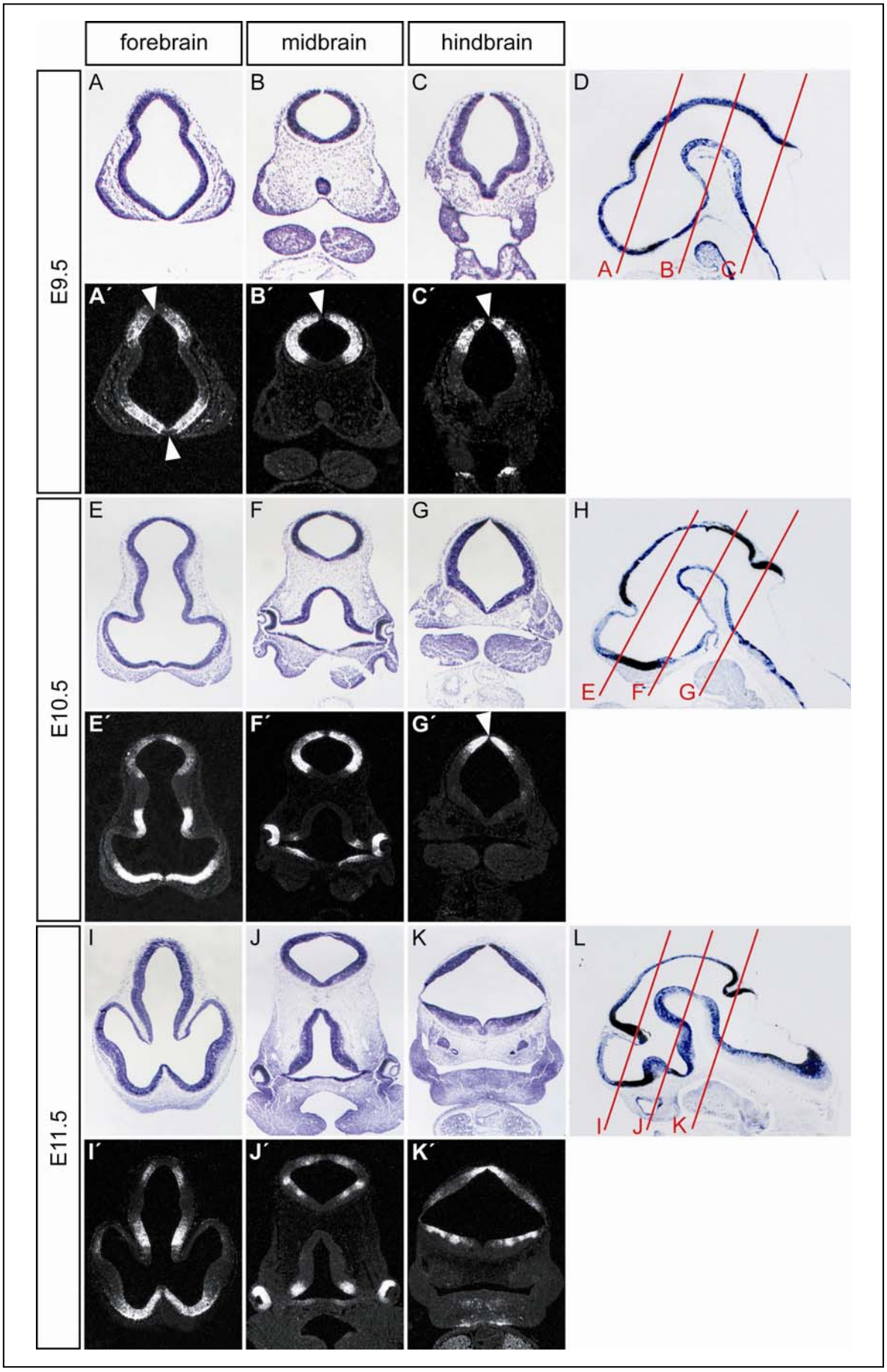
forebrain
midbrain
hindbrain
E9.5
E10.5
E11.5
A
B
C
D
A´
B´
C´
E
F
G
H
E´
F´
G´
I
J
K
L
I´
J´
K´

Figure 6

Figure 6 *Fgf15* expression in wild type embryos from E9.5 to E11.5 on coronal/oblique sections. Dorsal is at the top. (A-K) Brightfield images of (A´-K´). (A´-K´) Darkfield images of corresponding sections. Planes of sections are indicated by red lines in (D, H, L). (A-D) At E9.5, *Fgf15* was expressed in the anterior telencephalon and in the AP of the diencephalon (A´). The ANR in the telencephalon and the RP in the diencephalon did not show *Fgf15* expression (arrowheads in A´). In the midbrain, *Fgf15* was expressed in the AP, while the RP and BP/FP did not show *Fgf15* expression (arrowhead in B´). In the anterior hindbrain, *Fgf15* transcripts were restricted to the dorsal part of the neural tube, with a gap in the RP (arrowhead in C´). (E-H) At E10.5, *Fgf15* expression recapitulated the pattern at E9.5 (E´-G´). In addition, *Fgf15* was expressed in the developing retina and in the neuroepithelium of the optic stalk (F´). (I-L) At E11.5, *Fgf15* was expressed in the anterior telencephalon, in the dorsal thalamus and the AP of the diencephalon (I´). In the midbrain, *Fgf15* expression comprised the AP of the neural tube. Furthermore, it was expressed in the retina and the entrance to the optic stalk. In the hindbrain, *Fgf15* was expressed in the RP, the AP and the BP of the neural tube, whereas it was not expressed in the FP.

To define the ventral border of *Fgf15* expression in the D/V axis more precisely, colocalization experiments for *Fgf15* and *Shh* mRNAs on coronal/oblique sections of E11.5 embryos were performed. *Shh* expression during mouse neural development has been shown to cover the FP and BP in the fore- and midbrain, whereas it narrows substantially in the hindbrain, comprising only the FP (Patten and Placzek, 2000; Jessell, 2000). In the neural tube of E11.5 embryos, the ventral border of the *Fgf15* expression domain abutted the dorsal border of the *Shh* expression domain in the fore-, mid- and hindbrain (Fig. 7B-D, F-H, J-L). This finding further supports the notion that the *Fgf15* negative domain in the ventral neural tube of E11.5 embryos comprised the FP and BP in the fore- and midbrain, and the FP in the anterior hindbrain.

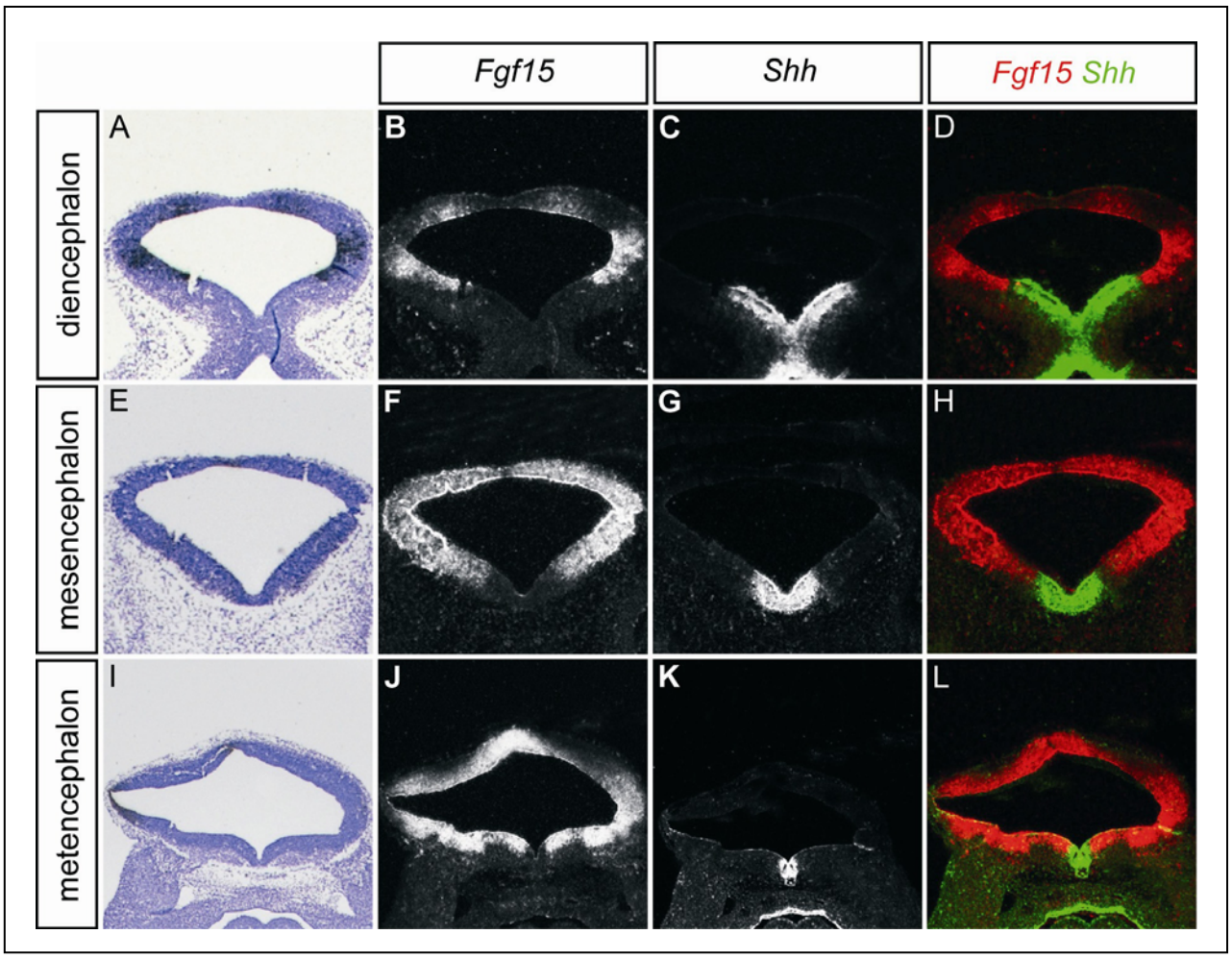

Figure 7 *Fgf15* expression is complementary to the *Shh* expression in the FP/BP of E11.5 wild type embryos. (A-L) Coronal sections of the neural tube, dorsal is at the top. (A, E, I) Brightfield images of (B, F, J). (C-D, F-H, J-L) Darkfield images of corresponding sections. (D, H, L) Pseudocolor overlays of consecutive sections hybridized with probes for *Fgf15* (red) and *Shh* (green). (A-D) In the diencephalon, *Fgf15* expression was complementary to the ventral *Shh* expression domain in the BP and FP. (E-H) In the midbrain, *Fgf15* transcripts also abutted the *Shh* domain in the BP and FP. (I-L) In the anterior hindbrain, the *Fgf15* expression domain spared the ventral *Shh* expression domain in the FP.

3.1.2 *Fgf15* deficient embryos on a CD1 genetic background displayed a neural phenotype

The prominent expression of *Fgf15* in the developing anterior neural tube suggested a role of this factor in neural development. To assess a possible function of Fgf15 during CNS development, a mouse line with a targeted deletion in the *Fgf15* gene was analyzed. This mouse line was originally established by J. R. McWhirter in the laboratory of C. Murre, University of California, and was first published by Wright et al., 2004. In this mouse line, a

1.6 kb fragment containing about 800 bp each of intron 2 and exon 3 is replaced by an MC1-NeopA expression cassette, with the direction of *Neo* transcription opposing that of *Fgf15* (Fig. 8). This results in a deletion of 108 amino acids (aa) of the C-terminus, comprising 52% of the Fgf15 protein, including a large part of the Fgf core homology region as well as a major part of sequences expected to be involved in Fgf receptor and heparin binding. Genotyping of mice and embryos was performed by triplex PCR, with a forward primer located in intron 2 (P1 in Fig. 8) and two different reverse primers, one binding in intronic sequence that was deleted in the mutant, and the other one binding in the *Neo* sequence of the MC1NeopA cassette (P2 and P3 in Fig. 8). This resulted in the amplification of a 500bp wild type fragment and a 370bp mutant fragment, respectively (Fig. 8D).

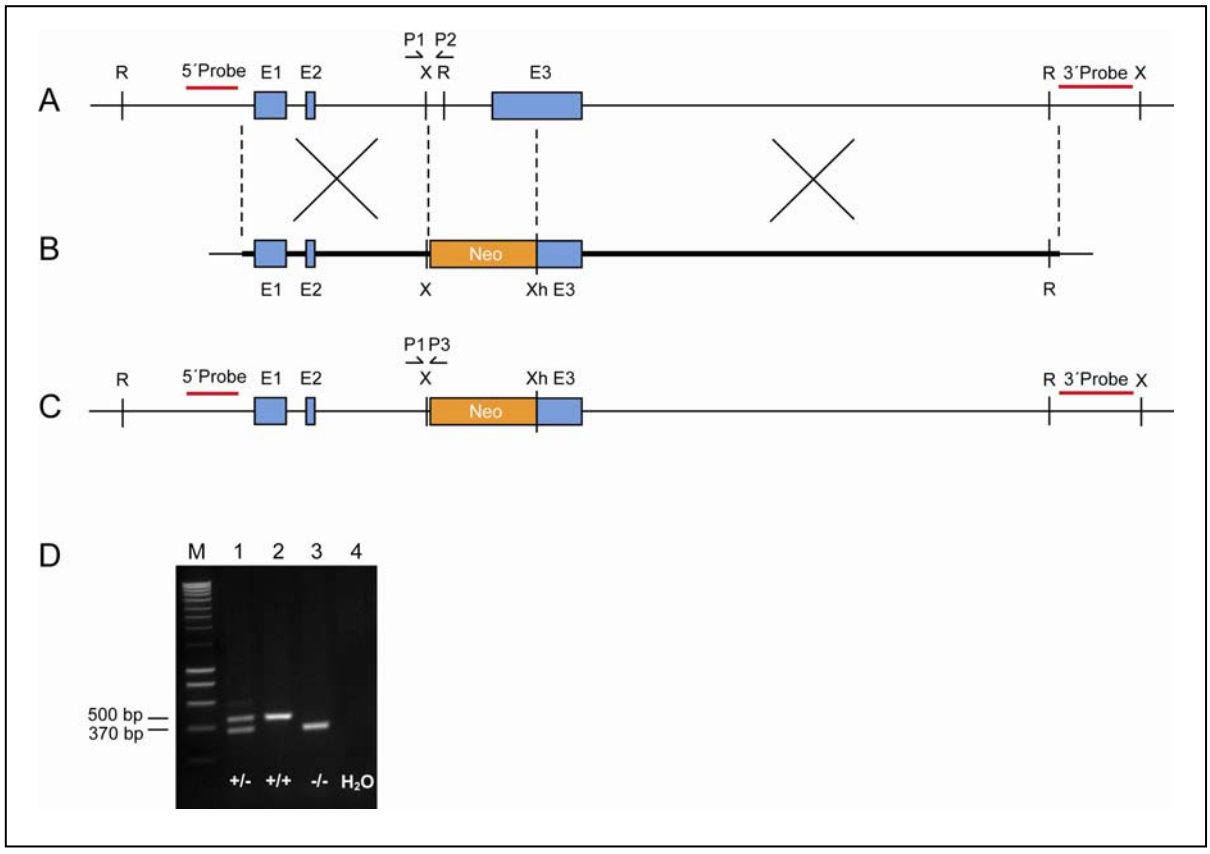

Figure 8 Targeting strategy used for the inactivation of *Fgf15* by Wright et al., 2004. (A) *Fgf15* genomic locus. (B) Targeting vector with a *Neo* cassette replacing part of intron 2 and exon 3. Homologous arms are depicted as bold black lines. (C) Targeted *Fgf15* allele after HR. P1: forward primer for genotyping PCR; P2: reverse primer for amplification of 500bp wild type fragment; P3: reverse primer for amplification of 370bp mutant fragment; E: exon; restriction sites: R *Eco*RI; X *Xba*I; Xh *Xho*I. (adapted from Wright et al., 2004). (D) Genotyping PCR of embryos from an $Fgf15^{+/-}$ heterozygous mating. Amplification of the wild type allele using primers 1 and 2 rendered a 500bp fragment (2), amplification of the targeted allele using primers 1 and 3 resulted in a 370bp fragment (3). Amplification of both bands in case of heterozygous animals (1). M: DNA Smart ladder; 4: water control.

The *Fgf15* knockout line was established on a mixed Sv129/C57Bl/6 background and was subsequently inbred to a pure C57Bl/6 background. Since analyses of this mouse line did not reveal a CNS phenotype on either of these genetic backgrounds (Wright et al., 2004; Vincentz et al., 2005), in the present study *Fgf15* heterozygous mice (*Fgf15*$^{+/-}$) from the original strain (i.e. on a Sv129/C57Bl/6 mixed genetic background) were backcrossed with CD1 outbred mice for 6 generations (F6). Homozygous mutant embryos from heterozygous matings were analyzed from F1 onwards. As no differences in the phenotype of homozygous mutant embryos between F1 and F6 were detected, the filial generation of the analyzed mutant embryos is not indicated.

Adult offspring from matings of *Fgf15*$^{+/-}$ mice on a CD1 genetic background resulted in only 1 homozygous *Fgf15*$^{-/-}$ mutant out of 207 born mice (0.48%). This is in accordance with embryonic or early postnatal lethality reported by Wright et al. (2004) and Vincentz et al. (2005), indicating that the phenotype of embryonic lethality was preserved on an outbred genetic background. The time point of lethality reported in previous studies varied from later than E12.5 to postnatal day (P) 21 (Wright et al., 2004; Vincentz et al., 2005). To determine the time point of embryonic lethality on a CD1 genetic background more precisely, litters from heterozygous intercrosses were dissected at E12.5, E13.5, E14.5 and E18.5. While the distribution of wild type, heterozygous and homozygous mutant embryos was close to the mendelian ratio up to E13.5, the percentage of homozygous mutant embryos at E14.5 and E18.5 dropped to 2.6% and 0%, respectively. This finding indicates that most *Fgf15*$^{-/-}$ embryos on a CD1 genetic background die between E13.5 and E14.5.

Mutant embryos of heterozygous intercrosses were inspected by gross morphology and on histological sections. While no apparent defects were detectable in *Fgf15*$^{-/-}$ embryos until stage E11.5, an obvious morphological phenotype occurred in 10% of all E12.5 and E13.5 homozygous mutants (Fig. 9). The chorion of these embryos showed no blood filled vessels, the embryos were generally pale and seemed to lack a proper blood supply. They were smaller in size than wild type and heterozygous littermates and showed an overall growth retardation (Fig. 9). While eye morphology appeared grossly normal, the facial and head structures seemed not well developed (Fig. 9B, G, E, J). Given this already evident phenotype by gross morphology, the anatomy of affected embryos was further examined by histological analysis of sections from E13.5 mutant embryos (Fig. 10). Affected embryos showed a massive infolding of the anterior neural tube. The neuroepithelium showed multiple deep indentations in the dorsal fore-, mid- and hindbrain, whereas the defects were less severe in the ventral neural tube (Fig. 10A). This was confirmed on coronal/oblique sections of E13.5

mutant embryos, which showed that dorsal neural tissue folded up massively and formed invaginations into the lumen of the neural tube (Fig. 10B-D).

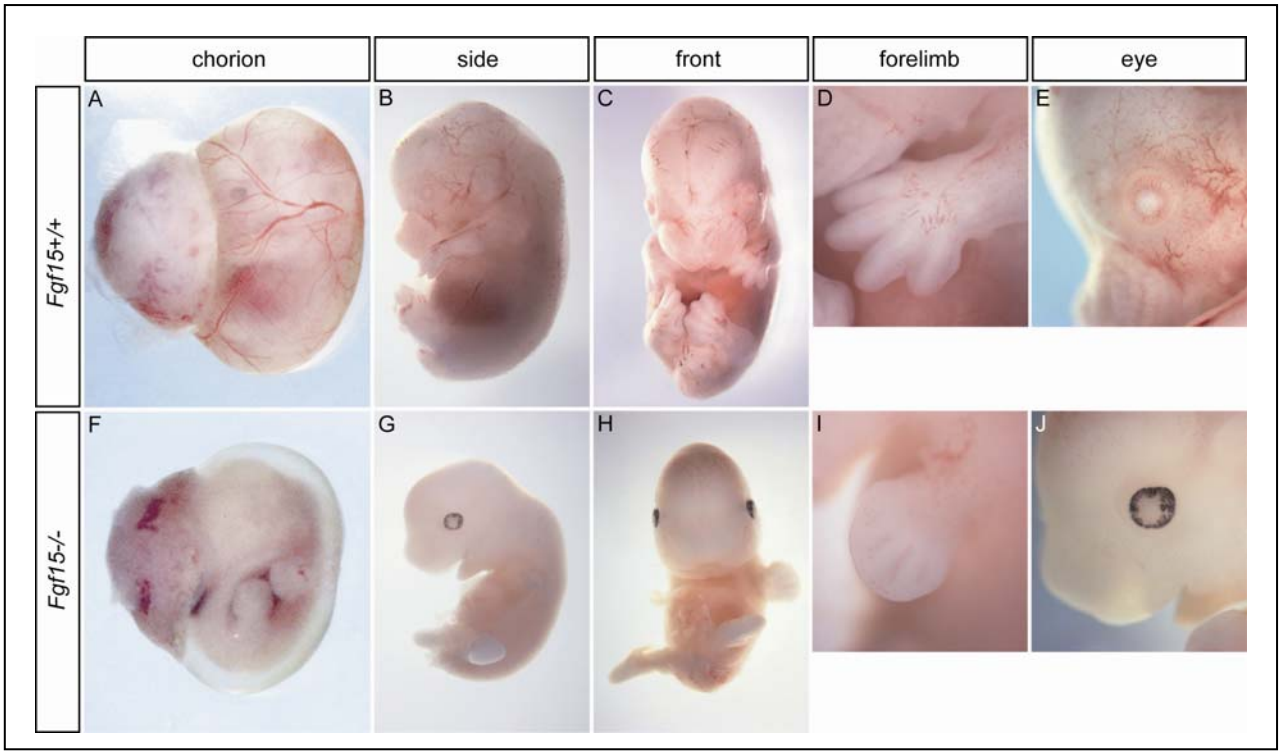

Figure 9 Morphological defects and growth retardation in 10% of *Fgf15*$^{-/-}$ embryos on an outbred (CD1) genetic background at E12.5 and E13.5. A representative E13.5 *Fgf15*$^{-/-}$ embryo is shown in (F-J) with a wild type littermate in (A-E). No blood filled vessels were obvious in the chorions of mutant embryos and in the embryos themselves (F, G, compare with A, B). The embryos appeared pale, suggesting that they lacked a proper blood supply. Compared to wild type littermates, the embryos were growth retarded (compare forelimbs in D, I) and craniofacial structures were not well developed (E, J), while the eyes appeared grossly normal (different pigmentation in (E, J) as a result of the mixed C57Bl/6/CD1 background).

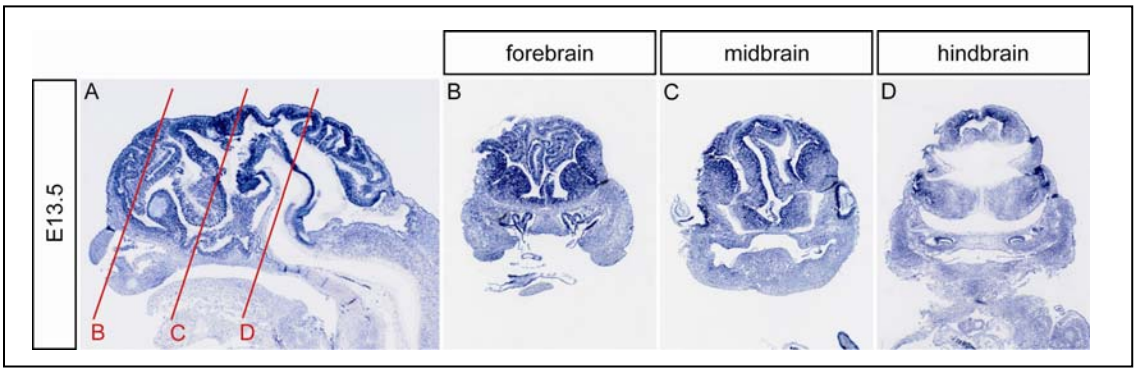

Figure 10 Massive infolding of anterior neural tissue in E13.5 *Fgf15*$^{-/-}$ embryos displaying aberrant morphology. Cresyl violet staining on sagittal and coronal sections of a representative mutant embryo. Anterior is to the left in (A), dorsal is to the top in (B-D). Plane of sections in (B-D) are depicted as red lines in (A). (A) Sagittal section showing the severe infolding of predominantly dorsal neural tissue. (B-C) Coronal/oblique sections revealed a strong invagination of folded neural tissue into the lumen of the neural tube in the forebrain (B), and to a lesser extent in the midbrain (C) and hindbrain (D).

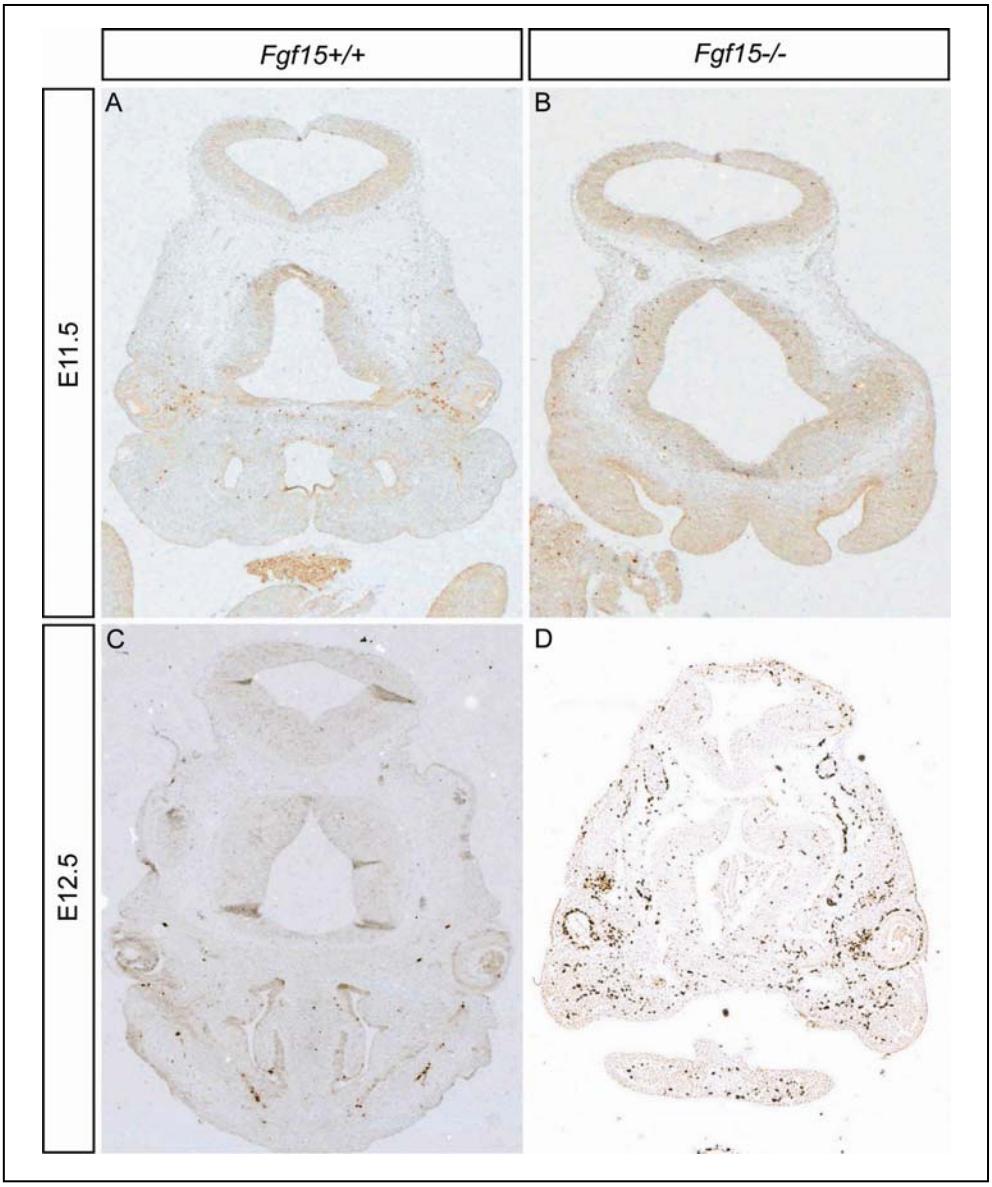

Figure 11 Apoptosis was strongly increased in *Fgf15*$^{-/-}$ embryos at E12.5. (A-D) Immunostaining for cleaved caspase 3 on coronal sections at midbrain level of wild type (A, C) and mutant embryos (B, D). Dorsal is to the top. (A, B) At E11.5, staining for cleaved caspase 3 was comparable between wild type and mutant embryos with very few labeled cells. (C, D) At E12.5, cleaved caspase 3 staining was markedly increased in *Fgf15*$^{-/-}$ mutants with morphological defects (D) compared to wild type littermates (C).

In addition to the aberrant morphology, the affected embryos were apparently starting to disintegrate and their tissue was very fragile, indicating that these embryos might already be dying at the time of dissection. To test this hypothesis, immunohistochemistry against cleaved caspase 3, a marker expressed in apoptotic cells, was performed on E11.5 and E12.5 embryos. At E11.5, only few cells were labeled for cleaved caspase 3 and no difference between wild type and mutant embryos was detected (Fig. 11A, B, n=8). However, one day later a massive increase in cleaved caspase 3 staining could be observed in *Fgf15*$^{-/-}$ embryos showing the

described morphological defects (Fig. 11C, D, n=2). This finding indicates that these embryos undergo massive apoptosis from E12.5 on, prior to embryonic lethality occurring around E14.5. Whether this increased apoptosis was a direct or indirect consequence of the loss of Fgf15 is not clear, but it should be noted that apoptosis was not restricted to *Fgf15* expressing tissues.

The pale appearance of embryos showing the described morphological defects, in addition to the apparently poor blood supply in the chorion, raised the possibility that the observed phenotype was a consequence of placental defects. To test this hypothesis, the expression of genes encoding the vascular endothelial growth factor receptors *Vegfr1* and *Vegfr2* was examined in placentas of E13.5 wild type and mutant embryos. *Vegfr1* mRNA was strongly expressed in the labyrinth and maternal decidua, whereas *Vegfr2* transcripts were detected in

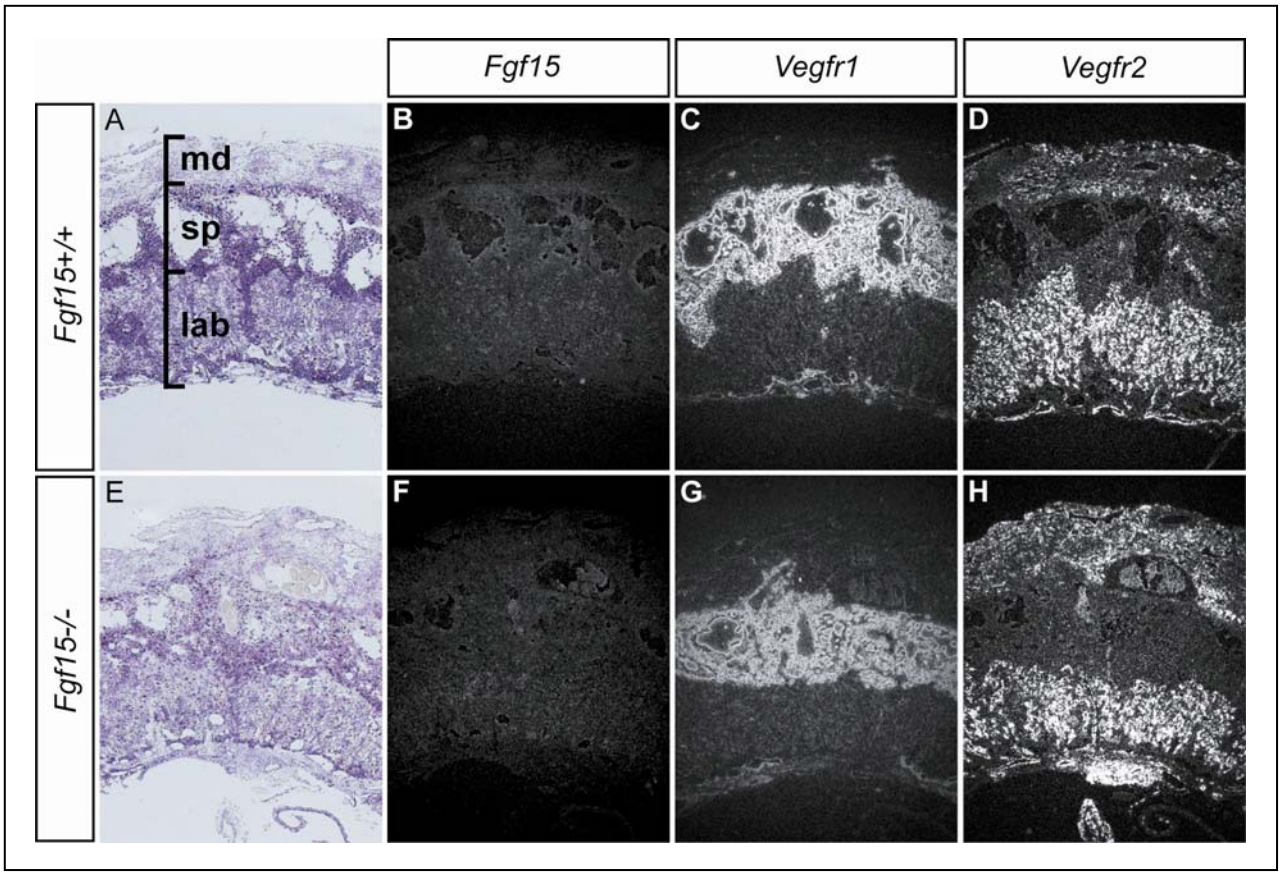

Figure 12 Patterning of *Fgf15*$^{-/-}$ placentas at E13.5 was normal. (A-H) Transverse sections through wild type (A-D) and mutant placentas (E-F). (A, E) Brightfield images of (B, F). (B-D, F-G) Darkfield images of corresponding sections. (B) *Fgf15* was not expressed in wild type placentas. (C, G) The spongiotrophoblast, strongly expressing *Vegfr1*, appeared to be normal in *Fgf15*$^{-/-}$ placentas. (D, H) The maternal decidua as well as the labyrinth also seemed to be unaffected by the loss of *Fgf15*, as assessed by the normal expression of *Vegfr2* in these tissues. md maternal decidua; sp spongiotrophoblast; lab labyrinth.

the spongiotrophoblast of wild type and mutant placentas (Fig. 12C, G and D, H). Signal intensity and expression pattern of both markers did not show obvious differences between wild type and mutant placentas. Moreover, *Fgf15* mRNA was not expressed in placental tissue in the wild type (Fig. 12B). These findings suggest that, although subtle defects cannot be ruled out completely, the gross morphology of mutant placentas seemed not to be affected by the loss of *Fgf15* and that the apparent poor blood supply of *Fgf15*$^{-/-}$ embryos was very likely not a consequence of placental defects.

Another possible explanation for the pale appearance of the affected embryos could be a defect in vascularization of the embryo itself. To assess whether blood vessels were formed in *Fgf15*$^{-/-}$ embryos, an immunostaining for von-Willebrand-factor (VWF) was performed. VWF is a multimeric protein complex involved in the adhesion of platelets to vascular endothelial

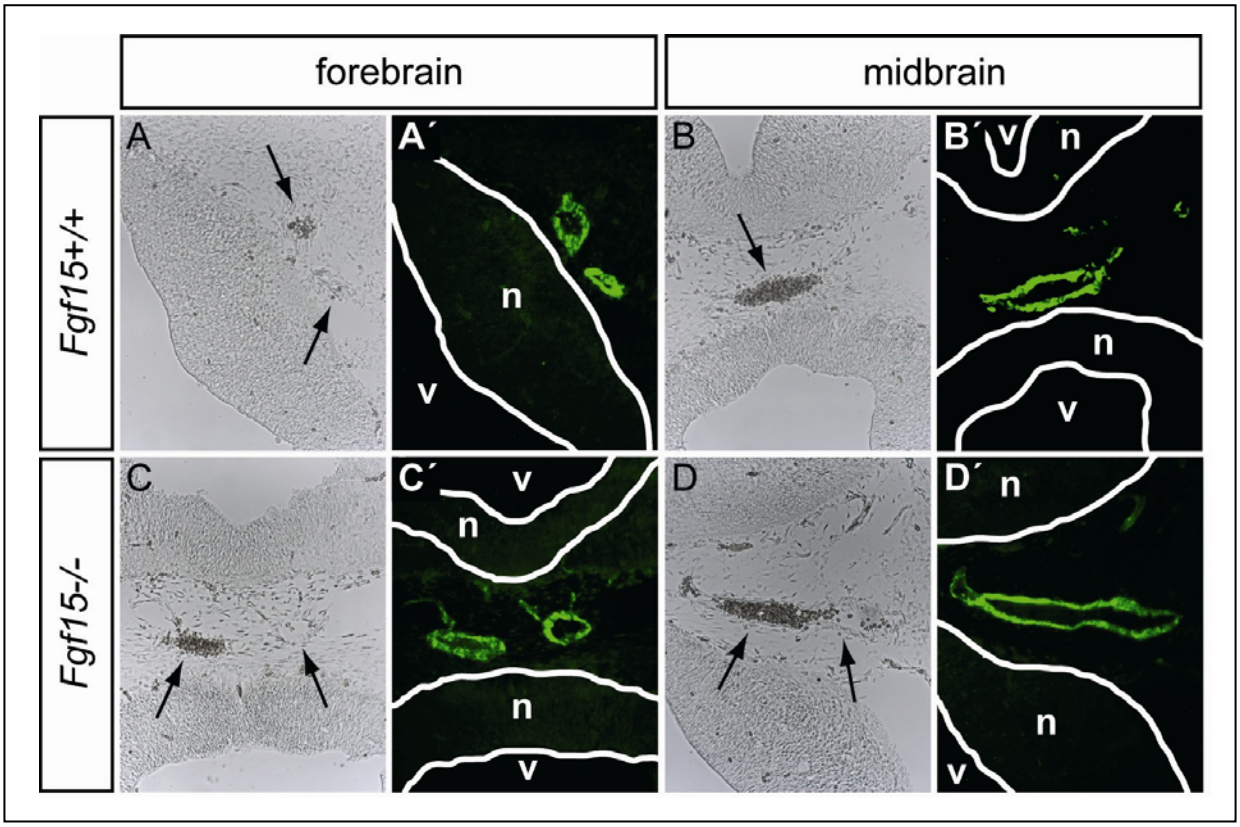

Figure 13 Formation of blood vessels appeared not to be affected in *Fgf15*$^{-/-}$ embryos at E11.5. (A-D) Brightfield images of (A´-D´). Neuroepithelium is outlined in white in (A´-D´). Representative sections of wild type and mutant littermates are shown, labeled with an antibody against VWF (an endothelial marker) displaying vessels of the PVP. Positions of blood vessels are marked by arrows. Comparable fluorescent immunostaining for VWF (green) in wild type (A-B´) and mutant littermates (C-D´) revealed that the PVP was present in *Fgf15*$^{-/-}$ embryos. n neuroepithelium; v ventricle.

cells (Sadler, 1998), and was therefore used as a vascular endothelial marker. In E11.5 wild type and mutant embryos, blood vessels were readily detectable by VWF staining, with no obvious differences between genotypes (Fig. 13 shows representative stainings of blood vessels from the perineural vascular plexus (PVP) (Bauer et al., 1993) in wild type embryos and *Fgf15*$^{-/-}$ littermates). The appearance of VWF-stained blood vessels in mutant embryos suggests that angiogenesis takes place in the absence of Fgf15, and that the apparent poor blood supply of *Fgf15*$^{-/-}$ embryos is very likely not due to a defective vascularization of the tissue.

It was shown by Vincentz et al., 2005, that loss of *Fgf15* leads to heart defects during embryonic development. The first alterations in cardiac development were reported to appear at E11.5 in mutant embryos, resulting in obvious morphological anomalies not before E12.5, while earlier stages seemed unaffected. Therefore, as placental structures and vascularization appeared to be unaffected by the loss of *Fgf15*, the reported cardiac phenotype could account for the apparently poor blood supply, and might lead to several other aspects of the described defects of *Fgf15*$^{-/-}$ embryos, including embryonic lethality. In order to analyze a putative neural-specific function of *Fgf15* during embryonic development, an important issue was to exclude secondary effects caused by cell death or disintegration of tissue. Therefore, we restricted our analysis of the *Fgf15*$^{-/-}$ mouse line on embryonic stages before E12.5.

3.1.3 Patterning appeared not to be affected in the anterior neural tube of *Fgf15*$^{-/-}$ embryos at E11.5

Since several studies have demonstrated that Fgfs are involved in patterning events in various tissues during development, including the CNS, we first tested whether patterning of the anterior neural tube was affected by the loss of *Fgf15*. To this end, the expression of several genes characteristic for distinct regions in the A/P and D/V axes of the neural tube was analyzed in wild type and mutant embryos.

In the A/P axis, the expression domain of the gene encoding Pax6, a homeobox containing transcription factor, comprises the alar plate of the entire forebrain, with its posterior boundary demarcating the junction between diencephalon and mesencephalon (Warren and Price, 1997; Mastick et al., 1997). As shown in Fig. 14C, D, the expression of *Pax6* mRNA in the forebrain was not changed in E11.5 mutant embryos (n=6) compared to wild type littermates. The gene encoding the homeobox transcription factor En1 is expressed in the

caudal part of the mesencephalon, across the MHB and in the rostral third of rhombomere1 in the hindbrain at E11.5. The expression of *En1* mRNA in mutant embryos was comparable to that in wild type littermates (Fig. 14E, F, n=5). The gene encoding the secreted factor Fgf8 is expressed in a narrow ring in the most rostral part of rhombomere 1 (Suzuki-Hirano et al., 2005; Maruoka et al., 1998) and marks the isthmic tissue (Wassef and Joyner, 1997). As Fig. 14G, H shows, *Fgf8* expression was unaltered in *Fgf15* mutant embryos at E11.5 (n=5).

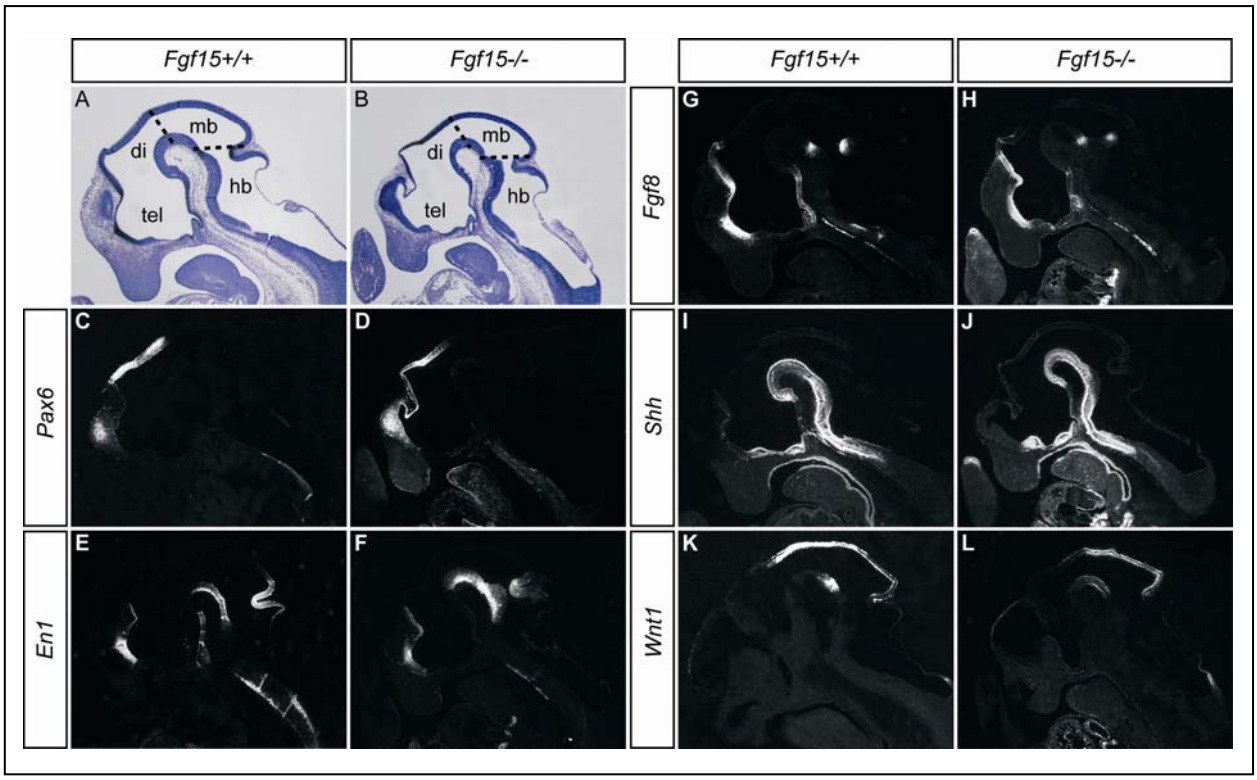

Figure 14 A/P patterning in the anterior neural tube appeared not to be affected in *Fgf15*$^{-/-}$ embryos at E11.5, as assessed by the expression of *Pax6*, *En1*, *Fgf8*, *Shh* and *Wnt1*. (A-L) Sagittal sections of the anterior neural tube of wild type (A, C, E, G, I, K) and mutant embryos (B, D, F, H, J, L). (A, B) Brightfield images of (G, D). (C-L) Darkfield images of corresponding sections. Expression of *Pax6* (C, D), *En1* (E, F), *Fgf8* (G, H), *Shh* (I, J) and *Wnt1* (K, L) was similar in wild type and mutant embryos. Note the smaller size of mutant embryos compared to wild type littermates. tel telencephalon; di diencephalon; mb midbrain; hb hindbrain; approximate boundaries between di and mb and between mb and hb are indicated by broken lines in (A, B).

Shh is expressed ventrally along the entire length of the neural tube (Patten and Placzek, 2000; Jessell, 2000). While in the spinal cord and rhombencephalon the expression domain is restricted to the FP, the expression broadens substantially in the mid- and caudal forebrain territory, covering the entire BP and FP, and expanding even more dorsally in a narrow domain corresponding to the zona limithans intrathalamica (ZLI) (Echelard et al., 1993;

Kiecker and Lumsden, 2004). In the A/P axis, there was no difference in *Shh* expression detectable between wild type and mutant embryos (Fig. 14I, J, n=6). *Wnt1* is expressed in the RP of the midbrain and caudal diencephalon and in two ventral domains flanking the FP within the cephalic flexure (Parr et al., 1993; Panhuysen et al., 2004). The expression of *Wnt1* was unaltered in *Fgf15*$^{-/-}$ embryos (Fig. 14K, L, n=5).

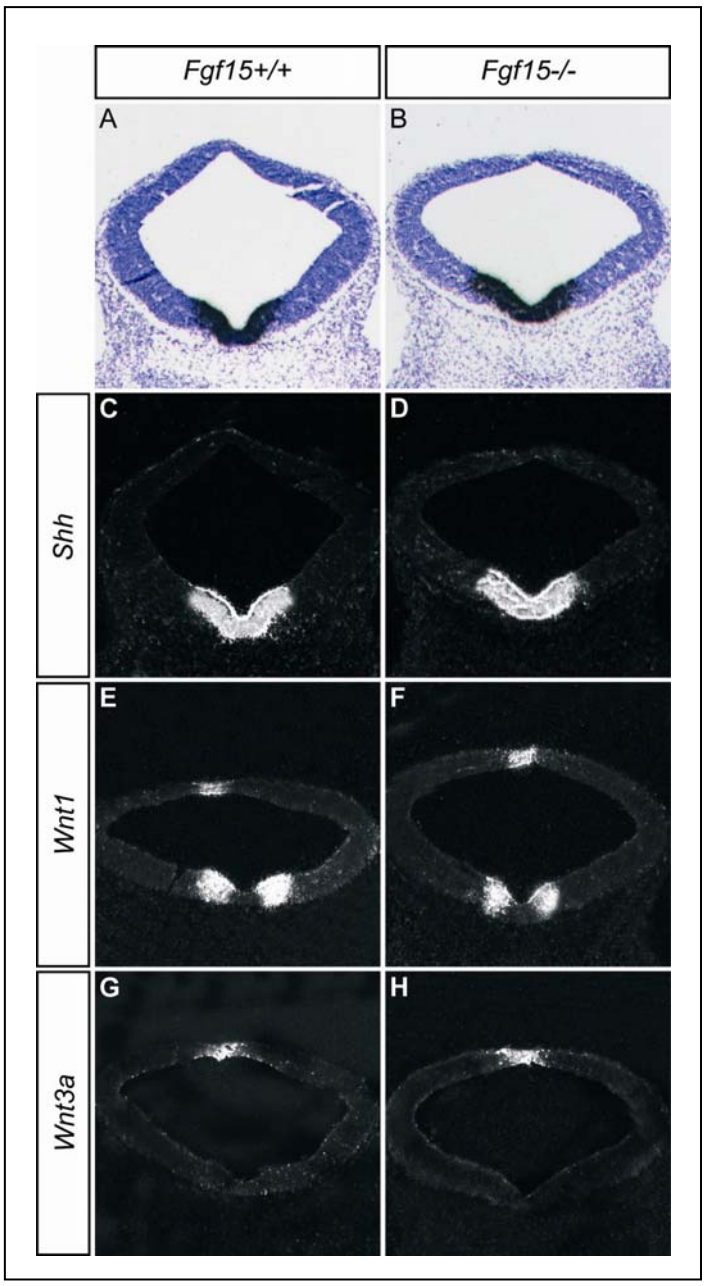

Figure 15 D/V patterning in the anterior neural tube appeared not to be affected in *Fgf15*$^{-/-}$ embryos at E11.5, as assessed by the expression of *Shh*, *Wnt1* and *Wnt3a*. (A-H) Coronal midbrain sections of wild type (A, C, E, G) and mutant embryos (B, D, F, H). (A, B) Brightfield images of C, D. (C-H) Darkfield images of corresponding sections. Expression of *Shh* (C, D), *Wnt1* (E, F), and *Wnt3a* (G, H) was not changed in the anterior neural tube of *Fgf15*$^{-/-}$ embryos.

To test whether D/V patterning was affected in *Fgf15*$^{-/-}$ embryos, the expression patterns of *Shh*, *Wnt1* and *Wnt3a*, which is expressed in the RP along almost the entire length of the neural tube (Parr et al., 1993), were analyzed on coronal/oblique sections of E11.5 wild type and mutant embryos (Fig 15). None of these genes showed an altered expression pattern (n=6, 8 and 6, respectively) in *Fgf15*$^{-/-}$ embryos (Fig. 15D, F, H) compared to wild type littermates (Fig. 15C, E, G). Taken together, the expression analysis of the above mentioned genes did not provide any evidence for a patterning activity of Fgf15 in the anterior neural tube.

3.1.4 Proliferation was increased in 10% of *Fgf15*$^{-/-}$ embryos at E11.5

The infolding particularly of dorsal neural tissue in 10% of E12.5 and E13.5 mutant embryos raised the possibility that in these embryos excess neural tissue may be generated by increased proliferation. As the cranial cavity would restrict exuberant dilatation of the neuroepithelium, this extra neural tissue would subsequently fold up and invaginate into the lumen of the neural tube. To examine whether increased proliferation might cause the infolding of neural tube tissue in *Fgf15*$^{-/-}$ embryos, the abundance and distribution of proliferating cells in the neuroepithelium of wild type and mutant littermates at E11.5 was analyzed.

Phosphorylated histone H3 is exclusively expressed in the nucleus of proliferating cells during the M-phase of the cell cycle (Hans and Dimitrov, 2001). In wild type E11.5 embryos, a subset of cells in the ventricular zone (VZ) of the neuroepithelium was labeled by an antibody against phosphorylated histone H3 (Fig. 16A). In *Fgf15*$^{-/-}$ littermates, phospho-histone H3-expressing cells were also localized to the VZ, but the number of labeled cells appeared to be slightly increased (Fig. 16B, C, n=6). To test this quantitatively, labeled cells were counted in relation to the area of the neuroepithelium of the corresponding section, because in general, *Fgf15*$^{-/-}$ embryos at E11.5 were smaller in size than wild type littermates (see e.g. Fig. 14), which was reflected by a reduced size of the neuroepithelial area (table 5 in appendix 7.4). The number of labeled cells per 1000µm^2 was increased from 0.77±0.08 in wild type to 0.87±0.06 in mutant embryos in the forebrain, from 0.60±0.04 to 0.73±0.08 and from 0.58±0.02 to 0.70±0.12 in the mid- and hindbrain, respectively (n=6 wt, 6 mut; table 3 and Fig. 16D; mean±standard deviation). Given the strong variation between single embryos and the resulting high standard deviations, these results were not statistically significant ($p > 0.1$, student's t-test). This finding indicates that the number and distribution of mitotic cells in the neuroepithelium of E11.5 embryos is not strongly affected by the loss of *Fgf15*.

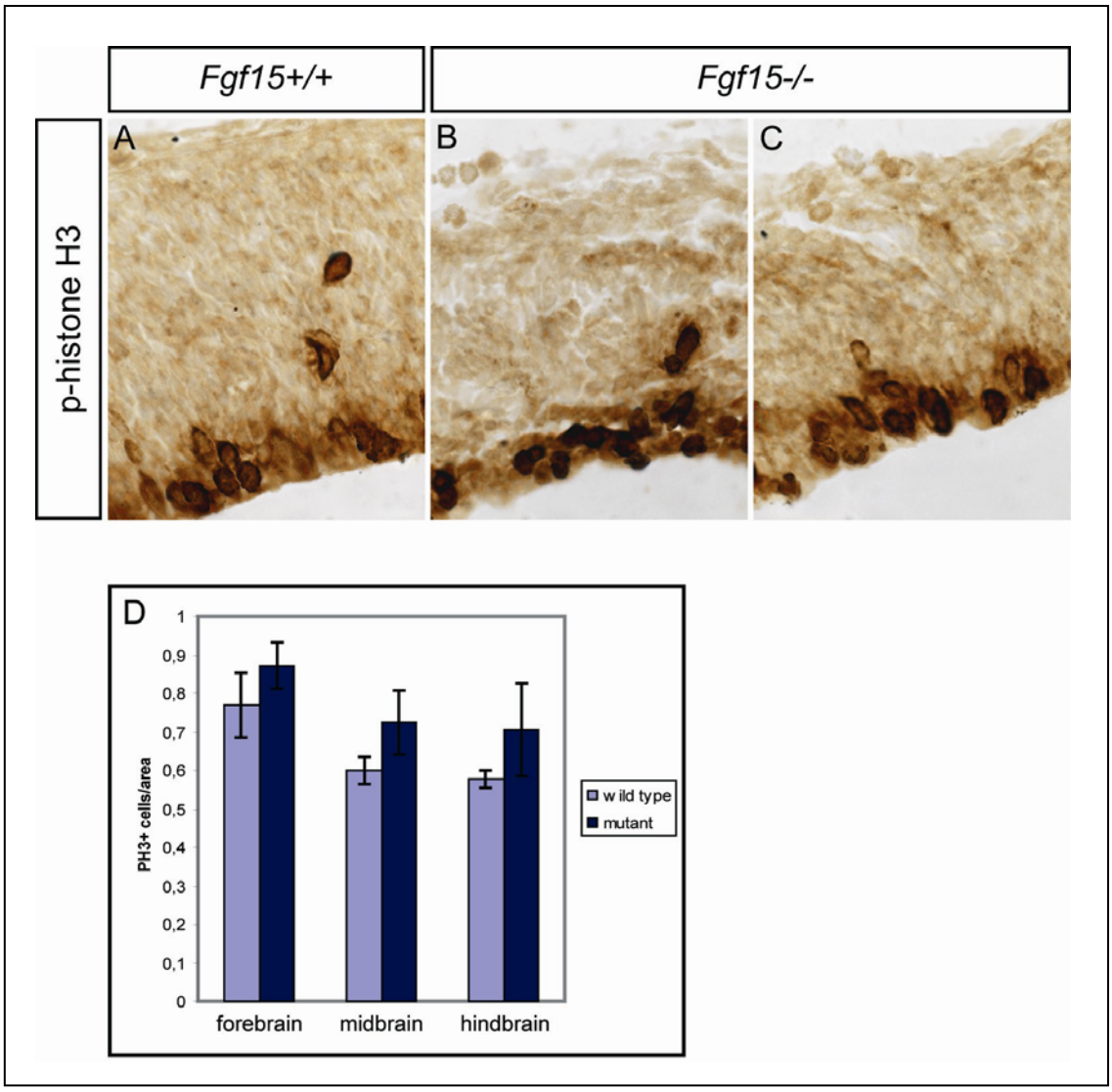

Figure 16 Mitotic cells were not significantly increased in *Fgf15*$^{-/-}$ embryos at E11.5. (A-C) Immunostaining for phospho-histone H3 (PH3) in the neuroepithelium of wildtype (A) and mutant littermates (B, C). Cells expressing nuclear phospho-histone 3 were mostly confined to the VZ in wildtype and mutant embryos. The number of labeled cells in mutant embryos appeared to be slightly increased compared to wild type littermates. (D) Counting of phospho-histone 3-labeled cells per 1000µm^2 of neuroepithelial area revealed that the differences between wildtype and mutant embryos were not significant (n = 6 wt, 6 mut; $p > 0.1$, students t-test).

To further analyze alterations of cell proliferation in *Fgf15* mutant embryos, labeling experiments with the thymidine analog BrdU were performed. Two different labeling paradigms were employed to label cells in the S-phase of the cell cycle. Pregnant mice of heterozygote matings were either given a single intraperitoneal BrdU injection 10min before dissection of the embryos, or three injections every 2h over a period of 6h before dissection of the embryos at E11.5. In the first paradigm, only those cells undergoing DNA replication in

the S-phase during the 10min labeling period before dissection incorporated BrdU. As expected, cells in the S-phase undergoing nucleokinesis were confined to the SVZ, and BrdU labeling was only detected in this region. In the second paradigm, all cells which underwent DNA synthesis during the 6h of cumulative labeling before dissection incorporated BrdU into the DNA. BrdU positive cells were distributed throughout the VZ and SVZ of the neuroepithelium, sparing only the MZ at the apical side, which contained cells that had exited the cell cycle before BrdU administration. No obvious differences of BrdU distribution in the neuroepithelium between wild type and mutant littermates could be detected after a single BrdU injection and after cumulative BrdU labeling, respectively (Fig. 17A-C, n=6 and D-F, n=8).

The expression of Ki67, a basic nuclear protein expressed in proliferating cells throughout the entire cell cycle (Scholzen and Gerdes, 2000), was used to further assess aberrant proliferation in *Fgf15*$^{-/-}$ embryos. In E11.5 wild type embryos, Ki67 expression was detected in the VZ of the neuroepithelium (Fig. 17G). The same pattern of expression was observed in the majority of mutant embryos (Fig. 17H, n=9/10), with the exception of one out of 10 embryos which showed an aberrant distribution of Ki67 positive cells in the neuroepithelium. In this embryo, the number of labeled cells appeared to be increased compared to wild type littermates and these cells were no longer confined to the VZ but were dispersed throughout the entire neuroepithelium (Fig. 17I, n=1/10).

Taken together, these findings do not indicate an obvious increase in the number of proliferating cells in the neural tube of *Fgf15*$^{-/-}$ embryos. However, the occurrence of 1 out of 10 mutant embryos (approximately 10% of *Fgf15*$^{-/-}$ embryos) showing aberrant and increased Ki67 immunoreactivity within the neuroepithelium strongly correlates with the proportion of mutant embryos displaying an evident morphological phenotype at E12.5 and E13.5. This correlation raises the possibility that in 10% of *Fgf15*$^{-/-}$ embryos, an increase and aberrant distribution of proliferating cells at E11.5 may lead to the generation and subsequent infolding of excess neural tissue one to two days later in development. Whether embryos with increased Ki67 staining at E11.5 would indeed develop excess neural tissue and display an infolding of the anterior neural tube at E12.5 or E13.5 could not be determined in the conventional knockout mouse line.

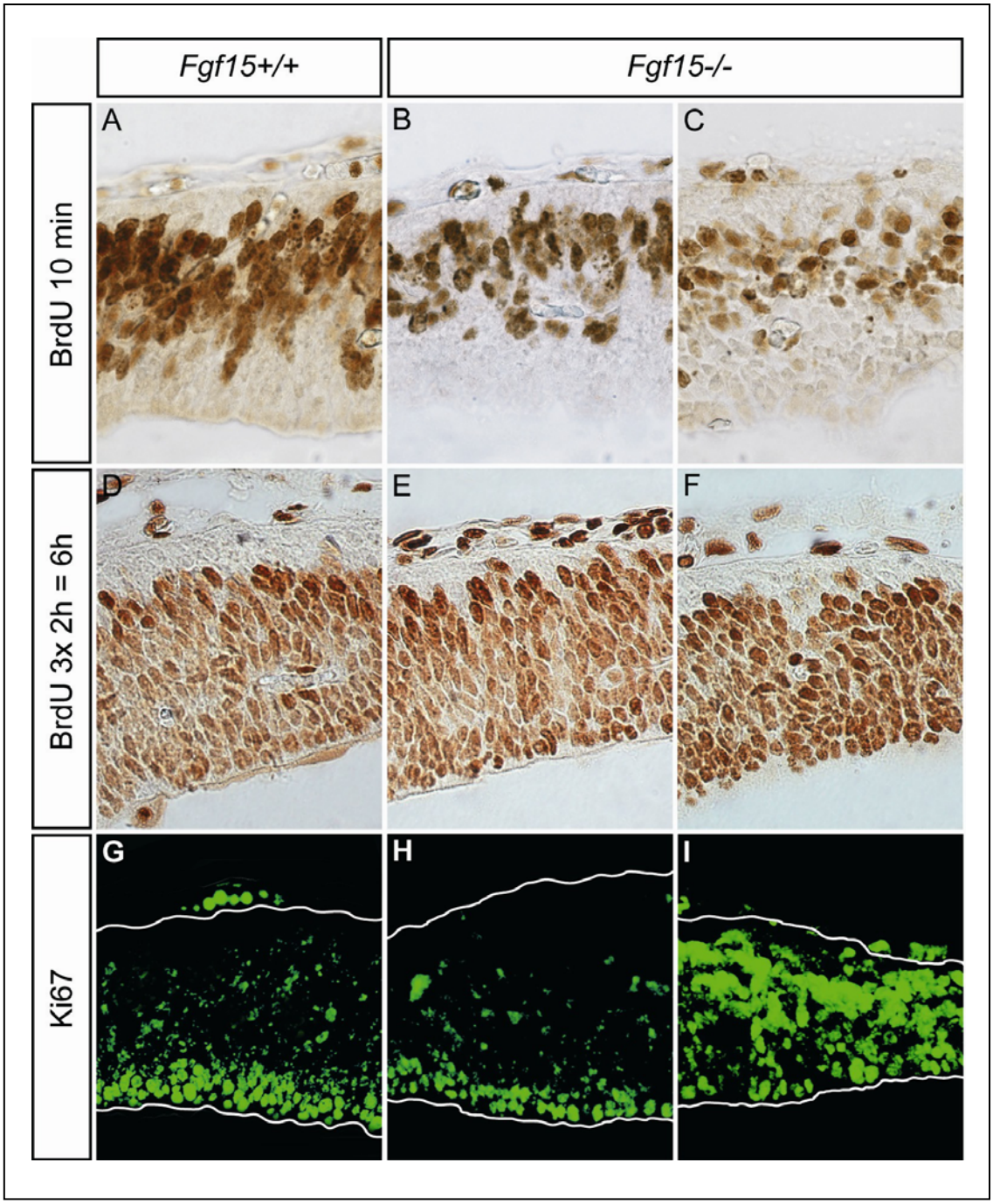

Figure 17 Neuroepithelial proliferation appeared to be increased in 10% of *Fgf15*$^{-/-}$ embryos at E11.5, as assessed by the expression of Ki67. (A-I) Coronal sections from dorsal neuroepithelium of the anterior neural tube of wild type (A, D, G) and mutant embryos (B, C, E, F, H, I). Neuroepithelium in (G-I) is outlined in white. (A-C) A single BrdU injection 10min before dissection resulted in a similar pattern of labeled cells in the SVZ of wildtype (A) and mutant embryos (B, C). (D-F) Cumulative BrdU labeling with 3 injections every 2h over 6h before dissection labeled cells in the VZ and SVZ of wild type (D) and mutant embryos (E, F) in a similar pattern. (G, H) Immunostaining for Ki67 labeled mostly cells in the VZ of wild type and 90% of *Fgf15*$^{-/-}$ embryos. (I) In 10% of *Fgf15*$^{-/-}$ embryos, Ki67 staining appeared to be increased and was ectopically expanded into the SVZ and MZ.

3.1.5 Cell cycle exit was affected in *Fgf15* mutant embryos

Aberrant proliferation results from defects in the control of the cell cycle. One possible mechanism that leads to an increase in proliferating cells over time is a failure of progenitor cells to exit the cell cycle correctly. To examine whether cell cycle withdrawal was affected in *Fgf15*$^{-/-}$ embryos, pregnant mice of timed heterozygous matings were injected with BrdU at E10.5 (t_0), embryos were dissected at E11.5 (t_{24}) and double immunodetection of BrdU and Ki67 was performed. At t_0, all cells in the cell cycle expressed Ki67, while only cells in the S-phase of the cell cycle undergoing DNA synthesis incorporated BrdU. Cells which incorporated BrdU at t_0 and had exited the cell cycle at t_{24}, i.e. entered G_0 phase, did not express Ki67 anymore and were thus BrdU positive but Ki67 negative. Cells which incorporated BrdU at t_0 and remained in the cell cycle at t_{24} still expressed Ki67 and were therefore BrdU$^+$/Ki67$^+$ double positive. Cells that were not in the S-phase of the cell cycle at t_0 but had entered the cell cycle by t_{24} were BrdU negative and Ki67 positive (Fig. 18A). In addition to alterations in the number of cells remaining in the cell cycle, it was also examined whether such cells appeared at ectopic locations in the neuroepithelium of *Fgf15*$^{-/-}$ embryos. Since proliferating cells are confined to the VZ in the wild type and migrate out into the MZ only after cell cycle exit, an ectopic localization of BrdU$^+$/Ki67$^+$ double positive cells in the SVZ and MZ would further argue for a perturbed cell cycle exit in *Fgf15*$^{-/-}$ embryos (Fig. 18A). In *Fgf15* mutant embryos, the number of BrdU$^+$/Ki67$^+$ double positive cells in the anterior neural tube was increased compared to wild type littermates (Fig 18B, n=5/5). Furthermore, these cells were no longer confined to the VZ of the neuroepithelium but were also located in the SVZ and MZ. 20% of *Fgf15*$^{-/-}$ embryos showed a more pronounced phenotype, with a marked increase in the number of Ki67 positive cells throughout the neuroepithelium (similar to the 10% of mutant embryos displaying aberrant Ki67 staining described in 3.1.4) and a strong increase in the number of double labeled cells (Fig. 18B, right panel). The ratio of 20% of mutant embryos displaying this increased Ki67 expression and pronounced decrease in cell cycle exit is twice as high as the percentage of mutant embryos showing increased Ki67 expression reported in 3.1.4, but this discrepancy can probably be attributed to the smaller sample size in the latter experiment. Cell countings revealed that the number of BrdU positive cells (i.e. cells incorporating BrdU in the S-phase at t_0) was comparable between wildtype and mutant embryos (107±1.5 (wt) and 103±1.7 (mut), n=5 wt, 5 mut). The number of Ki67 positive cells (including double labeled cells) was slightly but significantly increased in mutants (31.4±0.7 (wt) and 35.4±0.8 (mut), $p<0.005$, Fig. 18C). To

determine the number of cells which remained in the cell cycle, the ratio T_C of $BrdU^+/Ki67^+$ double positive cells per BrdU positive cells was calculated, i.e. T_C was defined as

$$T_C = n(\text{cells in the cell cycle at } t_0 \textit{ and } t_{24}) / n(\text{cells in the cell cycle at } t_0).$$

The value for T_C was increased by 60% in *Fgf15*$^{-/-}$ embryos compared to wild type littermates and this difference was highly significant (15.1±0.4 (wt) and 24.3±0.6 (mut), $p<0.001$, Fig.18C). In summary, the finding of an increased number of cells which remained in the cell cycle over a period of 24 hours, together with the ectopic location of these cells in the SVZ and MZ of the neuroepithelium, indicate that cell cycle exit was perturbed in *Fgf15*$^{-/-}$ embryos. It should be noted that while an increase in the total number of proliferating cells was obvious in only 10% of mutant embryos, a failure of cell cycle withdrawal was observed in all analyzed *Fgf15*$^{-/-}$ embryos to varying degrees.

During neurogenesis, proliferating progenitor cells exit the cell cycle and start to differentiate into neurons. As discussed in the introduction, the transition from proliferation to differentiation and the control of cell cycle exit are tightly regulated by a complex network of extracellular and intracellular factors (Edlund and Jessell, 1999; Galderisi et al., 2003; Ohnuma and Harris, 2003). The finding of a failure to exit the cell cycle of neuroepithelial cells in *Fgf15*$^{-/-}$ embryos suggested a possible involvement of Fgf15 in the regulation of cell cycle withdrawal and neurogenesis. To examine whether neurogenesis was affected by the loss of Fgf15, we analyzed the expression of markers for neuroepithelial precursor cells and differentiating neurons, respectively.

Nestin is an intermediate filament which has been shown to be expressed in the radial processes of undifferentiated CNS precursor cells (Lendahl et al., 1990; Hartfuss et al., 2001). Immunohistochemistry for Nestin revealed a stronger staining in the neuroepithelium of mutant embryos than of wild type littermates at E11.5 (Fig. 19A, B, n=9/10). At E12.5, Nestin expression in mutant embryos was also substantially stronger than in wild type littermates, although this result should be taken with caution, given the already evident disintegration of neural tissue in the analyzed embryos (Fig. 19C, D, n=2). Notably, however, the increase in Nestin expression in mutant embryos at E12.5 was strongest in domains corresponding to *Fgf15* expressing regions in wild type embryos (Fig. 19E, F), a finding that strongly argues for a CNS-specific function of Fgf15 in this context.

The expression of Doublecortin (Dcx) and class III-β-tubulin (TuJ1) were examined to determine alterations in neuronal differentiation, as both proteins have been shown to be

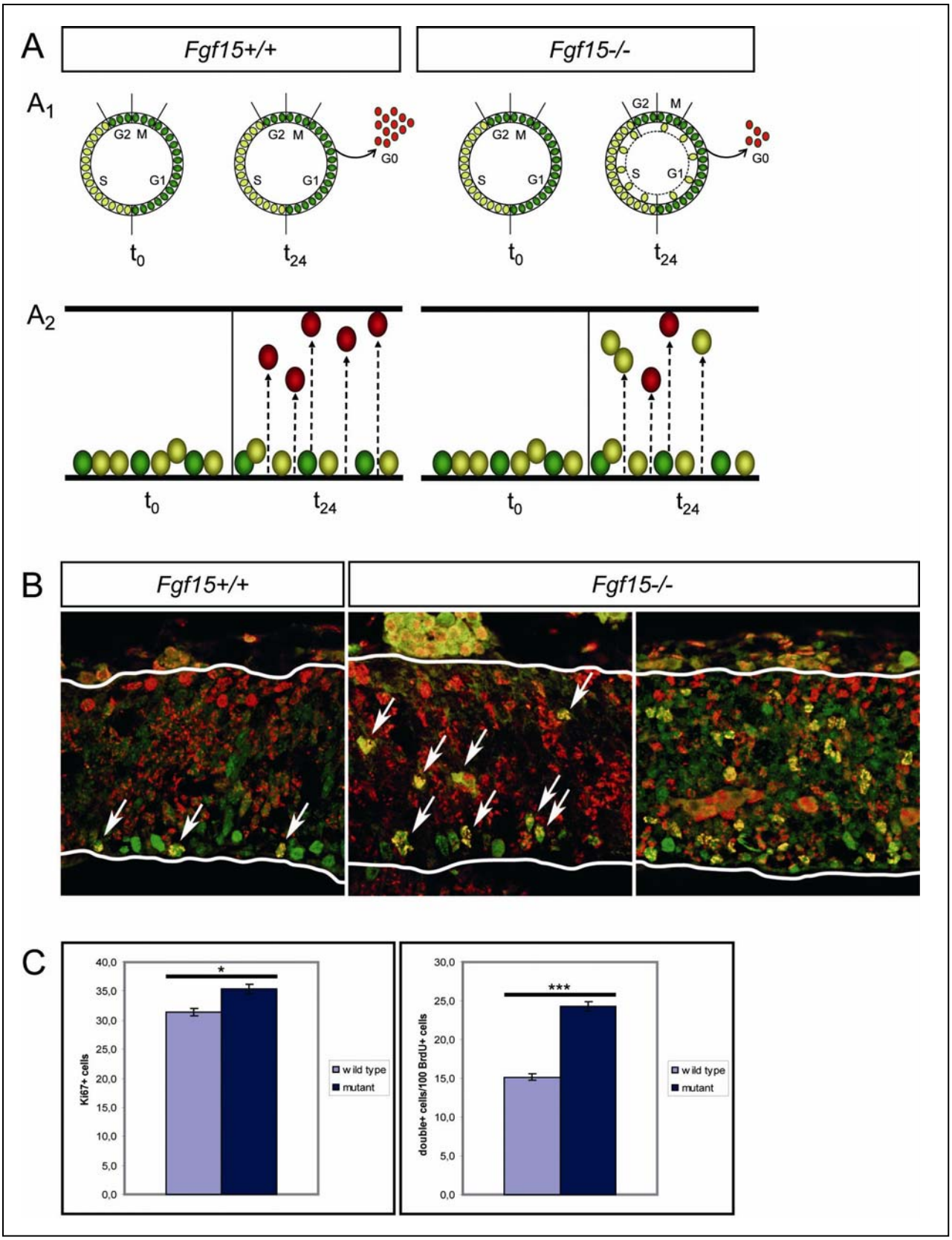
A
Fgf15+/+
Fgf15-/-
A1
G2 M
S
G1
G0
t0
t24
A2
B
Fgf15+/+
Fgf15-/-
C
Ki67+ cells
40,0
35,0
30,0
25,0
20,0
15,0
10,0
5,0
0,0
*
wild type
mutant
double+ cells/100 BrdU+ cells
***

Figure 18

Figure 18 Cell cycle exit was defective in *Fgf15*$^{-/-}$ embryos at E11.5. (A) Depiction of the experimental concept of the cell cycle exit assay. (A_1) Injection of a pregnant mouse at t_0 labels cells in S-phase with BrdU. At t_0, all BrdU$^+$ cells express Ki67 (yellow ovals). Cells in other phases of the cell cycle do not incorporate BrdU and are only Ki67$^+$ (green ovals). 24 hours later (t_{24}), embryos are dissected and immunostained for BrdU and Ki67. A fraction of cells that had incorporated BrdU at t_0 stay in the cell cycle (BrdU$^+$/Ki67$^+$; yellow ovals), the remaining BrdU$^+$ cells exit the cell cycle and enter G_0 (BrdU$^+$/Ki67$^-$; red ovals). In case of a failure to exit the cell cycle in *Fgf15*$^{-/-}$ embryos, the fraction of cells staying in the cell cycle (yellow ovals) would be increased, while the number of cells entering G_0 (red ovals) would be decreased. (A_2) As neuroepithelial cells exit the cell cycle and become postmitotic, they migrate out of the VZ into the SVZ and MZ. Therefore, at t_{24} only BrdU$^+$/Ki67$^-$ cells (red ovals) are located outside the VZ in the wildtype. Ectopic localization of BrdU$^+$/Ki67$^+$ cells (yellow ovals) outside the VZ would therefore further argue for a cell cycle exit defect in *Fgf15*$^{-/-}$ embryos. (B) Fluorescent immunostaining for BrdU (red) and Ki67 (green) on coronal sections from the anterior neuroepithelium of wild type and mutant embryos. The neuroepithelium is outlined in white, ventricular surface at the bottom. In wild type embryos at t_{24}, BrdU$^+$/Ki67$^+$ cells (yellow) were located in the VZ of the neuroepithelium (white arrows), as were Ki67$^+$ cells (green), while BrdU$^+$ cells (red) were located mostly in the MZ (left panel). The number of BrdU$^+$/Ki67$^+$ cells (yellow) was increased in *Fgf15*$^{-/-}$ embryos, and a fraction of these cells was ectopically located in the SVZ and MZ (middle panel, white arrows). In 20% of *Fgf15*$^{-/-}$ embryos, the number of BrdU$^+$/Ki67$^+$ cells (yellow) was strongly increased, as was the number of Ki67$^+$ cells (green). Both types of immunopositive cells were dispersed throughout the neuroepithelium (right panel). (C) The amount of Ki67$^+$ cells was increased by 13% in mutant embryos (left panel). The number of double labeled cells/100 BrdU$^+$ cells was significantly increased by 61% in mutant embryos (mean±standard error of mean; * $p < 0.005$; *** $p < 0.001$; student's t-test).

expressed in early postmitotic neurons (des Portes et al., 1998; Gleeson et al., 1998; Gleeson et a., 1999; Menezes and Luskin, 1994; Lee et al., 1990). E11.5 wild type embryos showed a similar expression of Dcx and TuJ1, both proteins being exclusively expressed in cells occupying the MZ of the neuroepithelium (Fig. 20A, C). In mutant littermates, Dcx and TuJ1 expression were also confined to cells within the MZ, but the number of labeled cells appeared to be decreased compared to wild type littermates (Fig. 20B, D, n=5/8 and 8/12, respectively). At the pial surface of the neuroepithelium of wild type embryos, at least 3 layers of Dcx- and TuJ1-expressing cells were detected, whereas in mutant embryos only one Dcx- and TuJ1-positive cell layer was detected.

The increased expression of the neural precursor marker Nestin, concomitant with the decreased expression of the early postmitotic neuronal markers Dcx and TuJ1, suggests that in the absence of Fgf15, neural progenitor cells fail to exit the cell cycle and remain in a proliferative state, thus generating less postmitotic neurons and increasing the number of proliferating progenitor cells. Since neurogenesis is believed to begin between E9.5 and E10.5, the interval to which the present analysis was restricted (E11.5) may have been too early for a more pronounced phenotype. Furthermore, it remains unclear whether Fgf15 is

involved specifically in neurogenesis or whether the generation of astrocytes and/or oligodendrocytes, which take place later in development, would be similarly affected by the loss of Fgf15.

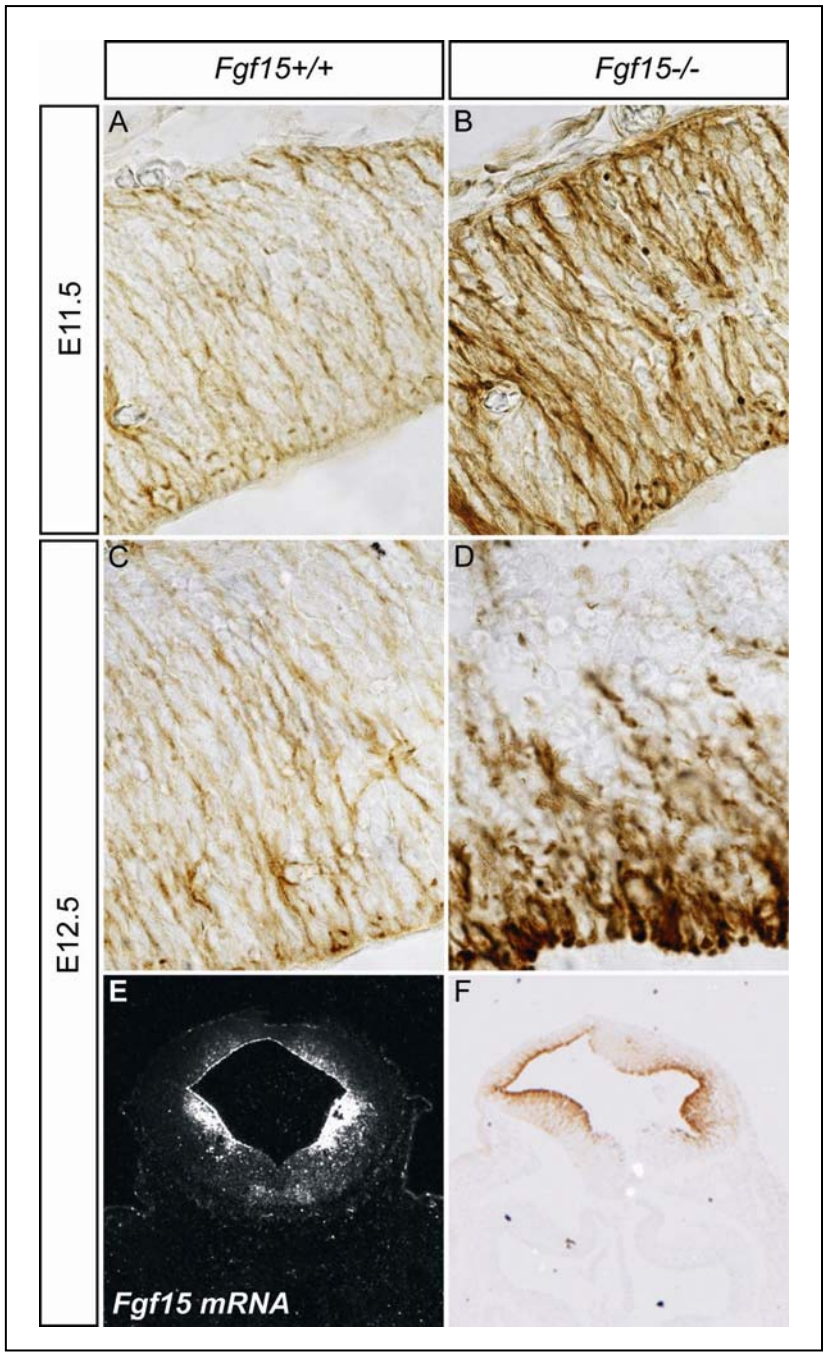

Figure 19 Nestin expression was increased in the neuroepithelium of *Fgf15* mutant embryos at E11.5 and E12.5. (A-F) Coronal sections from the neural tube of wild type (A, C, E) and mutant embryos (B, D, F). (E, F) Overview images at lower magnification than A-D. (A, B) At E11.5, Nestin expression was stronger in *Fgf15*$^{-/-}$ embryos (B) than in wild type littermates (A). (C-F) In E12.5 *Fgf15*$^{-/-}$ embryos displaying morphological defects (D), Nestin expression was also stronger than in wild type littermates (C), although this finding remains questionable due to the apparent disintegration of tissue in (D). Notably, however, the increased Nestin expression in *Fgf15*$^{-/-}$ embryos was strongest in domains that normally express high levels of *Fgf15* in the wild type (compare E and F).

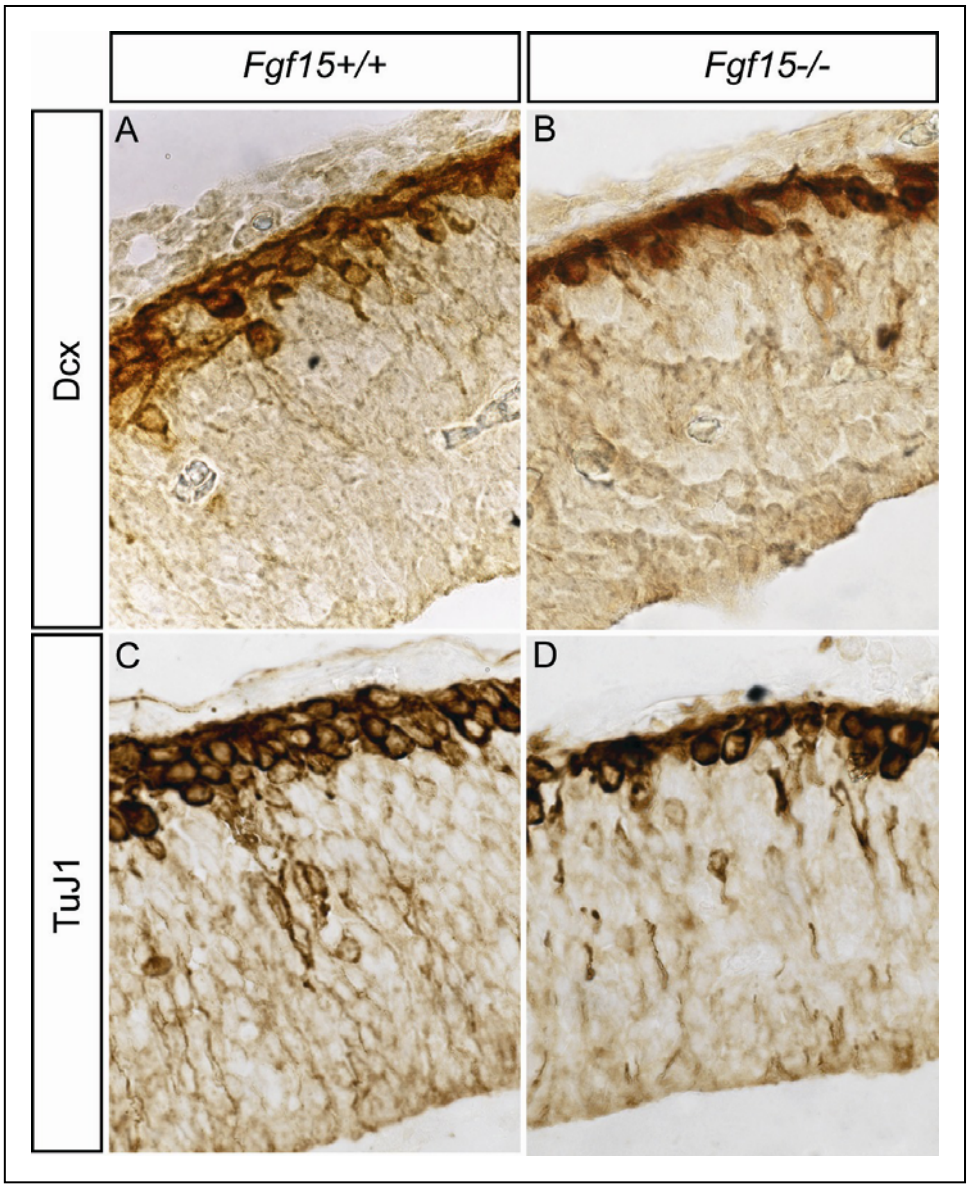

Figure 20 Expression of Dcx and TuJ1 appeared to be reduced in the neuroepithelium of *Fgf15*$^{-/-}$ embryos at E11.5. (A-D) Coronal sections from the neural tube of wild type (A, C) and mutant embryos (B, D). (A, B) Dcx expression was confined to the MZ in wild type and *Fgf15*$^{-/-}$ embryos. In wild type embryos, at least 3 cell layers of Dcx labeled cells were discernible (A), whereas in mutant embryos only 1 layer of labeled cells was apparent (B). (C, D) Staining for TuJ1 resulted in a similar pattern of labeled cells, with at least 3 layers of labeled cells in the MZ of wild type embryos (C), and only 1 layer of TuJ1-positive cells in the MZ of mutant littermates (D).

3.1.6 Perturbed cell cycle exit in *Fgf15*$^{-/-}$ embryos was accompanied by a misexpression of neurogenic and proneural genes

If the hypothesis of perturbed neurogenesis was true, an up-regulation of neurogenic genes and a down-regulation of proneural genes in the neuroepithelium of *Fgf15*$^{-/-}$ embryos would be expected. Therefore, the expression of neurogenic and proneural genes was assessed in wild type and mutant embryos. First, the expression of the neurogenic genes *Hes1*, *Hes3* and *Hes5* was analyzed in *Fgf15*$^{-/-}$ embryos at E11.5. The expression of *Hes1* appeared to be unaffected by the loss of Fgf15 (data not shown). The expression of *Hes3* in the midline of the dorsal isthmic organizer territory appeared to be increased and slightly broadened in its A/P extent in *Fgf15*$^{-/-}$ embryos compared to wild type littermates (Fig. 21A-D, n=4/5). Since the expression of *Fgf8* at the MHB appeared to be unaffected in *Fgf15*$^{-/-}$ embryos (Fig. 14G, H), this broadened expression of *Hes3* was most likely not due to an expansion of the isthmic organizer territory. This finding suggests that the pool of undifferentiated, *Hes3* expressing progenitor cells at the MHB (Hirata et al., 2001) was moderately enlarged in *Fgf15*$^{-/-}$ embryos. In case of *Hes5* expression, marked differences were detected in *Fgf15*$^{-/-}$ embryos compared to wild type littermates. In wild type embryos, *Hes5* expression showed a distinct boundary in the neuroepithelium, with strong expression in the VZ and SVZ, and no expression in the MZ (Fig. 21E, F, I, J). In contrast, in *Fgf15* mutant embryos this boundary was not discernible and *Hes5* expression was ectopically expanded into the MZ of the neuroepithelium (Fig. 21G, H, K, L, n=4/5). Furthermore, *Fgf15*$^{-/-}$ embryos displayed an ectopic expression of *Hes5* in areas where *Hes5* was not expressed at all in the wild type neuroepithelium (Fig. 21E, G, n=4/5). These alterations in the expression pattern of *Hes5* suggest that in the absence of Fgf15 cells that migrate out of the VZ and SVZ to the MZ of the neuroepithelium fail to exit the cell cycle, thus remaining in a proliferative progenitor state, as indicated by sustained expression of *Hes5*. In addition, regions where most cells are already differentiating in the wild type and have down-regulated *Hes5* expression, still appear to contain a substantial amount of undifferentiated, *Hes5* expressing cells in the mutant.

Next, the expression of the proneural genes *Mash1*, *Ngn1*, *Ngn2* and *NeuroD* was analyzed in *Fgf15*$^{-/-}$ embryos at E11.5. Mash1, Ngn1 and Ngn2, which mediate cell specification towards a neuronal fate at the onset of neurogenesis, are mostly expressed in the VZ and SVZ of the neuroepithelium, where precursors begin differentiation, but not in the MZ, where differentiated neurons are situated. NeuroD is expressed later in neurogenesis, in cells that already started differentiation, and consequently, expression of NeuroD is found in

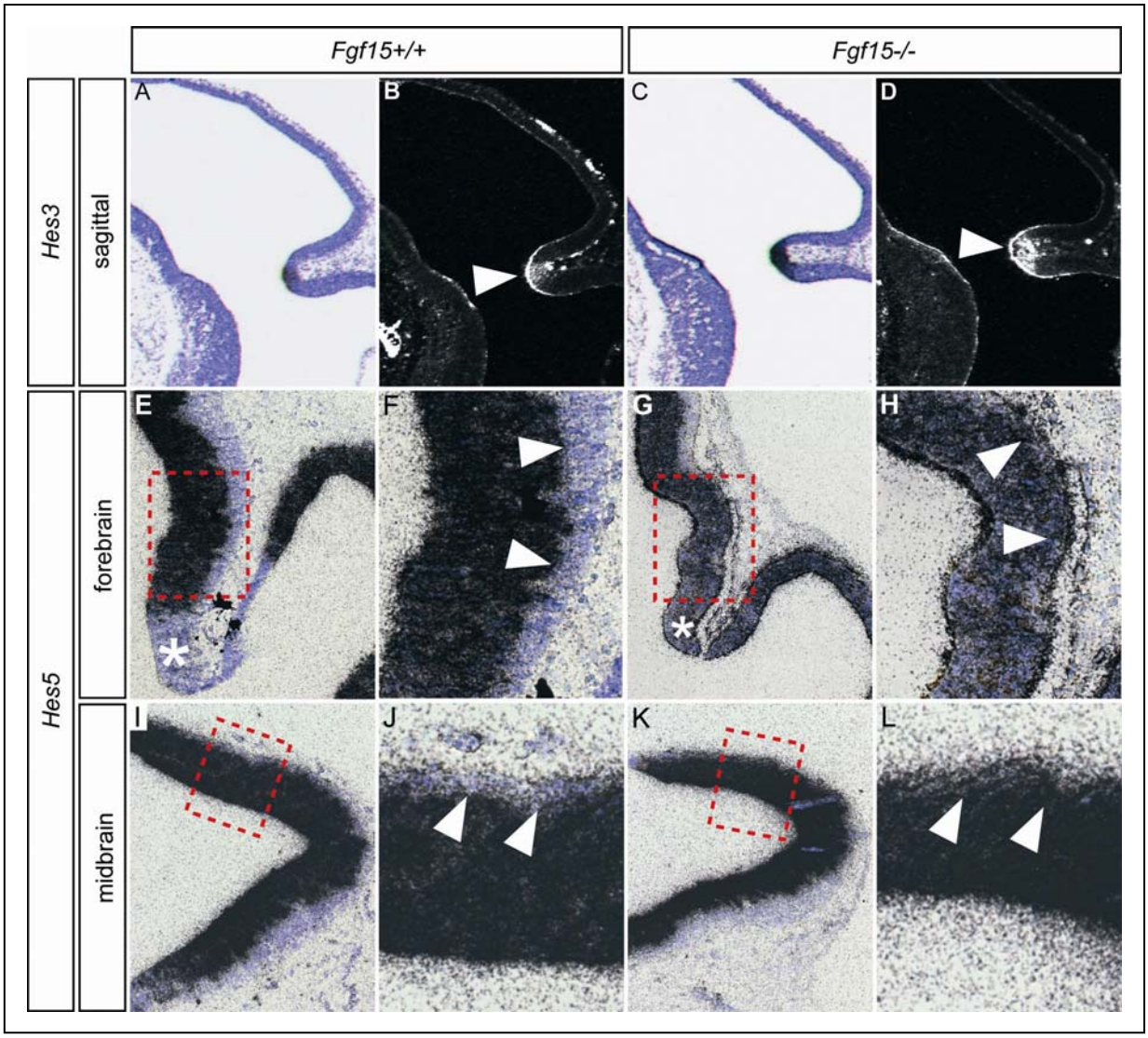

Figure 21 Increased and ectopic expression of *Hes3* and *Hes5* in the neuroepithelium of *Fgf15*$^{-/-}$ embryos at E11.5. (A-D) Sagittal sections showing the mid-/hindbrain region of wild type (A, B) and *Fgf15*$^{-/-}$ embryos (C, D), anterior is to the left. (A, C) Brightfield images of (B, D). (E-L) Coronal/oblique sections from the forebrain (E-H) and midbrain (I-L) of wild type (E, F, I, J) and *Fgf15*$^{-/-}$ embryos (G, H, K, L). (F, J and H, L) Higher magnifications of areas outlined by red dotted rectangles in (E, I and G, K). (A-D) Expression of *Hes3* was restricted to the dorsal isthmic organizer territory both in wild type and mutant embryos (arrowheads). In the absence of *Fgf15*, *Hes3* expression appeared to be increased and slightly broadened in its A/P extent (D). (E, F and I, J) In the neuroepithelium of wild type embryos, *Hes5* expression displayed a sharp boundary (arrowheads), with strong expression in the VZ and SVZ and no expression in the MZ. (G, H and K, L) In *Fgf15*$^{-/-}$ embryos, this boundary was not apparent, and *Hes5* expression was expanded into the MZ (arrowheads). Furthermore, *Hes5* was ectopically expressed in areas where it was not expressed at all in the wild type (asterisks in E and G).

the SVZ and MZ, not in the VZ. The expression of *Mash1*, *Ngn1*, and *Ngn2* was down-regulated in the neuroepithelium of mutant embryos compared to wild type littermates (Fig. 22, n=5/6). Interestingly, the strongest down-regulation was observed in the AP of the neural tube, an area where *Fgf15* is highly expressed in the wild type (compare with Fig. 6 and 7). In

the BP and FP, where *Fgf15* is not expressed, decrease of *Mash1* and *Ngn1* expression was less severe than in the AP, and *Ngn2* expression in this domain appeared to be not affected at all (Fig. 22, n=5/6). The reduction of *NeuroD* expression was even more pronounced than of early proneural genes (Fig. 22G, H, n=5/7). Its expression was almost completely lost in the AP of the neural tube, while only a small expression domain was detected ventrally. The decreased expression of early proneural genes in *Fgf15*$^{-/-}$ embryos is in line with the increased/ectopic expression of neurogenic genes in the mutant neuroepithelium and points to an inability of neural cells to initiate or correctly progress through the neuronal differentiation program, which consequently results in an even more severe down-regulation of the late proneural gene *NeuroD*.

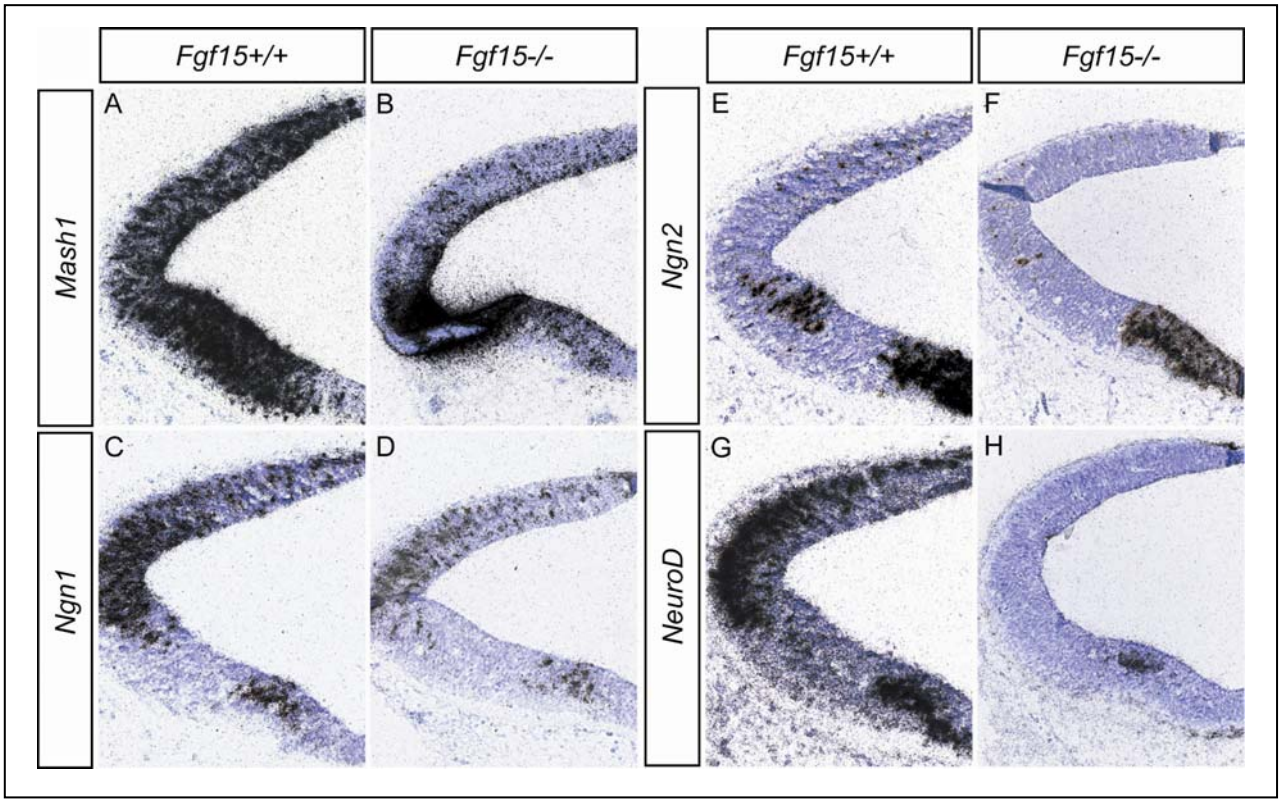

Figure 22 Expression of the proneural genes *Mash1*, *Ngn1*, *Ngn2* and *NeuroD* was down-regulated in the neuroepithelium of *Fgf15*$^{-/-}$ embryos at E11.5. (A-H) Coronal sections at midbrain level of wild type (A, C, E, G) and mutant embryos (B, D, F, H). Expression of *Mash1* (A, B), *Ngn1* (C, D), *Ngn2* (E, F) and *NeuroD* (G, H) was decreased in the neuroepithelium of *Fgf15*$^{-/-}$ embryos (B, D, F, H) compared to wild type littermates (A, C, E, G). This down-regulation was most pronounced in the AP of the neuroepithelium, a site of strong *Fgf15* expression in the wild type (compare with Fig. 6 and 7). The ventral expression domains of *Mash1*, *Ngn1* and *NeuroD* appeared less affected, and the ventral *Ngn2* expression domain was almost unaffected. Note that *NeuroD* expression was almost completely lost in the AP of mutant embryos, and only a very small expression domain was detected ventrally (G, H).

3.1.7 Expression of *Id* genes was increased in the neuroepithelium of *Fgf15*$^{-/-}$ embryos

The ectopic location of proliferating cells and the misexpression of neurogenic and proneural genes in the neuroepithelium of *Fgf15*$^{-/-}$ embryos suggests a role of Fgf15 in cell cycle exit and neurogenesis. To further test whether the failure of cell cycle exit in the absence of *Fgf15* compromised neuronal differentiation, the expression of *Id* genes was analyzed. *Id1* was weakly expressed in the VZ of the neuroepithelium of E11.5 wild type embryos (Fig. 23A, B), while *Id3* was expressed in the VZ and SVZ (Fig. 23D, E). In *Fgf15*$^{-/-}$ embryos, the expression of both *Id1* and *Id3* was increased (Fig. 23C, F, n=4/4). In addition, these two genes were ectopically expressed in the MZ of the neural tube. These findings, together with the previous results for the expression of neurogenic and proneural genes, indicate that in *Fgf15*$^{-/-}$ embryos a) more neuroepithelial cells remain in an undifferentiated, proliferating progenitor state, and that b) consequently the normal generation and segregation of postmitotic offspring in the MZ of the neuroepithelium was affected.

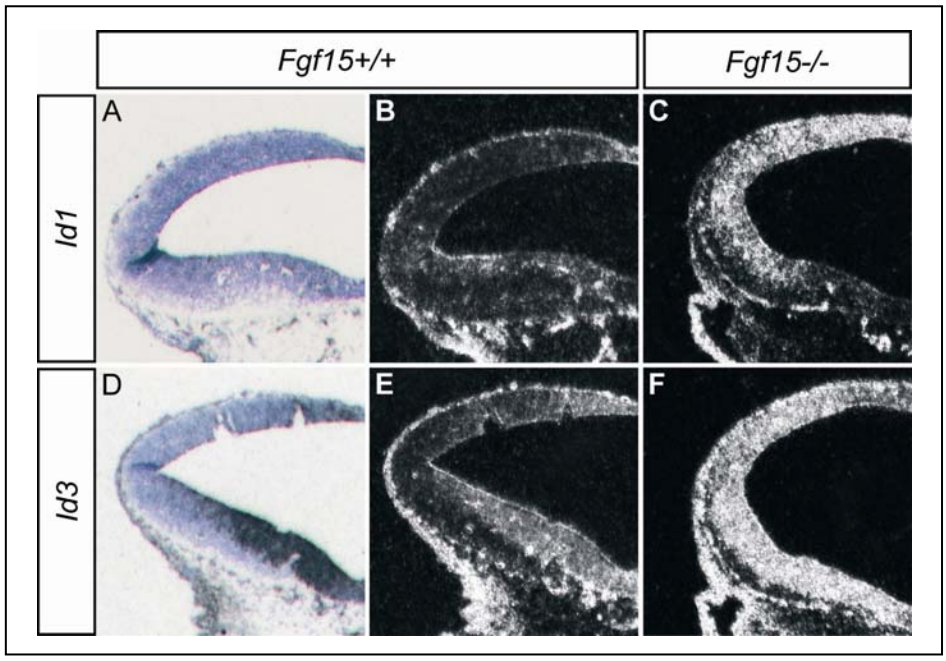

Figure 23 *Id1* and *Id3* expression was up-regulated and ectopically expanded in the neuroepithelium of *Fgf15*$^{-/-}$ embryos at E11.5. (A-F) Coronal sections of wild type (A, B, D, E) and mutant embryos (C, F). (A, D) Brightfield images of (B, E). (B, C, E, F) Darkfield images of corresponding sections. (A-C) The weak expression of *Id1* in the VZ of the neuroepithelium of wild type embryos (B) was increased and expanded into the SVZ and MZ in mutant embryos (C). Note that the domain of increased *Id1* expression corresponded to the expression domain of *Fgf15* in the wild type (compare C with Fig. 6J´and 7F). (D-F) *Id3* was expressed mostly in the VZ and SVZ of the neuroepithelium in wild type embryos (E). In mutant littermates, the expression was strongly increased in the VZ and SVZ and ectopically expanded into the MZ of the neuroepithelium (F).

3.1.8 p107 activity appeared to be unaffected by the loss of *Fgf15*

The previous results provide evidence that cell cycle exit and neurogenesis were perturbed in the absence of Fgf15 at E11.5. Since both processes are tightly linked together (see introduction), two possible roles of Fgf15 can be hypothesized: 1) Fgf15 may directly regulate cell cycle withdrawal of neural progenitors and 2) Fgf15 in addition may control the differentiation of neuronal precursors into neurons by an as yet unknown mechanism. A possible scenario for the first hypothesis could involve the regulation of one or several components of the cell cycle machinery through intracellular Fgf signaling induced by Fgf15. A recent study provides evidence that in differentiating chondrocytes, for example, Fgf signaling may directly regulate phosphorylation and thereby activation of the retinoblastoma protein p107 (Dailey et al., 2003). To test whether crucial components of the cell cycle exit machinery such as Rb proteins were affected by the loss of *Fgf15* and whether this effect might be mediated by the regulation of their phosphorylation state, Western blot experiments were performed to assess the level of expression and phosphorylation state of several cell cycle inhibitors. To this end, protein extracts were prepared from E11.5 wild type and *Fgf15*$^{-/-}$ embryo heads.

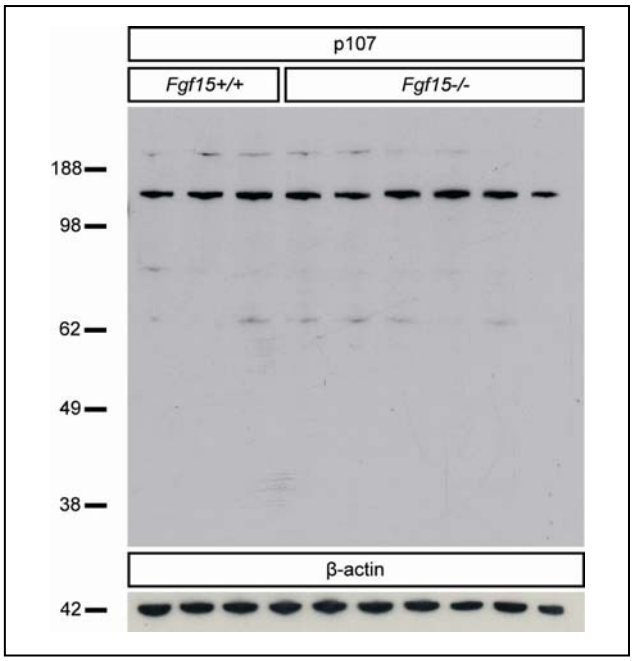

Figure 24 Differences in the phosphorylation level of p107 between wild type and *Fgf15*$^{-/-}$ embryos were not detectable by Western blot. Immunoblots of protein extracts from whole embryo heads of E11.5 wild type and mutant littermates were probed with antibodies against p107 and β-actin. Only a single band corresponding to the approximate molecular weight of p107 (107 kDa) was detected by an anti-p107 antibody both in wild type and *Fgf15*$^{-/-}$ protein extracts. β-actin detection served as loading control. Molecular weight in kDa is given to the left.

Only detection of p107 was successful in Western blot experiments. During the cell cycle, p107 is subjected to cyclic phosphorylation and dephosphorylation events, thereby changing from the inactive hyperphosphorylated form to the active hypophosphorylated form (see introduction). As the two forms differ in their molecular weight, they can be distinguished by Western blot analysis. As shown in Fig. 24, only a single band for p107 was detected at approximately the expected molecular weight (107 kDa), but it was not clear whether this band corresponded to the hyper- or hypophosphorylated form of p107. While this may indicate that the phosphorylation state of p107 and therefore its activity is unaffected by the loss of Fgf15, it is very likely that the applied experimental set up was not adequate to detect subtle differences in the phosphorylation state of p107. As neuroepithelial cells make up only a small fraction of the entire head tissue, and of those, only a subset are expected to show a difference in p107 phosphorylation, this difference might be diluted beyond detection level in the applied protein extracts.

Nevertheless, the evident and marked decrease in cells that exit the cell cycle correctly in the neuroepithelium of *Fgf15*$^{-/-}$ embryos strongly suggests that the cell cycle machinery underlying the control of cell cycle exit may be affected in these embryos. Therefore, a wider selection of cell cycle regulators beside p107 will have to be examined. In addition, *in vitro* experiments using neural primary cell cultures may provide a means to overcome the dilution effect addressed above and allow the detection of differences in the phosphorylation state of cell cycle inhibitors.

3.1.9 Generation of a conditional *Fgf15* mutant mouse line

The embryonic lethal phenotype of *Fgf15*$^{-/-}$ mice made an analysis of later developmental stages than E12.5 impossible. As neurogenesis starts at around E9.5-10.5 and proceeds until around E14.5, followed by the generation of astrocytes and oligodendrocytes (Zigmond et al., 1999), the defects observed at E11.5 in the mutant may become even more pronounced at later stages of development, and may affect not only neurogenesis but also astrocyte and/or oligodendrocyte development, as well as neurogenic processes in the adult brain. To address these issues, a conditional allele of *Fgf15* was cloned and introduced into a murine embryonic stem (ES) cell line. Crossing the corresponding mutant mouse line with different Cre-expressing mouse lines would allow for the time- and region-specific inactivation of *Fgf15* (Sternberg and Hamilton, 1981).

A targeting vector was designed for electroporation into mouse ES cells to generate genetically engineered ES cells via homologous recombination (HR). The PNTFlp vector was used as template (Fig. 25B). The vector contains a neomycin resistance gene and a thymidine kinase (TK) gene, both under the control of a PGK promoter. The TK gene is located directly upstream of the insertion site of the 5' homologous arm and will thus not be integrated into the genome by HR, which allows the negative selection of clones that underwent unspecific recombination or incomplete HR. The key element of the vector consists of a flipase (Flp) gene under the control of the promoter of the testis-specific angiotensin-converting enzyme (tACE). The selection cassette comprises the neomycin resistance gene and the flipase gene and is flanked by two frt sites. The tACE promoter is only active in male germ cells (Zhou et al., 1996). Following germ line transmission, the Flp will thus be activated and recombine the two frt sites of the vector, resulting in the deletion of the complete selection cassette (Dymecki, 1996, Fig. 25C, D). In addition, the vector contains a loxP site, which will not be affected by the Flp-mediated deletion.

The genomic regions used as homologous arms for HR were amplified by PCR, using a BAC clone from a commercially available BAC library (Clone RP23-332 B 13, ResGen, Invitrogen). The 5' homologous arm comprised 5406 bp, containing the three exons and two introns of the *Fgf15* gene, while the 3' homologous arm comprised 2969 bp of genomic sequence immediately downstream of exon 3 (Fig. 25A). In case of the 3' homologous arm, two *Xho*I sites were introduced with the PCR primers. The PCR fragments were subcloned into the pCRII TOPO vector (Invitrogen). A loxP site together with an additional *Xho*I restriction site was introduced into intron 2 in the 5' homologous arm 1214 bp upstream of exon 3. To this end, the pCRII vector containing the 5' arm was digested with *Mfe*I and the loxP site was ligated into the vector via *Mfe*I restriction sites. The direction of insertion of the loxP site was determined by DNA sequencing. The modified 5' arm was excised from the pCRII vector using *Fse*I and *Bam*HI, purified via gel extraction and ligated into the PNTFlp vector which had been digested with *Fse*I and *Bgl*II. The 3' arm was excised from the pCRII TOPO vector using the introduced *Xho*I sites, purified via gel extraction and ligated into the target vector, which had been linearized with *Sal*I. As this cloning step was bidirectional, the resulting clones were analyzed by restriction analysis. The final targeting vector was sequenced to rule out point mutations and to confirm the correct orientation of the introduced loxP site. Using this targeting vector, after HR and excision of the selection cassette the correctly targeted *Fgf15* locus will contain two loxP sites flanking 1.2kb of intron 2 as well as exon 3 (Fig. 25D). Crossing the corresponding mouse line with a Cre-expressing mouse strain

will therefore result in the deletion of 108 amino acids (aa) of the C-terminus of the Fgf15 protein, similar to the deletion in the conventional *Fgf15* mutant mouse line described in 3.2. In addition, the entire 3' UTR of the *Fgf15* mRNA will be deleted (Fig. 25 E).

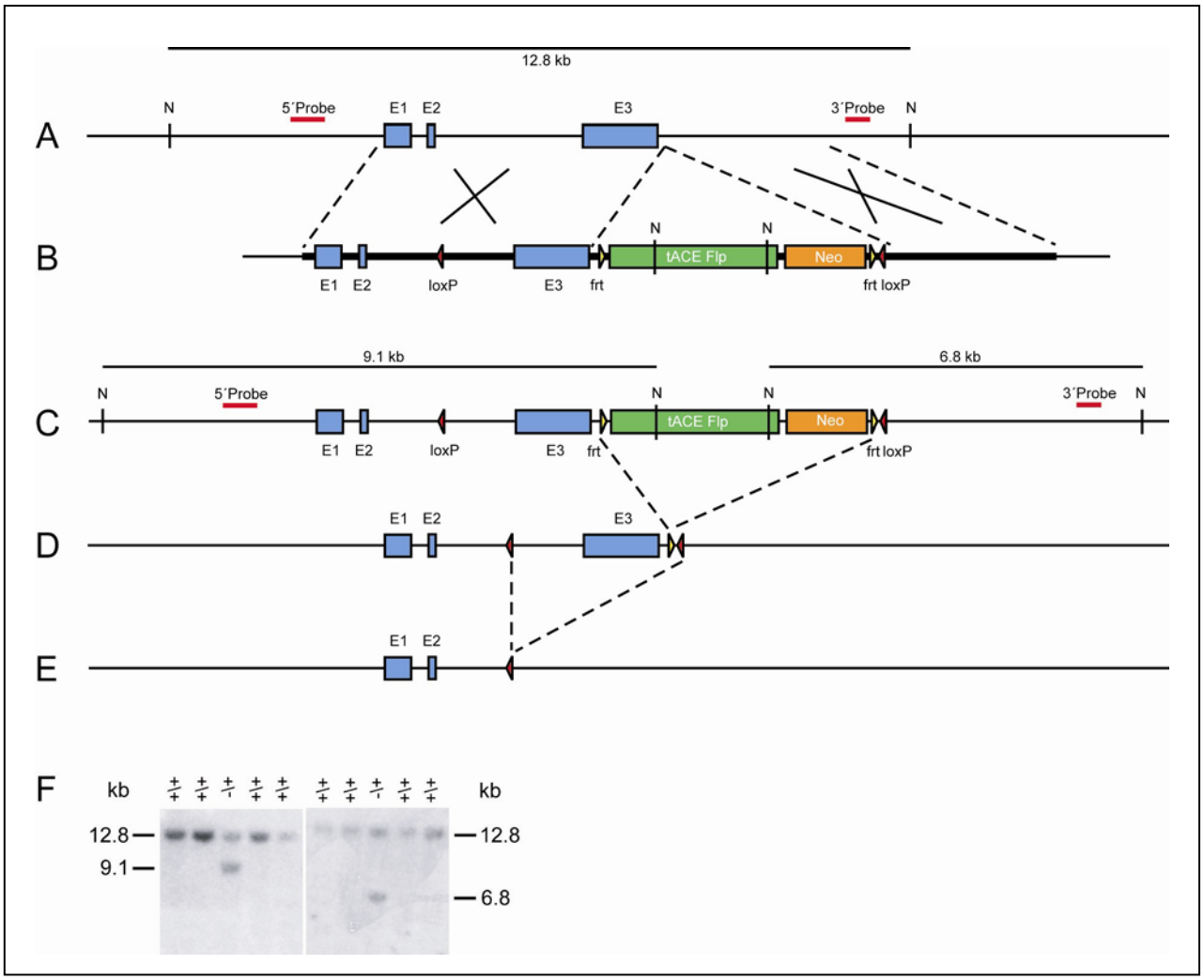

Figure 25 Targeting strategy for the generation of a conditional *Fgf15* deficient mouse line. (A) Genomic structure of the wildtype *Fgf15* locus. (B) Targeting vector with homologous regions indicated by broken lines. (C) Following HR, restriction digest with *Nsi*I resulted in a 12.8 kb wildtype fragment, and two mutant fragments of 9.1 kb (5' probe) and 6.8 kb (3' probe). (D) Removal of the Neo-Flp selection cassette during spermatogenesis in male chimeric animals by Flp-mediated recombination. (E) Cre-mediated recombination results in the inactivation of *Fgf15* due to excision of exon 3 (~50% of coding sequence). (F) Southern blot analysis of mouse ES cell clones after HR with the *Fgf15* conditional targeting vector. The 5' probe hybridized to the 12.8 kb wild type fragment and the 9.1 kb mutant fragment. The 3' probe hybridized to the 12.8 kb wild type fragment and the 6.8 kb mutant fragment. E: exon; N: *Nsi*I restriction site; tACE: testes-specific promotor of the angiotensin-converting enzyme; Flp: Flipase; Neo: neomycin resistance gene.

The targeting vector was linearized with *Apa*LI and electroporated into IDG3.2 ES cells. This cell line was derived from embryos of the F1 generation of mixed Sv129/C57Bl/6 matings. The cells were then subjected to a double selection both with G418 geneticin and gancyclovir. G418 geneticin was used to select for clones which exhibited neomycin resistance, i.e. which had incorporated the targeting vector into the genome. Gancyclovir was used to negatively select for clones that had undergone unspecific recombination or incomplete HR. The resulting clones were analyzed by Southern blot to identify correctly recombined clones. The isolated DNA of 768 clones was digested with *Nsi*I, which would result in a 12.8 kb wild type fragment and two mutant fragments of 9.1 kb and 6.8 kb, respectively. Probes hybridizing to sequences located outside the targeted region at the *Fgf15* locus were used for the Southern blot, with the 5' probe recognizing the 12.8 kb and 9.1 kb fragment, and the 3' probe recognizing the 12.8 kb and 6.8 kb fragment (Fig. 25A, C). One correctly targeted clone out of 768 analyzed clones was identified by Southern blot (Fig. 25F) and was subsequently expanded for blastocyst injection. The ES cells were injected into CD1 blastocysts and chimeras were identified by the extent of brown fur color. Chimerism of approximately 50-80% was obtained. 8 male chimeras were bred with CD1 wild type females, but no germline transmission was observed after the analysis of more than 40 litters, as assessed by the uniform white fur color of the offspring. Electroporation of ES cells and subsequent blastocyst injection of correctly targeted clones will therefore have to be repeated.

3.2 Wnt signaling in mesDA neuron development

The secreted glycoprotein Wnt1 has recently been demonstrated to play a pivotal role in the development of mesDA neurons (Prakash et al., 2006). It is unknown, however, how the extracellular Wnt1 signal is transduced in neuronal precursors within the mesDA domain. Wnt1 has been shown to act via the canonical Wnt pathway by binding to Fzd proteins that function as cellular receptors in all three intracellular Wnt signaling cascades (Huang and Klein, 2004). As there are 10 known *Fzd* genes in mouse and human, I wanted to identify the candidate receptors to transduce the Wnt1 signal in the process of mesDA neuron generation. To act as Wnt1 receptor in mesDA neuron development, the putative receptor must fulfill two conditions: 1) it has to be expressed in close vicinity to Wnt1-secreting cells and 2) it has to be present in the region where mesDA neurons arise. Therefore, ISH probes for all 10 mouse *Fzd* genes were cloned and a detailed expression analysis of the *Fzd* genes was performed in the mouse anterior neural tube, including the colocalization with *Wnt1* and mesDA markers. E9.5 to E12.5 mouse embryos were analyzed, as these stages are considered to be the crucial interval for the establishment of the mesDA progenitor domain and the generation of the first mesDA neurons (Prakash et al., 2006; reviewed in Prakash and Wurst, 2006).

3.2.1 Expression of *Frizzled* receptors in early mouse neural development

3.2.1.1 Expression of *Fzd1-10* at E9.5 of mouse embryonic development

Fzd genes were differentially expressed during neural development. *Fzd1* was weakly expressed throughout the anterior neural tube and strongly expressed in the surrounding mesenchyme (Fig. 26A, A´). *Fzd2* was expressed similarly, with weak expression throughout the neural tube and prominent expression in the mesenchyme (Fig 26B, B´). However, *Fzd2* showed a stronger expression in the forebrain than in the midbrain and rostral hindbrain neuroepithelium (Fig. 26B). In the caudal midbrain only a weak expression of *Fzd1* and *Fzd2* was detected in the VZ of the neuroepithelium which was difficult to distinguish from background levels (Fig 26A´, B´). *Fzd3* was expressed strongly throughout the entire neural tube both in the A/P and D/V axes of the embryo (Fig. 26C, C´). *Fzd4* was not expressed in the neuroepithelium of the anterior neural tube, but was expressed in the mesenchyme

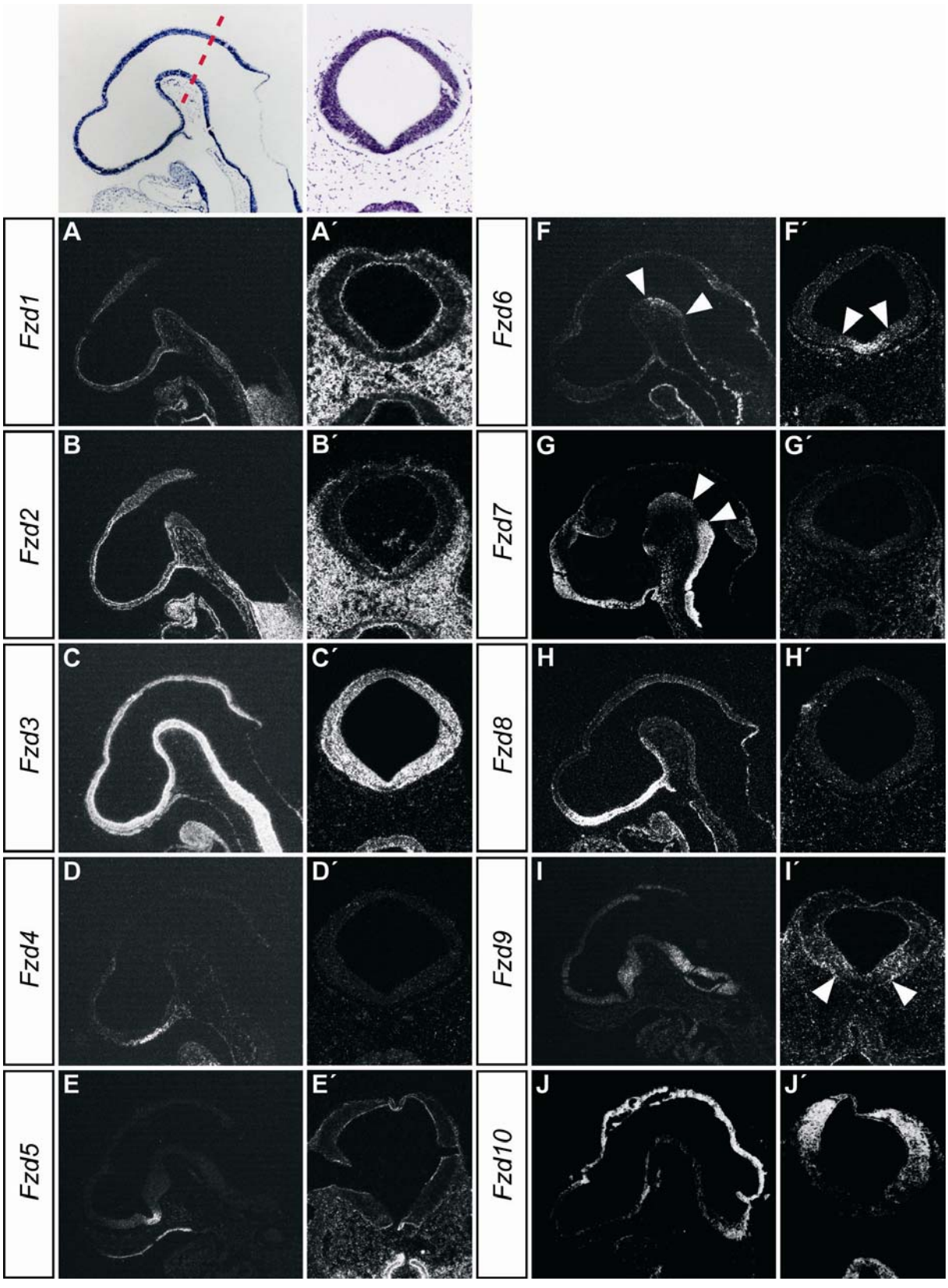
Fzd1
A
A´
Fzd6
F
F´
Fzd2
B
B´
Fzd7
G
G´
Fzd3
C
C´
Fzd8
H
H´
Fzd4
D
D´
Fzd9
I
I´
Fzd5
E
E´
Fzd10
J
J´

Figure 26

Figure 26 Expression of *Fzd1-10* genes in the anterior neural tube of E9.5 mouse embryos. Radioactive *in situ* hybridizations on sagittal (A-J) and coronal sections (A´-J´) with the indicated probes. Top row shows brightfield images of (H, C´) with coronal plane of section depicted as a broken red line. Anterior is to the left in sagittal sections, dorsal is to the top in coronal sections. (A, A´, B, B´) *Fzd1* and *Fzd2* were expressed in a similar pattern with very weak expression in the neural tube. Expression was confined to the ventricular zone of the midbrain neuroepithelium (A´, B´). (C, C´) *Fzd3* was strongly expressed throughout the entire neural tube. (D) *Fzd4* was expressed in the mesenchyme underlying the rostroventral telencephalon. (E) *Fzd5* was expressed in a highly restricted domain in the ventral telencephalon. (D´, E´) *Fzd4* and *Fzd5* were not expressed in the caudal midbrain. (F, F´) *Fzd6* was expressed in the FP and BP of the caudal cephalic flexure with its posterior limit approximately at the MHB (arrowheads in F, F´ delimit *Fzd6* expression along its A/P and D/V extent). (G, G´) *Fzd7* was strongly expressed in the ventral hindbrain and at lower levels in the anterior cephalic flexure, resulting in a gap of expression in the caudal cephalic flexure (between arrowheads in G). (H, H´) *Fzd8* was strongly expressed in the rostroventral telencephalon but not in the midbrain. (I, I´) *Fzd9* was expressed in a caudal to rostral gradient in the hindbrain and the cephalic flexure. In the D/V axis, *Fzd9* was expressed in the dorsal part of the BP and ventral part of the AP (arrowheads in I´ demarcate the ventral boundary of expression). (J, J´) *Fzd10* was strongly expressed in the dorsal diencephalon, midbrain and hindbrain (J), comprising most of the AP and the RP in the caudal midbrain (J´).

underlying the rostroventral telencephalon (Fig. 26D, D´). *Fzd5* was transcribed in a very restricted domain in the ventral telencephalon (Fig. 26E, E´). *Fzd6* expression appeared to be restricted to the dorsal and ventral posterior midbrain in the anterior neural tube. Coronal sections through the ventral expression domain revealed that *Fzd6* expression was restricted to the FP and ventral part of the BP of the neural tube (Fig. 26F, F´). *Fzd7* was strongly expressed in the ventral hindbrain, with a sharp border of expression approximating the position of the MHB, as well as in the head mesenchyme (Fig. 26G). In the caudal cephalic flexure, *Fzd7* expression showed a gap but continued in the rostral ventral midbrain (Fig. 26G). No *Fzd7* transcripts were detected on cross-sections through the posterior midbrain (Fig. 26G´). *Fzd8* was expressed strongly in the rostroventral telencephalon and part of the ventral diencephalon (Fig. 26H) but not in the midbrain or hindbrain territory (Fig. 26H´). *Fzd9* appeared to be weakly expressed in the ventral hindbrain and in a caudal to rostral gradient in the cephalic flexure (Fig. 26I). In the caudal midbrain, *Fzd9* transcripts were detected in the BP and ventral part of the AP, complementary to the expression of *Fzd6* (Fig. 26I´, compare with Fig. 26F´). *Fzd10* was expressed strongly in the dorsal diencephalon, mid- and hindbrain (Fig. 26J), comprising most of the alar plate and the roof plate at the level of the caudal midbrain (Fig. 26J´).

3.2.1.2 Expression of *Fzd1–10* at E10.5 of mouse embryonic development

At E10.5, *Fzd1* and *Fzd2* expression became more refined. Both *Fzd1* and *Fzd2* were expressed in the ventral midbrain, diencephalon and in the entire telencephalon, while only *Fzd2* appeared to be weakly expressed dorsally in the midbrain (Fig. 27A, B). In the caudal part of the cephalic flexure, a gap in the expression domain of *Fzd1* and *Fzd2* became evident that was not apparent at E9.5 (Fig. 27A, B, compare with Fig. 27A, B). Coronal sections of the caudal midbrain showed a very faint expression of *Fzd1* and *Fzd2* in the VZ of the neuroepithelium that was hardly above background levels. However, both genes were strongly expressed in the mesenchyme (Fig. 27A´, B´). *Fzd3* continued to be expressed strongly in the entire neural tube, similar to its expression at E9.5 (Fig. 27C, C´). *Fzd4* was now expressed dorsally and ventrally in the anterior diencephalon, and a domain of strong *Fzd4* expression was detected in the anterior head mesenchyme (Fig. 27D). *Fzd5* was expressed in the rostroventral telencephalon at this stage (Fig. 27E). Neither *Fzd4* nor *Fzd5* were expressed in the midbrain (Fig. 27D´, E´). *Fzd6* still showed the highly restricted expression in the caudal midbrain, but an additional expression domain appeared in the dorsal telencephalon (Fig. 27F, F´). The ventral expression domain of *Fzd6* in the midbrain comprised the caudal half of the cephalic flexure up to approximately the position of the MHB, while the dorsal domain was restricted to the most posterior part of the midbrain (the isthmic region) (Fig. 27F). Coronal sections through the ventral mesencephalic expression domain revealed that *Fzd6* expression was restricted to the FP and ventral half of the BP (Fig. 27F´). *Fzd7* continued to be strongly expressed in the ventral hindbrain up to approximately the position of the MHB, displaying a gap in the ventral caudal midbrain. A faint *Fzd7* expression resumed in the anterior cephalic flexure (Fig. 27G). Weak expression of *Fzd7* was detected in the VZ at the AP/BP boundary (Fig. 27G´). *Fzd8* was still transcribed in the ventral telencephalon, similar to *Fzd5*, although expression levels appeared to be weaker than at E9.5 (Fig. 27H, compare with E and 26H). *Fzd8* expression was not detected in the midbrain (Fig. 27H´). *Fzd9* was now strongly expressed in the ventral and dorsal hindbrain and at lower levels in a caudal to rostral gradient in the midbrain (Fig. 27I). In the caudal midbrain, *Fzd9* expression was detected in the BP, sparing the FP (Fig. 27I´), and in the most dorsal part of the AP, adjacent to the RP which did not express *Fzd9*. *Fzd10* continued to be strongly expressed in the dorsal diencephalon, mid- and hindbrain, showing a sharp boundary in the rostral diencephalon and was not expressed in the telencephalon (Fig. 27J). In the D/V axis of the caudal midbrain, *Fzd10* was expressed in

the RP and lateral walls of the neural tube, sparing the most ventral part of the BP and the FP (Fig. 27J´).

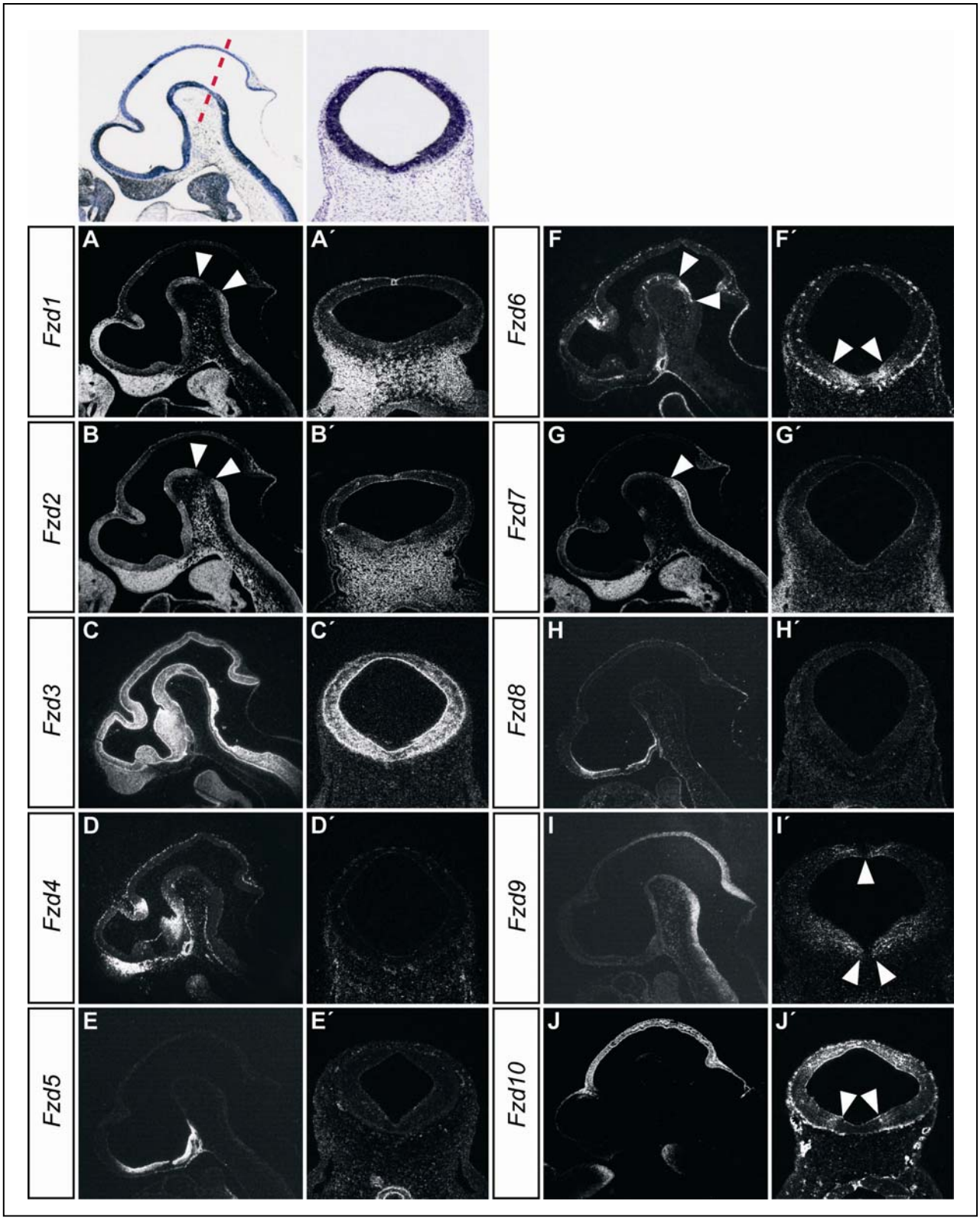

Figure 27

Figure 27 Expression of *Fzd1-10* in the anterior neural tube of E10.5 embryos. Radioactive *in situ* hybridizations on sagittal (A-J) and coronal sections (A´-J´) with the indicated probes. Top row shows brightfield images of (B, C´) with coronal plane of section depicted as a broken red line. Anterior is to the left in sagittal sections, dorsal is to the top in coronal sections. (A, B) *Fzd1* and *Fzd2* were expressed throughout the ventral neural tube with a gap in the caudal cephalic flexure (arrowheads in A, B). (A´, B´) Coronal sections through the posterior midbrain showed very weak expression of *Fzd1* and *Fzd2* in the ventricular zone of the neuroepithelium. (C, C´) *Fzd3* was expressed strongly throughout the entire neural tube. (D) *Fzd4* was expressed in the dorsal and ventral anterior diencephalon and in the anterior head mesenchyme. (E) *Fzd5* was expressed in the rostroventral telencephalon. (D´, E´) *Fzd4* and *Fzd5* were not expressed in the caudal midbrain. (F, F´) *Fzd6* was expressed in the caudal part of the cephalic flexure, comprising the FP and part of the BP (arrowheads in F, F´ demarcate the boundaries of expression in the A/P and D/V axes). (G, G´) *Fzd7* was strongly expressed in the hindbrain, with the anterior limit of expression approximately at the position of the MHB (arrowhead in G), and at lower levels in the rostral cephalic flexure (G), resulting in a gap of expression in the caudal ventral midbrain (G, G´). (H, H`) *Fzd8* was expressed in the rostroventral telencephalon and ventral diencephalon (H), but not in the midbrain (H´). (I, I´) *Fzd9* was expressed in a caudal to rostral gradient in the hindbrain and midbrain (I). In addition to the ventral expression at E9.5, *Fzd9* was also expressed dorsally, but displaying a gap in the ventral and dorsal midline (arrowheads in I´). (J, J´) *Fzd10* was expressed dorsally in the diencephalon, midbrain and hindbrain (J). In the caudal midbrain, *Fzd10* was expressed in the RP, the AP and the dorsal part of the BP (arrowheads in J´ delimit its ventral border of expression).

3.2.1.3 Mouse *Fzd* genes were differentially expressed in the caudal ventral midbrain where mesDA neurons arise

The expression analysis of the 10 *Fzd* genes in E9.5 and E10.5 mouse embryos revealed that *Fzd4*, *Fzd5*, *Fzd8* and *Fzd10* were not expressed at all in the ventral midbrain and thus could be excluded as putative Wnt1 receptors in mesDA neuron development. In order to further narrow down the list of candidate receptors, the expression of the remaining 6 *Fzd* genes in the cephalic flexure at E10.5 was examined more closely.

Both *Fzd1* and *Fzd2* were expressed in the ventral midbrain, but their expression displayed a distinct gap in the caudal part of the cephalic flexure (Fig. 28C, D). In pseudocolored overlays this gap corresponded closely to the expression domain of *Fzd6* (Fig. 28F and insets in C, D). *Fzd3* was strongly expressed in the entire neuroepithelium, including the mesDA progenitor domain in the ventral midbrain and overlapping with the *Fzd6* expression domain (Fig. 28E, and inset). *Fzd6* was expressed in a highly restricted domain in the caudal ventral midbrain. *Fzd7* expression displayed a sharp border at the caudal end of the *Fzd6* expression domain and was weakly expressed in the VZ of the anterior cephalic flexure, resulting in a similar gap as for *Fzd1* and *Fzd2*, which again corresponded to the *Fzd6* domain

in the ventral midbrain (Fig. 28G). *Fzd9* was expressed in a caudal to rostral gradient in the ventral hindbrain and posterior ventral midbrain, showing a partial overlap with the caudal *Fzd6* expression domain (Fig. 28H).

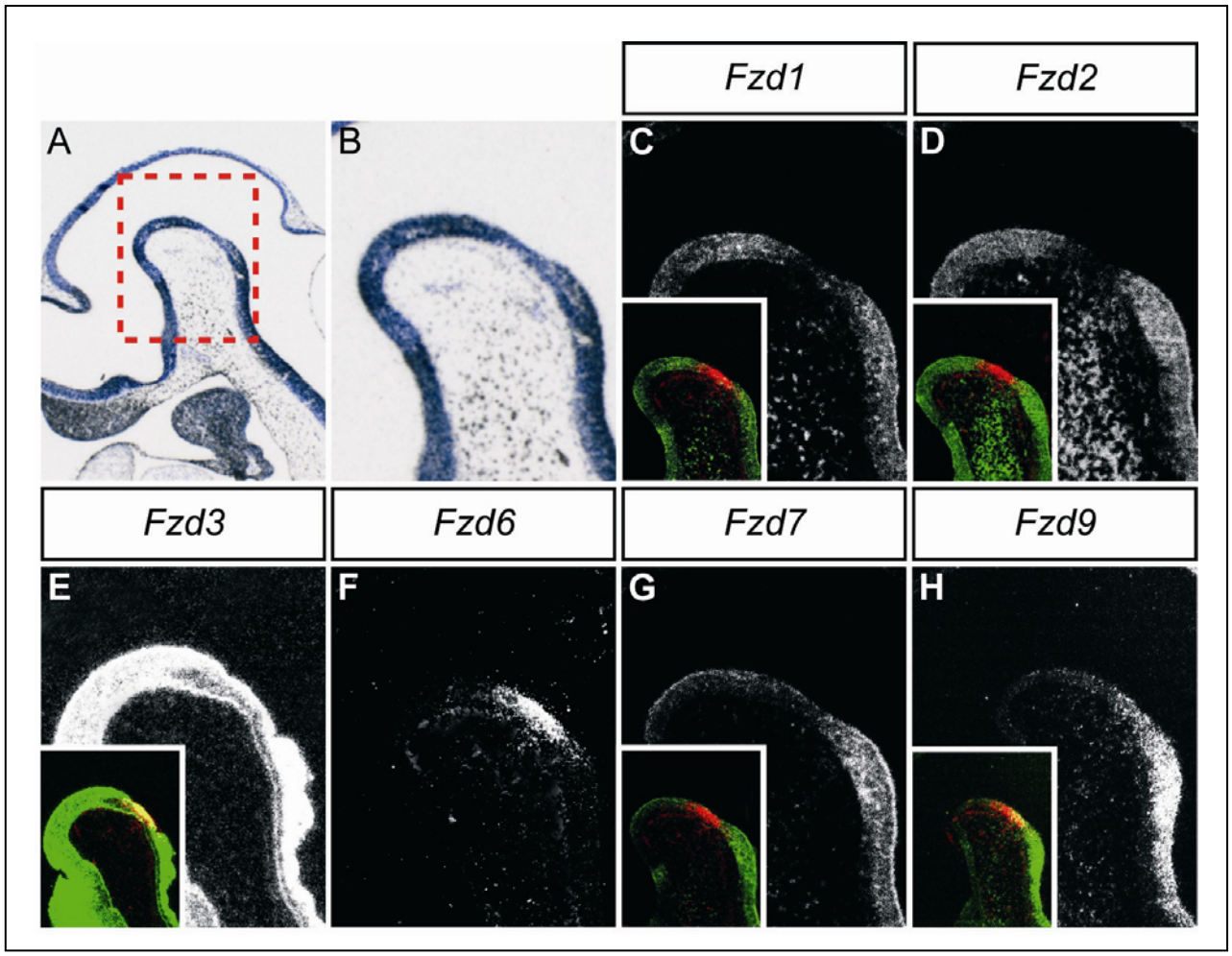

Figure 28 Comparison of the expression of *Fzd1*, *Fzd2*, *Fzd3*, *Fzd6*, *Fzd7* and *Fzd9* in the cephalic flexure of E10.5 mouse embryos. (A-H) Sagittal sections of E10.5 embryos, anterior is to the left. (B-H) Higher magnifications of the region outlined by the red dotted rectangle in (A). (A, B) Brightfield images of (C). (C-H) Darkfield images of corresponding sections. Insets in (C-E, G, H) are pseudocolor overlay images with (F), *Fzd6* in red and *Fzd1, 2, 3, 7, 9* in green. (C, D) *Fzd1* and *Fzd2* were expressed in a complementary pattern to *Fzd6* in the cephalic flexure. (E) *Fzd3* was expressed throughout the ventral midbrain, thus overlapping with *Fzd6* expression. (G) *Fzd7* was very weakly expressed in the VZ of the anterior cephalic flexure, resulting in a gap corresponding to the *Fzd6* expression domain in the caudal ventral midbrain. (H) *Fzd9* was expressed in a gradient in the most caudal part of the midbrain, thus overlapping partially with *Fzd6* expression.

This close inspection of *Fzd* gene expression therefore revealed that these receptors displayed a peculiar expression pattern in the caudal ventral midbrain just rostral to the MHB, the domain where mesDA neurons are assumed to arise. Of the 10 murine *Fzd* genes, only *Fzd3*, *Fzd6* and *Fzd9* were expressed in the caudal ventral midbrain, and of these, *Fzd6* expression was restricted specifically to this region, whereas *Fzd3* and *Fzd9* were expressed in a broader domain. Most notably, the *Fzd6* expression domain in the caudal ventral midbrain coincided with the gap in the expression of *Fzd1*, *Fzd2* and *Fzd7*. Taken together, these results suggest that Fzd6, possibly together with Fzd3 and/or Fzd9, is very likely the receptor transducing the Wnt1 signal for the generation of mesDA neurons.

3.2.2 *Fzd6* was coexpressed with *Wnt1* in the caudal ventral midbrain

This analysis was further extended to test whether *Fzd6* was expressed in close vicinity to Wnt1-secreting cells in the ventral caudal midbrain (condition 1, see above). At E10.5, *Fzd6* was expressed in the neuroepithelium of the caudal cephalic flexure (Fig. 27F, 28F, 29B), overlapping with the *Wnt1* expression domain in this region. Wnt1 expression, however, extended rostrally into the anterior cephalic flexure (Fig. 29C). At E11.5, the *Fzd6* and *Wnt1* expression domains appeared now to completely overlap in the caudal cephalic flexure (Fig. 29E, F). At E12.5, the expression of *Fzd6* and *Wnt1* still coincided almost completely in the ventral caudal midbrain (Fig. 29H, I). While *Fzd6* and *Wnt1* appeared to be expressed throughout the entire neuroepithelium, comprising the VZ, SVZ and MZ at E10.5, their expression appeared to be restricted to the VZ at E12.5 (compare Fig. 29B, C with H, I). Taken together, the colocalization of *Fzd6* and *Wnt1* transcripts at the critical stages of mesDA neuron development (E9.5-E12.5) therefore demonstrates that the Fzd6 receptor fulfills condition 1), i.e. it is expressed in close vicinity to Wnt1-secreting cells is thus a good candidate to transduce the Wnt1 signal necessary for mesDA neuron generation.

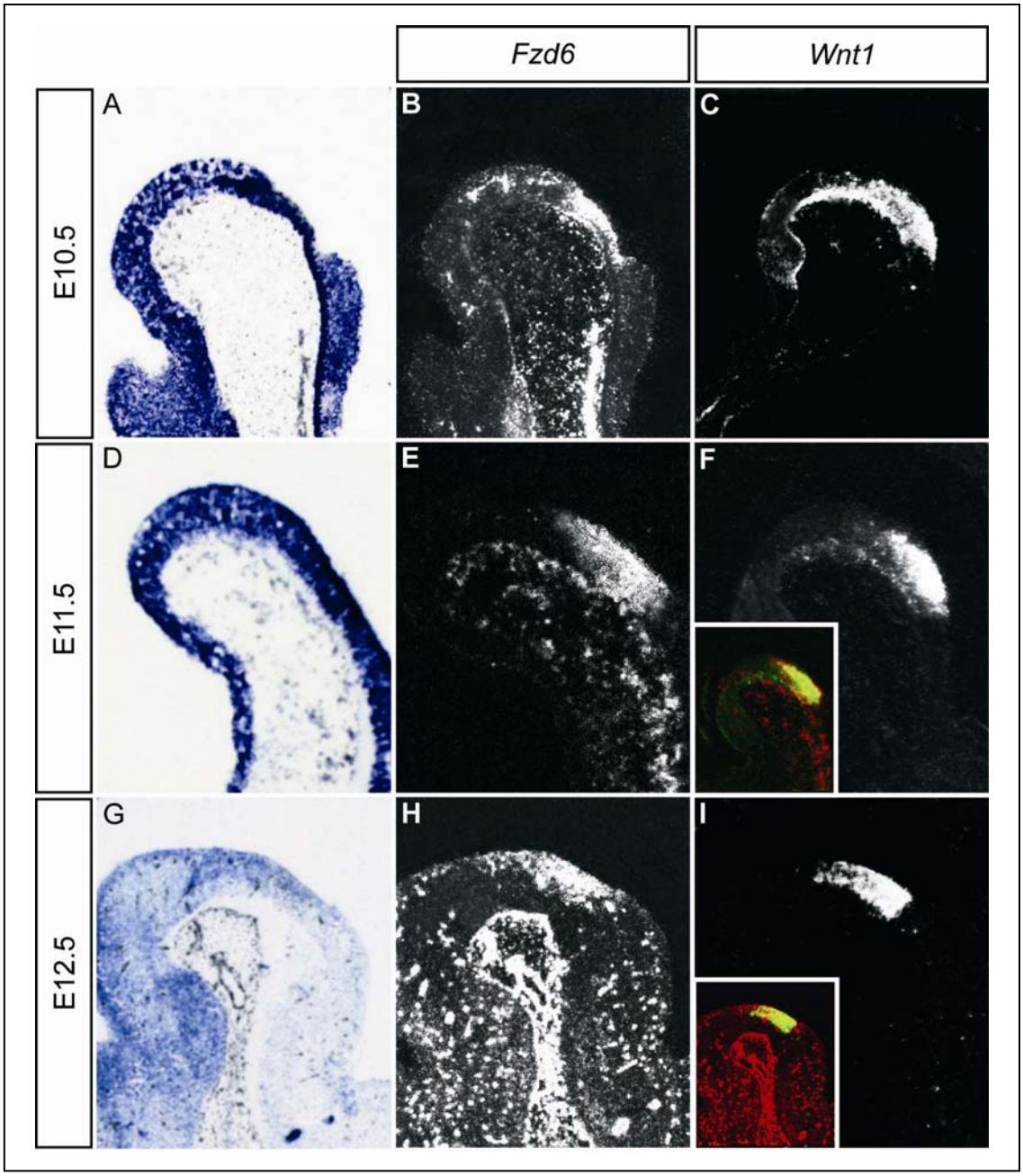

Figure 29 Coexpression of *Fzd6* and *Wnt1* in the cephalic flexure between E10.5 and E12.5. (A-I) High magnifications of the cephalic flexure in sagittal sections from E10.5 (A-C), E11.5 (D-F) and E12.5 embryos (G-I). Anterior is to the left. (A, D, G) Brightfield images of (B, E, H). (B, C, E, F, H, I) Darkfield images of corresponding sections. Insets in F, I are pseudocolor overlay images with E, H, *Fzd6* in red and *Wnt1* in green. (B, C) At E10.5, *Fzd6* and *Wnt1* overlapped in the caudal ventral midbrain, with *Wnt1* expression extending more rostrally than *Fzd6* expression. (E, F) At E11.5, *Fzd6* and *Wnt1* continued to be coexpressed in the caudal cephalic flexure, now with a very similar A/P extent of expression. (G-I) At E12.5, *Fzd6* and *Wnt1* expression coincided almost completely in the caudal cephalic flexure. Note that the expression of *Fzd6* and *Wnt1* appeared to comprise the VZ, SVZ and MZ of the neuroepithelium at E10.5, but appeared to become restricted to the VZ at E12.5 (compare B, C with H, I).

3.2.3 *Fzd6* expression showed an almost complete overlap with *Aldh1a1* expression but only a marginal overlap with *Nr4a2*, *Th* and *Pitx3* expression

It is assumed that Wnt1 signals cell-autonomously for the generation of mesDA neurons. Therefore, mesDA progenitors/precursors are required to express the candidate Fzd receptor to receive and transduce the Wnt1 signal (condition 2, see above). The expression of *Fzd6* mRNA was compared to the expression of early and late markers for mesDA progenitors and neurons, respectively, to determine whether Fzd6 may function as a Wnt1 receptor in mesDA neuron development.

First, the expression of *Aldh1a1* was used to identify the mesDA progenitors (Wallen et al., 1999). At E10.5, *Aldh1a1* was expressed in the caudal cephalic flexure, including the entire *Fzd6* expression domain (Fig. 30B, C). On coronal sections, *Fzd6* and *Aldh1a1* expression domains overlapped substantially in the BP of the neural tube (Fig. 30E, F). Unlike *Fzd6*, *Aldh1a1* expression displayed a narrow gap in the medial FP of the neural tube (Fig. 30F). At E11.5, *Fzd6* and *Aldh1a1* were still expressed in a similar pattern in the BP of the neural tube, with *Fzd6* expression extending more laterally than *Aldh1a1* expression (Fig. 30H, I). *Fzd6* and *Aldh1a1* were not expressed in the FP at this stage. Note that while at E10.5 both genes were expressed throughout the entire width of the neuroepithelium (i.e. in the VZ, SVZ and MZ), *Fzd6* expression appeared to be restricted to the VZ and SVZ at E11.5, whereas *Aldh1a1* was also expressed in the MZ (Fig. 30H, I). These results suggest that mesDA progenitors indeed express *Fzd6*, further supporting a possible role of Fzd6 in the transduction of the Wnt1 signal early during mesDA neuron generation.

Next, *Fzd6* expression was compared to the expression of *Th*, *Pitx3* and *Nr4a2* at E11.5 and E12.5 to address the question whether Fzd6 may also play a role during later differentiation of mesDA precursors. At E11.5, *Th*, *Pitx3* and *Nr4a2* were expressed in the outer layer of the neuroepithelium (presumably the MZ) which was mostly devoid of *Fzd6* transcripts. Furthermore, their expression domain in the cephalic flexure extended far more rostrally than *Fzd6* expression (Fig. 31B-E). An overlap in the expression of these genes and *Fzd6* expression was detected only in the MZ of the most caudal part of the cephalic flexure (insets in Fig. 31C-E). At E12.5, *Th*, *Pitx3* and *Nr4a2* appeared to be mostly confined to the SVZ and MZ of the neural tube in the caudal midbrain (Fig. 31H-J), whereas *Fzd6* expression appeared to be more restricted to the VZ (Fig. 31G). Pseudocolored images of consecutive sections confirmed the mutually exclusive expression of *Fzd6* and the mesDA neuronal

markers in the caudal cephalic flexure at this stage (insets in Fig. 29H-J). The differential expression of *Fzd6* and *Th*, *Pitx3* and *Nr4a2* therefore suggests that only a few, if any, mesDA precursors/neurons may express *Fzd6* at later stages of mesDA neuron development (i.e. at E11.5 and E12.5).

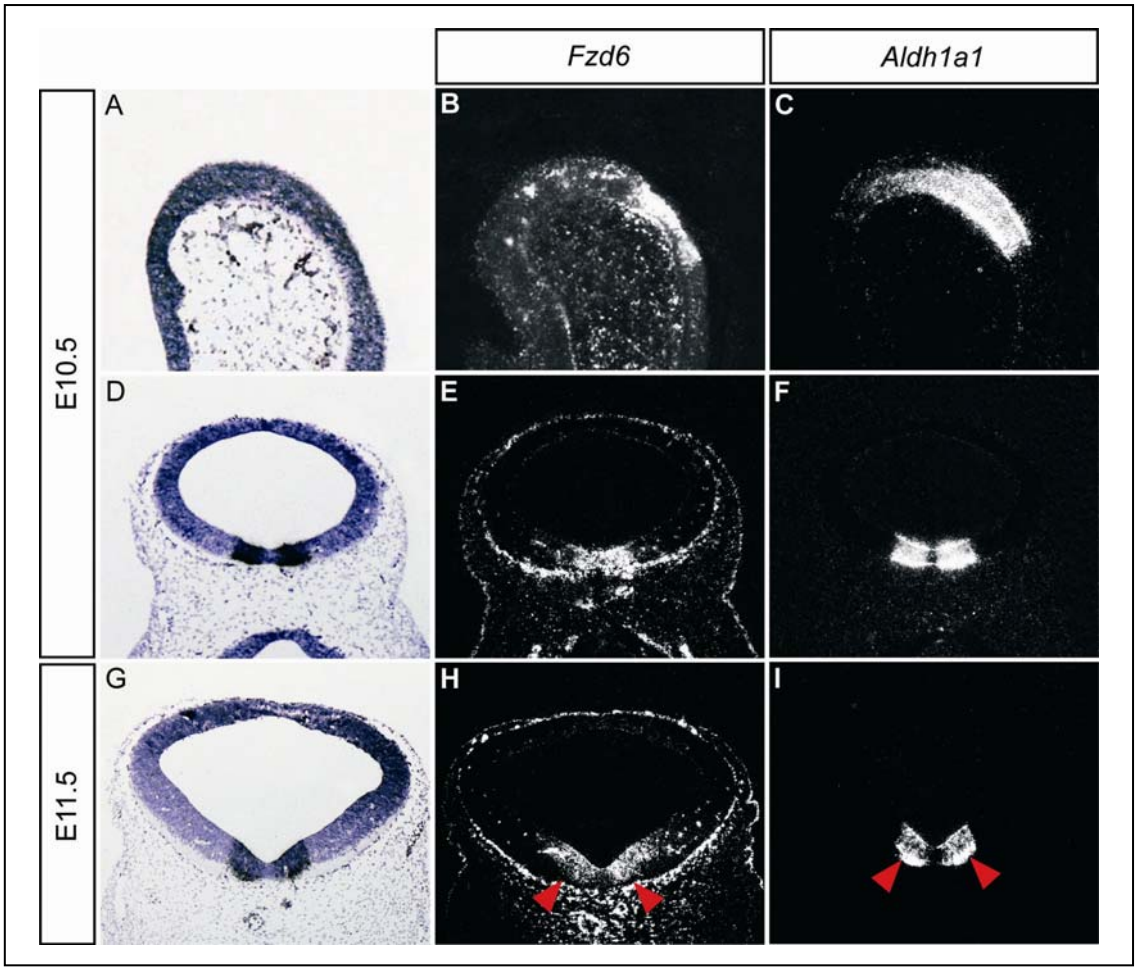

Figure 30 *Fzd6* expression overlapped with expression of *Aldh1a1*, a marker of early mesDA progenitors. (A-C) Sagittal sections showing the cephalic flexure of E10.5 embryos. Anterior is to the left. (D-I) Coronal sections of the caudal midbrain of E10.5 (D-F) and E11.5 embryos (G-I). Dorsal is to the top. (A, D, G) Brightfield images of (C, F, I). (B, C, E, F, H, I) Darkfield images of corresponding sections. (A-C) At E10.5, *Fzd6* and *Aldh1a1* expression overlapped in the cephalic flexure, with *Aldh1a1* expression extending more rostrally than *Fzd6* expression. (D-F) Coronal sections showed an overlap of the *Fzd6* domain with the *Aldh1a1* domain in the BP. Unlike *Fzd6*, *Aldh1a1* displayed a gap in the medial FP. (G-H) At E11.5, *Fzd6* and *Aldh1a1* continued to be coexpressed in the BP of the neural tube, while both genes were not expressed in the medial FP at this stage. At E10.5, *Fzd6* and *Aldh1a1* expression spanned the entire width of the neuroepithelium (i.e. the VZ, SVZ and MZ) (E, F), whereas at E11.5 *Fzd6* expression appeared to be restricted to the VZ and SVZ, while *Aldh1a1* was expressed also in the MZ (red arrowheads in H, I).

Taken together, the detailed expression analysis of the *Fzd* genes during early mouse neural development lead to the identification of Fzd6 as a putative candidate, very likely together

with Fzd3 and/or Fzd9, to function as a receptor for the Wnt1 signal required early for the establishment of the mesDA progenitor domain. The overlap of *Fzd6* expression with *Aldh1a1* expression at E10.5 and E11.5 demonstrates that Fzd6 also fulfills condition 2), as it is expressed in mesDA progenitors early in mesDA neuron development. Furthermore, although only a minimal, if any, overlap was detected between the expression of *Fzd6* and *Pitx3* at E11.5 and E12.5, the induction of *Pitx3* expression could be initiated by Fzd6-mediated Wnt1 signaling in mesDA progenitors before E11.5, the time point at which Pitx3 expression is first detected.

The analysis regarding the function of Fzd receptors in mesDA neuron development *in vivo* is currently in progress. In a first approach, two conventional knockout mouse lines for *Fzd3* and *Fzd6*, respectively, are used to generate embryos in which either one or both of these receptors are inactivated. This work will be the subject of a separate thesis in our group.

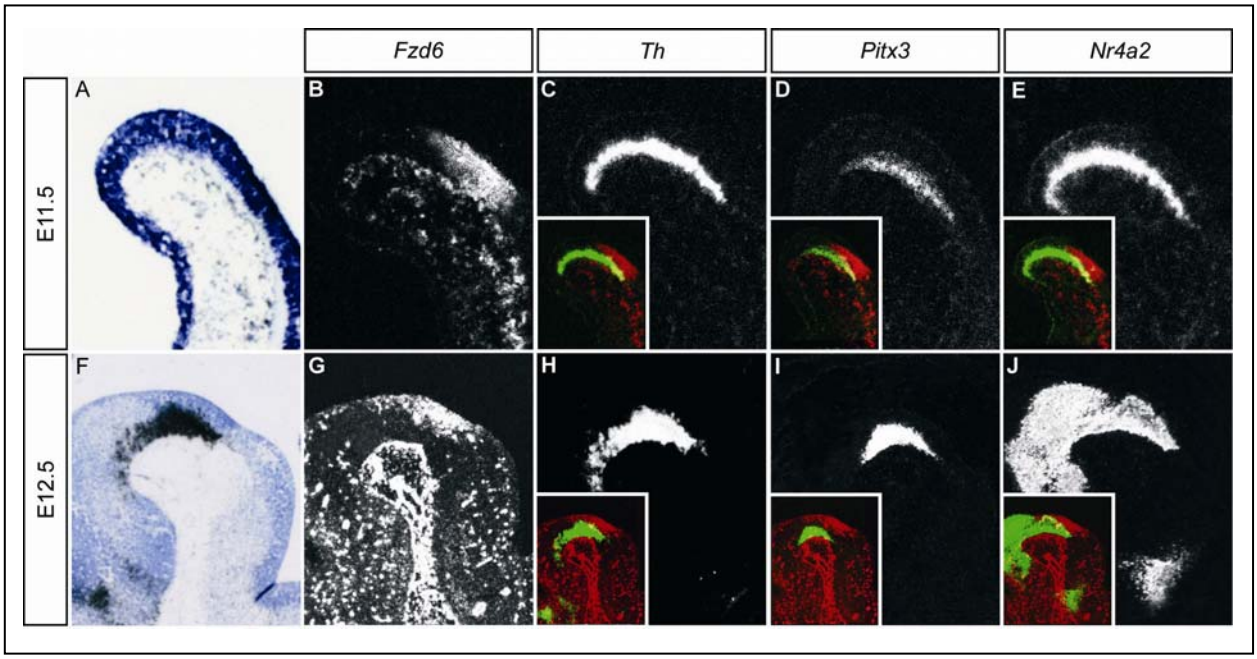

Figure 31 Comparison of *Fzd6* expression with *Th*, *Pitx3* and *Nr4a2* expression in the ventral midbrain of E11.5 and E12.5 mouse embryos. (A-J) Sagittal sections of the cephalic flexure of E11.5 (A-E) and E12.5 embryos (F-J). Anterior is to the left. (A, F) Brightfield images of (B, H). (B-E, G-J) Darkfield images of corresponding sections. Insets in (C-E, H-J) are pseudocolor overlay images of consecutive sections hybridized with *Fzd6* (red) and *Th*, *Pitx3* or *Nr4a2* (green). (B-E) At E11.5, *Fzd6* expression overlapped with *Th*, *Pitx3* and *Nr4a2* expression only in the outermost layer of the neuroepithelium in the caudal cephalic flexure. (G-J) At E12.5, *Fzd6* expression appeared to be restricted to the VZ, whereas *Th*, *Pitx3* and *Nr4a2* were expressed mostly in the SVZ and MZ. Therefore, *Fzd6* was not coexpressed with *Th*, *Pitx3* and *Nr4a2* at this stage (insets in H-J).

3.2.4 Establishment of an *in vitro* system to examine Wnt signaling in mesDA neuron development

To further dissect whether a Fzd6-mediated Wnt1 signal can promote the specification of a mesDA fate to a certain extent, *in vitro* assays will have to be performed, using appropriate cell lines that can be manipulated *in vitro*. To this end, an adult rat hippocampal stem/progenitor (AHP) cell line was characterized and tested for its suitability for these experiments. The endogenous expression of major components of the Wnt/β-catenin signaling cascade, such as *Wnt3*, *Fzd1*, *Dvl1*, *Axin1*, *Gsk3β*, *β-catenin* and *Lef1*, has been determined in the AHP cell line by RT-PCR (Lie et al., 2005). Using this AHP cell line, it has recently been shown by Lie et al., 2005, that Wnt/β-catenin signaling is involved in adult neurogenesis in the hippocampus. Furthermore, upon application of Wnt ligands these cells can differentiate into DA neurons, as assessed by the expression of Th, *Nr4a2*, *Pitx3* and *Slc6a3* (D.-C. Lie, personal communication). Interestingly, in a stably transduced AHP cell line with a Wnt1-expressing retroviral vector (AHP-Wnt1), the number of DA neurons after differentiation is substantially higher (D.-C. Lie, personal communication), further supporting a crucial role of Wnt1 signaling in DA neuron generation. This cell line thus fulfills two essential requirements for *in vitro* experiments of Wnt signaling in mesDA neuron development: 1) the cells are responsive to Wnt ligands/Wnt signaling and express crucial components of the canonical Wnt/β-catenin pathway. 2) the cells possess the ability to differentiate into DA neurons *in vitro*. For future experiments, however, a precise knowledge of the complement of Fzd receptors and intracellular effectors of the Tcf/Lef family that are expressed in these cells was required. Therefore, the expression of all 10 rat *Fzd* genes, as well as of rat *Tcf7*, *Tcf7l1*, *Tcf7l2* and *Lef1*, was examined by RT-PCR in the AHP and AHP-Wnt1 cell lines. RT-PCR primers were designed based on the sequence of the rat transcripts annotated by NCBI (*Fzd1*, *Fzd2*, *Fzd3*, *Fzd4*, *Fzd5*, *Fzd9*, *Lef1*), predicted by NCBI (*Fzd6*, *Fzd7*, *Tcf7*) or based on the sequence of the mouse genes annotated by NCBI (*Fzd8*, *Fzd10*, *Tcf7l1*, *Tcf7l2*) (see appendix xxx for primer sequences and accession numbers). In all cases in which the rat mRNA sequence was known or predicted, nucleotide sequences displaying 100% homology between mouse and rat were chosen as primer binding sites.

Fzd1-5, *Fzd8-10*, *Tcf7*, *Tcf7l1*, *Tcf7l2* and *Lef1* mRNAs were expressed both in AHP and AHP-Wnt1 cells at equal levels except for *Fzd9* which appeared to be up-regulated in Wnt1-overexpressing cells. Interestingly, *Fzd6* and *Fzd7* transcripts were not detected in these cell lines (Fig. 32). Since the sequences of rat *Fzd6* and *Fzd7* mRNA have only been predicted, it

is however also possible that the actual nucleotide sequences of these transcripts differ from the predicted sequences in the regions used as primer binding sites, thus leading to a false negative result. To exclude this possibility, the experiment will have to be repeated using cDNA from rat embryos as positive control.

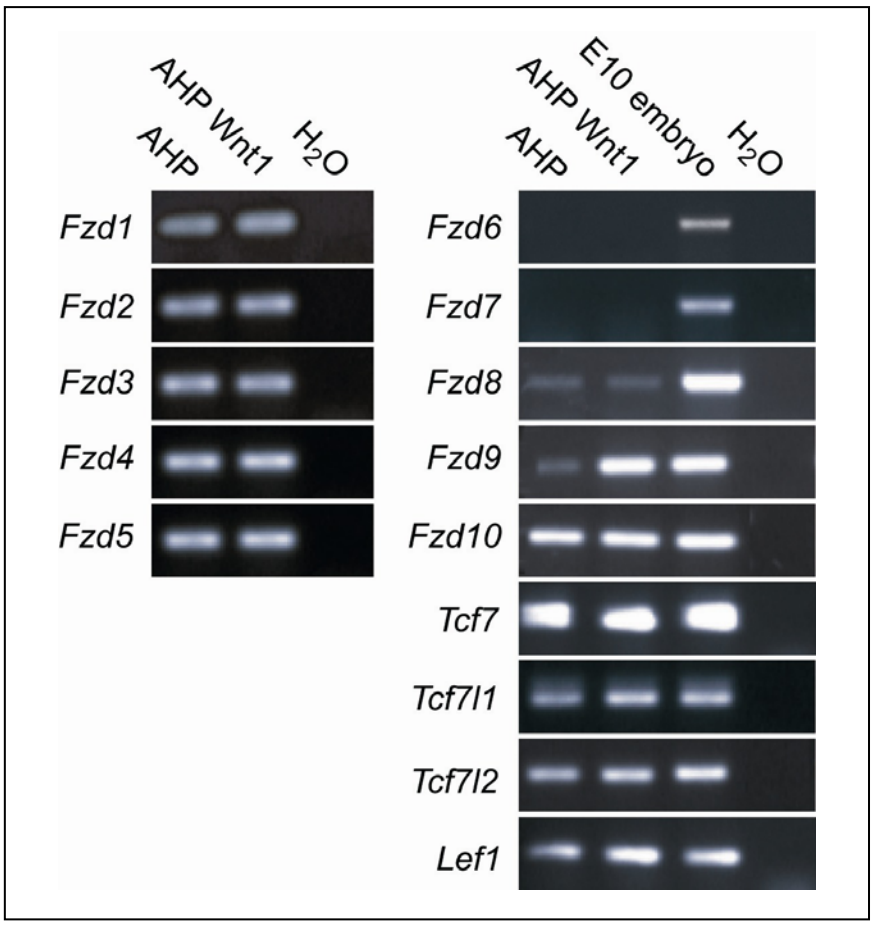

Figure 32 RT-PCR analysis for the detection of *Fzd1-10*, *Tcf7*, *Tcf7l1*, *Tcf7l2* and *Lef1* mRNA in AHP and AHP-Wnt1 cells. All analyzed genes except for *Fzd6* and *Fzd7* were detected in both cell lines. cDNA from E10.5 whole mouse embryos was used as positive control for the amplification of these genes. H_2O: water control.

As the expression pattern of *Fzd6* in mouse embryos suggests a specific role of this receptor in mesDA neuron development, one aim is to test the ability of Fzd6 and its downstream signaling cascade to even further promote (mes)DA differentiation in AHP and/or AHP-Wnt1 cells by overexpressing this receptor in these cell lines. To this end, both cell lines will be stably transfected with expression vectors encoding the mouse *Fzd6* cDNA. Since untranslated regions (UTRs) at the 5' or at the 3' end of the mRNA can influence the stability

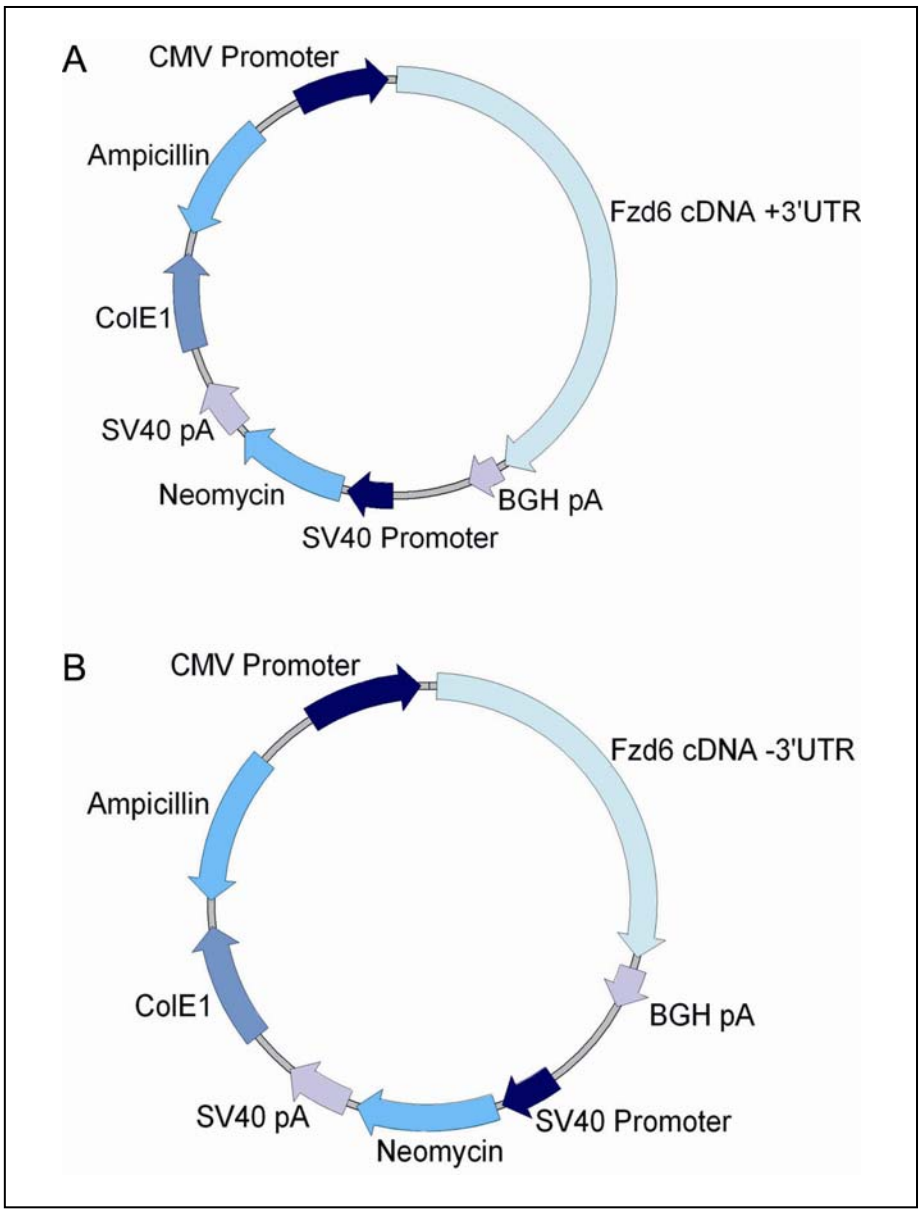

Figure 33 Design of the *Fzd6* expression vectors for stable transfection of AHP and AHP-Wnt1 cells. contained *Fzd6* cDNA fragments with (A) or without 3'UTR (B) were cloned into pcDNA3 vectors (Invitrogen). Expression of these cDNA fragments is driven by the CMV promoter. The neomycin resistance gene allows the selection of clones which integrated the vector into the genome and thus the generation of stably transfected cell lines. CMV Promoter: human cytomegalovirus immediate-early promoter/enhancer; BGH pA: bovine growth hormone polyadenylation signal; SV40 Promoter: simian virus 40 promoter; Neomycin: neomycin resistance gene; SV40 pA: simian virus 40 polyadenylation signal; ColE1: *E. coli* origin of replication; Ampicillin: ampicillin resistance gene.

of the transcript as well as the efficiency of translation, two different vectors were constructed: one containing a murine (m)*Fzd6* cDNA fragment including the 3' UTR and another containing a *mFzd6* cDNA fragment without the 3' UTR. In both vectors, the 5' UTR of the *mFzd6* cDNA was absent (Fig. 33A, B). *mFzd6* cDNA fragments with (3729bp) and

without 3' UTR (2146bp) were amplified from total RNA isolated from E10.5 mouse embryos by RT-PCR (see appendix xxx for the sequences of the *mFzd6* cDNA fragments). A *Bam*HI site was introduced with the forward primer and an *Eco*RV site was introduced with the two different reverse primers (see appendix xxx for primer sequences). The *mFzd6* cDNA fragments were ligated into the pcDNA3 vector (Invitrogen) which had been linearized with the restriction enzymes *Bam*HI and *Eco*RV and purified via gel extraction. The expression vectors were sequenced to confirm the correct orientation of the cDNA fragments and to rule out point mutations. AHP and AHP-Wnt1 cells will be transfected with these vectors. Since the pcDNA3 vector contains a neomycin resistance gene, cells which integrate the vector stably into the genome will be selected using G418 geneticin. The resulting mFzd6-expressing cell lines will be used to further characterize the Wnt1-Fzd6 signal transduction pathway in mesDA neuron development and to determine direct interactions between the Wnt1 ligand and its receptor Fzd6 *in vitro*.

4. Discussion

In this work, the roles of Fibroblast growth factor 15 and Wnt signaling in different aspects of central nervous system development were addressed. *Fgf15* was shown to be widely expressed in the developing neural tube, a specific role of this growth factor in CNS development, however, was hitherto unknown. The re-analysis of an *Fgf15* deficient mouse line revealed that this factor is involved in the regulation of cell cycle exit by neural progenitors and subsequent neurogenesis. Failure of neural progenitors to leave the cell cycle between E10.5 and E11.5 in *Fgf15*$^{-/-}$ embryos results in an up-regulation of neurogenic bHLH factors and a down-regulation of proneural bHLH factors in the mutant neuroepithelium and consequently to the generation of fewer postmitotic neurons. While Fgf15 signaling affects neurogenesis generally in the anterior neural tube, the function of Wnt signaling was specifically addressed in respect to the development of a restricted neuronal population, the DA neurons of the ventral midbrain. Here, Fzd6 was identified as a candidate receptor, together with Fzd3 and Fzd9, to transduce the Wnt1 signal required for the generation of mesDA neurons. The spatial and temporal expression pattern of these genes suggests a possible role of the corresponding receptors in the establishment of the mesDA progenitor domain between E9.5 and E10.5, as well as in the terminal differentiation of mesDA neurons.

4.1 The expression of *Fgf15* at midgestational stages of mouse embryonic development is complementary to the *Shh* expression in the anterior neural tube and displays a gap at the MHB

Fgf15 is expressed mostly in the AP of the anterior neural tube, sparing the RP dorsally and the FP/BP ventrally. At the MHB, *Fgf15* expression displays a narrow gap which comprises the anterior part of the isthmic *Fgf8* expression domain. Between E9.5 and E12.5, the gap in the *Fgf15* expression domain at the MHB narrows, following the retracting *Fgf8* expression. In the D/V axis, the expression of *Fgf15* is complementary to the *Shh* expression in the anterior neural tube. Since it has been proposed that Fgf15 may be a direct target of Shh signaling (Saitsu et al., 2005), it could be that either *Fgf15* expression is induced only by medium/low levels of Shh but suppressed by high levels of Shh, or that high levels of Shh induce a yet unidentified inhibitor of *Fgf15* expression. It remains unclear, however, whether

the Fgf15-mediated Shh signaling relay controlling *Ccnd1* and *Tcf7l2* expression (Ishibashi and McMahon, 2002) actually exists, as the expression of both *Ccnd1* and *Tcf7l2* were unaltered in *Fgf15*$^{-/-}$ embryos (data not shown). Moreover, the expression of *Fgf15* is normal in *Gli2*$^{-/-}$ mutant embryos (Saitsu et al., 2005), suggesting that the *Fgf15* promoter region that is activated by Gli2 in transgenic embryos may not contain all regulatory elements of *Fgf15* expression and thus may not recapitulate the *in vivo* situation correctly. Therefore, it is possible that loss of Shh affects the expression of Fgf15, Ccnd1 and Tcf7l2 independently from each other and that other factors may be involved in the proposed signaling relay mechanism.

4.2 Compromised blood supply and growth retardation of *Fgf15*$^{-/-}$ embryos likely result from cardiac defects

After backcrossing the original inbred Sv129/C57Bl/6 *Fgf15*$^{-/-}$ mouse line (Wright et al., 2004) to an outbred CD1 genetic background, morphological defects occur in 10% of all homozygous mutant embryos at the stages E12.5 and E13.5, which also include the neural tube. Affected embryos are generally growth retarded, appear to lack a proper blood supply and, most importantly, display an infolding of anterior neural tissue into the lumen of the neural tube. Since the morphology of the placenta and vascularization of the embryos seem to be unaffected in *Fgf15*$^{-/-}$ embryos, compromised blood supply and growth retardation can probably be attributed to the defects in heart development reported by Vincentz et al. (2005). In that study, it has been shown that loss of *Fgf15* affects the remodeling of cardiac neural crest cells, resulting in ventricular septal defects and alignment defects of the aorta and pulmonary trunk. Importantly, *Fgf15*$^{-/-}$ embryos were reported to be indistinguishable from wild type littermates until E11.5, when the first cardiac defects become obvious. This is in line with the present finding that morphological aberrations do not occur before E12.5 and that *Fgf15*$^{-/-}$ embryos at E11.5 are only slightly reduced in size. Furthermore, 5% of mutant embryos at E18.5 were reported not to show any heart defects, consistent with about 3% of mutant escapers which survive into adulthood (Vincentz et al., 2005), suggesting that the heart phenotype may also account for embryonic lethality.

The previous studies concerning *Fgf15* deficient mice used mouse lines either on a C57Bl/6 or on a mixed Sv129/C57Bl/6 background (Wright et al., 2004; Vincentz et al., 2005). The appearance of a CNS phenotype in *Fgf15*$^{-/-}$ embryos exclusively on a CD1 genetic

background suggests that genetic modifiers may exist in the C57Bl/6 and/or Sv129 inbred genetic backgrounds that are able to rescue the loss of *Fgf15* in the CNS. In the heterogenic outbred CD1 background, the variability of these 'modifier genes' appears to be rather high compared to the inbred, isogenic backgrounds C57Bl/6 and Sv129, resulting in the occurrence of a CNS phenotype with varying penetrance in *Fgf15*$^{-/-}$ embryos on the CD1 background. This is in line with numerous studies emphasizing the importance of the genetic background in the evaluation and interpretation of genetic mutations. Examples of genes displaying a CNS phenotype only or to a larger extent on a certain genetic background include *En1* (Bilovocky et al., 2003), *Pax2* (Schwarz et al., 1997), *p75*^{NGF} (Greferath et al., 2000) and *p130* (LeCouter et al., 1998). The specific differences between the C57Bl/6, Sv129 and CD1 genetic backgrounds responsible for the suppression of the *Fgf15* phenotype on the former two remain to be determined. The identification of an inbred genetic background that displays 100% penetrance of the Fgf15 phenotype would facilitate the analysis of the phenotype and may reveal further effects of the loss of *Fgf15* that may be suppressed by genetic modifiers present also in the CD1 genetic background. Furthermore, the analysis of such an inbred mouse strain represents the only possibility to identify these genetic modifiers of Fgf15 function.

4.3 Fgf15 is involved in the regulation of cell cycle exit of neuroepithelial progenitors during neurogenesis

The present study focused specifically on the CNS phenotype of *Fgf15*$^{-/-}$ embryos, since a function of this factor in neural development has not been reported previously. I provide evidence that in the anterior neural tube of *Fgf15*$^{-/-}$ embryos, cell cycle exit of neural progenitors is affected. At E11.5, the number of neuroepithelial cells which remain in the cell cycle is increased on average by more than 60% in *Fgf15*$^{-/-}$ embryos when compared to wild type littermates. It has been demonstrated that a twofold increase in the number of cells remaining in the cell cycle in the developing cortex leads to a dramatic enlargement of cortical tissue (Chenn and Walsh, 2002), resulting in an indentation of the neuroepithelium reminiscent of the infolding of neural tissue observed in 10% of *Fgf15*$^{-/-}$ embryos at E12.5 and E13.5. Notably, in both cases the increase in proliferating cells leads to a horizontal expansion of neural tissue, whereas the thickness of the neuroepithelium remains largely unaffected. While a failure of neural progenitors to exit the cell cycle is observed in virtually all *Fgf15*$^{-/-}$

embryos at E11.5, 1 out of 10 mutant embryos (approximately 10%) shows an increased proliferation at this stage (as assessed by Ki67 staining), and 1 out of 5 mutant embryos (approximately 20%) displays a much more pronounced cell cycle exit defect than the average (indicated by the increased number and ectopic location outside the VZ of $BrdU^+/Ki67^+$ double positive cells). These numbers appear to correlate well with the 10% of *Fgf15*$^{-/-}$ embryos displaying an infolding of neural tissue one day later in development. In these cases, a strongly increased number of cells that fail to exit the cell cycle may lead to a marked increase in the size of the progenitor pool and as a consequence to a dramatic enlargement of anterior neural tube tissue. The discrepancy between 10% of mutant embryos with increased proliferation and 20% of embryos with more pronounced cell cycle exit failure can probably be attributed to the small sample size in the cell cycle exit experiment. A possible explanation for the finding that only 10% of all *Fgf15*$^{-/-}$ embryos display a more distinct phenotype than the remainder of mutant embryos, may be the heterogeneity of the CD1 genetic background. While factors present in the C57Bl/6 and/or Sv129 genetic backgrounds appear to suppress the CNS phenotype of *Fgf15*$^{-/-}$ mice, factors in the CD1 genetic background reveal the effect of loss of Fgf15 in the anterior neural tube, and in 10% of CD1 embryos seem to further exacerbate this phenotype.

Given the paleness of the *Fgf15*$^{-/-}$ embryos and their apparently poor blood supply at E12.5, the generation of excess tissue could also be a secondary effect of hypoxia in neural tissue, as it has been shown that sub-lethal hypoxia induces neuronal proliferation (Bossenmeyer-Pourie et al., 1999). However, this seems to be unlikely in the case of the *Fgf15*$^{-/-}$ embryos, since it has been demonstrated that hypoxia-induced proliferation is accompanied by increased differentiation (Jin et al., 2002; Zhu et al., 2005), a finding that is in stark contrast to the observations in this work. Nevertheless, hypoxia resulting from the apparently poor blood supply of *Fgf15* mutant embryos could account for several aspects of the *Fgf15* phenotype, e.g. the widespread increase of apoptosis and the general growth retardation.

4.4 Failure to exit the cell cycle is accompanied by perturbed neurogenesis in *Fgf15*$^{-/-}$ embryos

The failure of neural progenitors to exit the cell cycle in *Fgf15*$^{-/-}$ embryos results in a failure of neuronal precursors to properly differentiate into neurons. While the expression of Nestin

is increased in the neuroepithelium of *Fgf15*$^{-/-}$ embryos, the number of postmitotic neurons in the MZ appears to be decreased (as assessed by TuJ1 and Dcx expression). Furthermore, the expression of the neurogenic bHLH genes *Hes3* and *Hes5* is increased in the neuroepithelium of mutant embryos, concomitant with a decrease in the expression of the proneural genes *Mash1*, *Ngn1*, *Ngn2* and *NeuroD*. The up-regulation of *Hes3* and *Hes5* and the down-regulation of *Mash1*, *Ngn1* and *Ngn2* in *Fgf15*$^{-/-}$ embryos indicates that already during the early steps of neurogenesis, neuroepithelial cells are not correctly specified towards a neuronal fate. Consequently, more downstream proneural genes such as *NeuroD* are even more affected in *Fgf15* mutant embryos, indicating that neuroepithelial cells do not progress through subsequent steps of neuronal differentiation. The perturbed differentiation is further confirmed by an up-regulation of the *Id* genes *Id1* and *Id3* in the anterior neural tube of *Fgf15*$^{-/-}$ embryos. The persistence of some TuJ1/Dcx positive cells in the MZ and the down-regulation but not complete loss of expression of proneural genes suggest that neuronal differentiation is not completely abolished in *Fgf15*$^{-/-}$ embryos, but that a fraction of cells fail to exit the cell cycle in the absence of *Fgf15* and therefore do not initiate their differentiation program. The function of Fgf15 in mouse neurogenesis may be similar, at least in part, to the role of Fgf19 in the zebrafish forebrain, where the inhibition of Fgf19 leads to the failure of GABAergic neuron and oligodendrocyte development (Miyake et al., 2005). In zebrafish embryos injected with a morpholino against *Fgf19* mRNA, neural cells in the forebrain are not specified towards a GABAergic or oligodendrocyte fate. While the function of zebrafish Fgf19 in neurogenesis appears to be more restricted to specific subpopulations of neuronal and glial cells, a common mechanism may initially be activated in mouse and zebrafish upon Fgf15/19 signaling, which promotes the differentiation of neuroepithelial cells towards a specific fate. Whether this mechanism involves the regulation of cell cycle exit also in zebrafish, however, has not been addressed. Furthermore, it should be noted that marked differences exist between the phenotypes of the mouse *Fgf15* knock-out and the *Fgf19* morpholino knock-down in zebrafish. Fgf19 promotes cell proliferation and is involved in the patterning of the forebrain in zebrafish (Miyake et al., 2005), whereas Fgf15 promotes cell cycle withdrawal and does not show obvious patterning activity (this work). The discrepancy between these findings may be explained by the low homology between Fgf15 and Fgf19 of only 51% on amino acid level (compared to >90% between all other Fgf orthologs) (Ornitz and Itoh, 2001). The low homology and functional diversity between these two orthologs suggests that Fgf15 and Fgf19 have diverged substantially and may have adopted partially different functions during vertebrate evolution.

The perturbed differentiation of neuronal precursors in *Fgf15*$^{-/-}$ embryos also results in a defective layering of the neuroepithelium. During wild type neurogenesis, neuronal precursors that exit the cell cycle and differentiate into neurons migrate towards the MZ of the neuroepithelium, a process that leads to the separation of progenitors/precursors located in the VZ and SVZ, and postmitotic neurons situated in the MZ. In *Fgf15*$^{-/-}$ embryos, in contrast, this separation is no longer evident. Although TuJ1/Dcx positive cells are still correctly located in the MZ of the neuroepithelium in *Fgf15*$^{-/-}$ embryos, the ectopic expression of *Hes5*, *Id1*, *Id3* and Ki67 in the MZ of mutant embryos indicates that a fraction of cells that migrate out of the VZ and SVZ and populate the MZ still remain in the cell cycle and retain an undifferentiated progenitor state in the absence of *Fgf15*.

Several aspects of the neural phenotype of *Fgf15*$^{-/-}$ embryos, e.g. the infolding of neural tissue, the down-regulation of the expression of proneural genes and the up-regulation of *Id1* expression, are more distinct in the dorsal than in the ventral neural tube, which correlates well with the expression pattern of *Fgf15* mRNA. This is most evident for the aberrant expression of Nestin in E12.5 embryos with morphological defects, which occurs specifically in areas which express high levels of *Fgf15* in the wild type. These findings further argue for a specific function of Fgf15 in the developing CNS which appears to be independent from secondary effects caused by cardiac defects or growth retardation.

The finding of a narrow territory at the position of the isthmic organizer which does not express *Fgf15* (corresponding to the anterior part of the isthmic *Fgf8* expression domain) further supports a function of Fgf15 in neurogenesis. It has been demonstrated that the isthmic organizer territory exhibits delayed neuronal differentiation, and that neurogenic bHLH transcription factors (Hes1 and Hes3 in mouse, Her5 in zebrafish) are involved in the maintenance of undifferentiated neural progenitors in this region (Hirata et al., 2001; Geling et al., 2003). Therefore, the specific absence of *Fgf15* transcripts in a region of delayed neurogenesis is in line with a putative role of this factor in promoting neuronal differentiation. Interestingly, while ectopic expansion of *Hes5* expression into the MZ is observed in the entire anterior neural tube of *Fgf15*$^{-/-}$ embryos, *Hes3* expression remains restricted to the isthmic organizer territory and is only marginally expanded in its A/P extent. This is in agreement with previous findings indicating that Hes5 plays a more general role in maintenance of neural progenitor cells in the developing CNS, whereas Hes3 seems to be more specific to the isthmic organizer territory (Hirata et al., 2001; Hatakeyama et al., 2004; Ross et al., 2003). Thus, while a deregulation of neurogenesis in *Fgf15*$^{-/-}$ embryos leads to a ubiquitous ectopic transcription of *Hes5* in the anterior neural tube, only progenitor cells

located in the isthmic organizer region seem to be competent to express *Hes3*. Why the expression of *Hes1* apparently remains unaffected by the loss of *Fgf15* is not clear. Since previous studies have shown that Hes1 is involved in the maintenance of neuronal progenitors (Ishibashi et al., 1995; Castella et al., 2000) and that it functions in a partially redundant manner with Hes3 and Hes5 (Ohtsuka et al., 1999; Hirata et al., 2001; Hatakeyama et al., 2004; Kageyama et al., 2005), an activation of Hes1 might have been expected in *Fgf15*$^{-/-}$ embryos. It should be noted, however, that in case of a transgenic mouse line expressing a constitutively active form of β-catenin, defects in cell cycle exit result in an ectopic expression of *Hes5*, but only to a marginal increase in *Hes1* expression (Chenn and Walsh, 2002), suggesting that the transcriptional control of these two factors is linked differently to cell cycle exit. This is in line with a previous report which demonstrated that the expression of *Hes5* is down-regulated upon inactivation of Notch1, whereas the expression of *Hes1* remains unaffected (de la Pompa et al., 1997).

4.5 The cell cycle exit defect in *Fgf15*$^{-/-}$ embryos may be mediated by hypoactive retinoblastoma proteins

The implication of Fgf15 as a factor that promotes cell cycle exit and neurogenesis is somewhat surprising, given the classical characterization of the gene family as growth factors and the accumulating evidence for the mitogenic activity of several Fgfs (Basilico and Moscatelli, 1992; Reuss and von Bohlen und Halbach, 2003). However, there are also more recent findings in non-neural systems suggesting a role of Fgf signaling in promoting differentiation and at the same time suppressing proliferation. During chondrogenesis, for example, activating mutations in Fgfr3 result in reduced growth of long bones due to decreased proliferation and premature differentiation of chondrocytes (Ornitz and Marie, 2002; Dailey et al., 2003), whereas loss of Fgfr3 function in mouse leads to overgrown and deformed long bones (Deng et al., 1996). In recent years considerable progress has been made towards an understanding of the mechanism(s) underlying these phenotypes. *In vitro* experiments using chondrocytic cell lines have shown that during chondrogenesis, Fgf signaling induces growth arrest and differentiation of chondrocyte precursors. This growth arrest is accompanied by the dephosphorylation of retinoblastoma proteins and the induction of p21 (a Cdk inhibitor) in chondrocyte precursors (Dailey et al., 2003), whereas an inactivation of retinoblastoma proteins abolishes the effect of Fgf signaling on growth arrest

(Laplantine et al., 2002). The dephosphorylation of the retinoblastoma protein p107 occurs immediately upon Fgf treatment, independently of transcriptional activity, while dephosphorylation of the retinoblastoma proteins Rb and p130 shows a considerable time delay and proves to be dependent on gene transcription. These findings have been interpreted in the way that the effect of Fgf signaling on p107 appears to be direct and initiates growth arrest, whereas the effect on Rb and p130 involves *de novo* gene transcription and is believed to maintain growth arrest. Furthermore, it has been suggested that the dephosphorylation of the retinoblastoma proteins may be mediated by an intracellular phosphatase that is activated upon Fgf signaling (Dailey et al., 2003).

A similar mechanism could underlie the Fgf15 activity in the neuroepithelium. The hypothesis that Fgf15 may regulate the phosphorylation levels and/or total protein levels of retinoblastoma and/or Cdki proteins, respectively, was therefore tested in the present work. However, only the detection of p107 in Western blot experiments of total protein extracts from whole embryo heads proved to be successful, and in these assays no differences neither in the phosphorylation state nor in the expression level of p107 could be detected. Nevertheless, the overt increase of neuroepithelial cells which aberrantly remain in the cell cycle in *Fgf15*$^{-/-}$ embryos at E11.5 strongly suggests that cell cycle regulators are affected by the loss of *Fgf15*. Whether a similar mechanism as in chondrocytes, involving the dephosphorylation of Rb proteins, is also active during neurogenesis or whether different or additional components of the cell cycle machinery are affected, still remains to be seen. However, the neural phenotypes displayed by mouse lines deficient for one or more members of the retinoblastoma protein family, are of striking similarity to observations reported here for *Fgf15* deficient mice.

Rb$^{-/-}$ embryos display an increased number of proliferating cells in the hindbrain and spinal cord, and these cells are ectopically located outside of the VZ (Jacks et al., 1992; Lee et al., 1994). In the peripheral nervous system (PNS) of these mice differentiation is impaired, as assessed by a down-regulation of βII-tubulin (Lee et al., 1994). In addition to a neural phenotype, *Rb*$^{-/-}$ mice exhibit defects in erythropoiesis, resulting in hypoxia and widespread apoptosis, which also affect the CNS and PNS. Brain-specific inactivation of *Rb* rescues the apoptosis observed in the CNS of *Rb*$^{-/-}$ embryos, whereas the increase of proliferating cells in the CNS and their ectopic localization outside of the VZ persist (MacPherson et al., 2003; Ferguson et al., 2002). Strikingly, these embryos display an increased brain size, with occasional large telencephalic protrusions in case of a telencephalon-specific inactivation of *Rb* (Ferguson et al., 2002). The latter observation, in particular, is reminiscent of the excess

neural tissue generated in 10% of *Fgf15*$^{-/-}$ embryos. In adult *p107*$^{-/-}$ mice, a marked increase in proliferating neural progenitors has been reported, and both *p107*$^{-/-}$ adult brains as well as E10.5 embryos exhibit increased numbers of neural stem cells (NSCs). The increase of NSCs is accompanied by an up-regulation of Notch signaling in *p107* deficient embryos at E14.5 (Vanderluit et al., 2004). In case of *p107*$^{-/-}$ mice, the increased size of the progenitor pool does not lead to an enlargement of the brain, since it has been shown that the enhanced rate of proliferation is balanced by increased apoptosis in neural tissue (Vanderluit et al., 2004). In *p130* deficient embryos, the number of proliferating cells at E10.5 is increased more than twofold specifically in the brain and spinal cord, concomitant with an impairment of motor neuron differentiation. Furthermore, the neuroepithelium in these embryos is not properly organized into layers and lacks a basement membrane (LeCouter et al., 1998).

Therefore, the inactivation of retinoblastoma proteins in mice results in partially similar neural phenotypes as the loss of *Fgf15*. In both cases, cell cycle exit is perturbed, leading to an increased size of the neuronal progenitor pool. The increased progenitor pool in *Fgf15*$^{-/-}$ embryos occasionally leads to an infolding of excess neural tissue into the lumen of the neural tube, and in conditional *Rb*$^{-/-}$ embryos to the generation of large telencephalic protrusions (Ferguson et al., 2002). The enhanced proliferation is accompanied by impaired neuronal differentiation in the CNS in case of *Fgf15*$^{-/-}$ and *p130*$^{-/-}$ embryos (LeCouter et al., 1998), and in the PNS in case of *Rb*$^{-/-}$ embryos (Lee et al., 1994). In both *Fgf15* and *p107* deficient embryos, Notch activity is increased, as assessed by an up-regulation of *Hes3* and *Hes5* in *Fgf15*$^{-/-}$ embryos and of *Notch1*, *Delta-like1* and *Hes1* in *p107*$^{-/-}$ embryos (Vanderluit et al., 2004). In light of the similar neural phenotypes between mice deficient for these retinoblastoma proteins and the *Fgf15*$^{-/-}$ mice, I therefore hypothesize that Fgf15 may activate, directly or indirectly, one or more members of the retinoblastoma protein family to initiate cell cycle exit and subsequently, neuronal differentiation in the anterior neural tube during embryonic development.

The idea that growth factors in general - in contrast to their original definition - may rather support cell cycle withdrawal and differentiation is supported by recent data from Siegenthaler and Miller (2005). In that study, it has been demonstrated that the transforming growth factor β1 (Tgf β1) promotes cell cycle exit in organotypic cortical slice cultures from rat embryos through the up-regulation of the Cdki p21. Therefore, a protein originally characterized as growth factor is involved in the control of cell cycle withdrawal by regulating components of the cell cycle machinery, a similar function to that proposed here for Fgf15 in the anterior neural tube.

4.6 The exceptional structure of the Fgf15 protein may account for its unique function in neural development

While Fgfs have been implicated in numerous processes in the developing CNS like proliferation, cell survival, cell migration, patterning and differentiation (Dono, 2003; Ford-Perriss et al., 2001; Reuss and von Bohlen und Halbach, 2003), the growth inhibitory function of Fgf15 in neural development appears to be distinct from any other member of the Fgf family. A possible explanation may be provided by the structural peculiarity of the Fgf15 protein compared to other Fgfs. A recent study has demonstrated that the protein structure of Fgf15 differs in two distinct features from the structure of other Fgf proteins (Harmer et al., 2004). First, a disulfide bond was identified which is not present in any other Fgf protein. Second, while Fgf proteins usually contain 12 β-strands, in Fgf15 the β11 strand is replaced by a helix domain. Interestingly, these variations from the common Fgf protein structure are conserved in human FGF19, the ortholog of murine Fgf15. It has been speculated that these unique structural features may explain the unusual receptor affinity of FGF19 exclusively to FGFR4 and its low affinity to heparin in *in vitro* assays (Xie et al., 1999; Harmer et al., 2004). In the mouse, *Fgfr4* expression is not detectable by radioactive *in situ* hybridization in the anterior neural tube during embryonic development (Blak et al., 2005), a finding that may be contradicting a possible function of Fgfr4 to transduce the Fgf15 signal during neurogenesis. However, since *Fgfr4* mRNA was detected by RT-PCR in the embryonic brain at E15 (Cool et al., 2002), a weak expression of *Fgfr4* in the anterior neural tube below detection level of radioactive *in situ* hybridization cannot be ruled out. The finding of co-expression of *Fgf15* and *Fgfr4* in the otic vesicles further supports a possible interaction of Fgf15 with Fgfr4 (Wright et al., 2003). On the other hand, *Fgfr1-3* are differentially expressed in the anterior neural tube (Blak et al., 2005) and may therefore also act as Fgf15 receptors in neural development. In addition, FGF19-FGFR4 binding has only been determined *in vitro*, and it is not known whether ligand-receptor pairing has been conserved throughout evolution. While a specific receptor for the transduction of the Fgf15 signal has not been identified to date, it is not clear whether ligand-receptor specificity underlies the differential response to different Fgfs at all, since all Fgfrs appear to signal through the same pathways, differing only in the amplitude of the signal (Dailey et al., 2005). Therefore, another mechanism beside receptor specificity may underlie the unique function of Fgf15 in neural development. It may be hypothesized, for example, that the structural peculiarity of the Fgf15 protein underlies an as yet unknown mechanism of ligand-receptor interaction or receptor activation. Another

explanation could be a specific interaction of Fgf15 with other extracellular modulators which is facilitated by its unique structure.

4.7 Direction of future experiments on Fgf15 function in neural development

As pointed out in the introduction, cell cycle exit and differentiation are tightly linked during neurogenesis. Cell cycle regulators have been shown to influence neural differentiation, while proneural/neurogenic bHLH factors affect cell cycle withdrawal (reviewed in Ohnuma and Harris, 2003). Therefore, at least two different functions of Fgf15 during neurogenesis are possible: 1) Fgf15 may directly promote cell cycle exit of neuroepithelial cells by regulating components of the cell cycle machinery. As a consequence of this defective cell cycle withdrawal, neuroepithelial cells would not initiate their differentiation program, resulting in the misexpression of neurogenic and proneural bHLH genes. 2) Conversely, Fgf15 could regulate the expression of neurogenic and/or proneural genes in neuroepithelial cells. The down-regulation of neurogenic genes and/or up-regulation of proneural genes in neural progenitors upon Fgf15 signaling would then result in cell cycle withdrawal of these cells. At present, the mechanism of Fgf15 activity in neurogenesis is not known. However, while an Fgf15-mediated regulation of neurogenic/proneural bHLH gene expression can only be speculated, the hypothesis of a direct role of Fgf15 in the regulation of the cell cycle exit machinery is supported by results obtained in chondrocyte differentiation experiments *in vitro* (Dailey et al., 2003; Laplantine et al., 2002) and by the striking similarities between the phenotypes of mice deficient for retinoblastoma proteins and Fgf15, respectively (Jacks et al., 1992; Lee et al., 1994; LeCouter et al., 1998; Ferguson et al., 2002; MacPherson et al., 2003; Vanderluit et al., 2004).

To address the mechanism of Fgf15-mediated cell cycle regulation, an *in vitro* system is currently being established using primary cell cultures of cortical cells from E12.5 mouse embryos. This system allows GOF experiments (using either an *Fgf15* expression vector or commercially available FGF19 protein (R&D Systems)), as well as rescue experiments by using primary cultures from *Fgf15*$^{-/-}$ embryos. In this system, the effect of Fgf15/FGF19 on cell cycle exit and neuronal differentiation will be tested. If the results of the *in vitro* experiments are consistent with the data obtained for *Fgf15*$^{-/-}$ embryos *in vivo*, a new attempt

to address the mechanism underlying cell cycle withdrawal by Fgf15 such as retinoblastoma protein dephosphorylation or Cdki up-regulation will be undertaken.

Another important issue is the function of Fgf15 later in embryonic development and in the adult. While I could show that early neurogenesis is affected in *Fgf15*$^{-/-}$ embryos, it is unclear whether this effect is restricted to the 'generic' differentiation into neurons, or whether loss of Fgf15 would also affect more specifically the differentiation of neuronal subpopulations as well as the generation of astrocytes and/or oligodendrocytes later in development, similar to the results obtained for Fgf19 in zebrafish concerning forebrain GABAergic neurogenesis and oligodendrogenesis (Miyaka et al., 2005). Another question arising from the present results is whether Fgf15 also plays a role in adult neurogenesis, as it was shown that *Fgf15* is expressed at early postnatal stages of mouse development in the rostral migratory stream (RMS), a site of adult neurogenesis, as well as in the granular and periglomerular layer of the olfactory bulb, a target region for neurons migrating along the RMS (Gimeno et al., 2003). In order to address these questions, the generation of a conditional *Fgf15* knock-out mouse line was started, which will allow the spatially and temporally restricted inactivation of *Fgf15* gene function, thereby circumventing the embryonic lethality as well as secondary effects caused by non-neural functions of Fgf15.

4.8 The Wnt1 signal required for the generation of mesDA neurons may be transduced by Fzd6

Like Fgfs, the large Wnt family of secreted glycoproteins has been implicated in numerous developmental, physiological and disease-related processes (Miller et al., 2002; Logan and Nusse, 2004; Yamaguchi et al., 2001). In the developing CNS, Wnt signaling has been shown to control proliferation, differentiation, cell survival and neural connectivity (Wurst and Bally-Cuif, 2001; Prakash and Wurst, 2004; Ciani and Salinas, 2005). A recent publication has implicated Wnt1 as a crucial factor in mesDA neuron development (Prakash et al., 2006). In that study, Wnt1 has been shown to exert two different functions in mesDA neuron generation. Early in this process, it is necessary for the establishment of the mesDA progenitor domain by regulating a characteristic genetic network in the caudal ventral midbrain. Later in development, Wnt1 is required for the terminal differentiation of mesDA neurons, probably by regulating the expression of *Pitx3*, as it has been shown that in the absence of Wnt1, no Pitx3-expressing cells are generated (Prakash et al., 2006). While these findings demonstrate that Wnt1 is involved in the regulation of the identity and fate of these neurons, the downstream signaling cascade that is activated in mesDA progenitors upon Wnt1 signaling has not been determined. To approach this issue, I examined the expression of the *Fzd* genes in early mouse neural development, as these encode the receptors for the secreted Wnt ligands (Huang and Klein, 2004). Fzd6 was identified as one receptor displaying a very specific expression pattern in the ventral midbrain and therefore is a possible candidate to act as receptor for Wnt1. However, other *Fzd* genes are also expressed in this region, making a redundancy between these receptors very likely.

Of the 10 murine *Fzd* genes, *Fzd3*, *Fzd6* and *Fzd9* are expressed in the caudal cephalic flexure during early neural development of the mouse. Other members of the Fzd family are either not expressed at all in the ventral midbrain (*Fzd4*, *Fzd5*, *Fzd8*, *Fzd10*) or display a gap in their expression in the caudal cephalic flexure (*Fzd1*, *Fzd2*, *Fzd7*). Strikingly, *Fzd6* expression is restricted specifically to the region where mesDA neurons arise, while *Fzd3* and *Fzd9* are expressed in a much wider domain. Furthermore, the gap in the expression of *Fzd1*, *Fzd2* and *Fzd7* corresponds closely to the *Fzd6* expression domain in the caudal cephalic flexure. Colocalization studies further demonstrated a close congruency of *Fzd6* and *Wnt1* expression in the cephalic flexure, suggesting that Fzd6 might indeed act as a Wnt1 receptor in the caudal cephalic flexure in early mouse neural development. At E10.5, *Wnt1* and *Fzd6* expression overlap in the caudal ventral midbrain, while *Wnt1* expression extends more

rostrally than *Fzd6*. Therefore, Fzd6 may transduce the Wnt1 signal in the caudal part of the cephalic flexure, whereas in the more rostral part, other members of the Fzd family may function as Wnt1 receptors. Both *Fzd6* and *Wnt1* are initially expressed throughout the entire width of the neuroepithelium at E10.5, but appear to be restricted mostly to the VZ by E12.5, suggesting that Fzd6-mediated Wnt1 signaling may be active in neural progenitors and precursors, but not in postmitotic neurons which are situated in the MZ, in line with what has been suggested by Prakash et al. (2006).

mesDA progenitors, identified by the expression of *Aldh1a1*, colocalize with *Fzd6* expression, although this was not resolved on a cellular level. Nonetheless, the coexpression of *Fzd6* and *Aldh1a1* in the mesDA progenitor domain suggests that mesDA neuronal progenitors receive the Wnt1 signal via the Fzd6 receptor. At E11.5, *Fzd6* expression is restricted to the VZ and SVZ, but absent from the MZ, indicating that neural progenitors and precursors but not postmitotic cells express *Fzd6* at this stage. *Aldh1a1*, in contrast, is also expressed in the MZ of the ventral midbrain, consistent with the notion that it is expressed by mesDA progenitors and postmitotic progeny alike (Wallen et al., 1999).

Fzd6 may also function as a Wnt1 receptor necessary for the induction of *Pitx3* expression during terminal differentiation of mesDA neurons. The expression of *Fzd6*, *Wnt1* and *Aldh1a1* overlap substantially at E10.5 and E11.5, a period shortly before (E10.5) or when (E11.5) Pitx3 is expressed in postmitotic mesDA neurons (Smidt et al., 1997; Smidt et al., 2004). The findings that *Fzd6* and *Wnt1* continue to be co-expressed in the VZ of the cephalic flexure at E12.5, but that both genes show only a minimal, if any, overlap with *Pitx3* expression at E11.5 and E12.5, further support that Wnt1 signaling may be required to initiate *Pitx3* transcription but is not necessary for its maintenance. This is in line with the temporal expression pattern of *Wnt1* and *Pitx3*, since *Wnt1* is expressed until E14.5 and is not expressed thereafter (data not shown), whereas *Pitx3* expression starts at E11.5 and persists into adulthood (Smidt et al., 1997). The co-expression of *Wnt1* and *Fzd6* at E11.5 and E12.5 further suggests that at these stages, the Wnt1-mediated induction of *Pitx3* transcription may continue in mesDA precursors located in the VZ, thus contributing to the increase in Pitx3-expressing postmitotic mesDA neurons in the MZ between E11.5 and E14.5 (Smidt et al., 2004; Maxwell et al., 2005).

4.9 Direction of future experiments on Wnt signaling in mesDA neuron development

Since Wnt1 has been implicated as a crucial factor in the generation of mesDA neurons, the lack of an appropriate receptor in cells that normally receive the Wnt1 signal in the caudal cephalic flexure should result in a similar mesDA phenotype as observed in *Wnt1*$^{-/-}$ embryos (Prakash et al., 2006). In the present study, three possible candidate receptors, Fzd3, Fzd6 and Fzd9, which may be involved in mesDA neuron development, were identified. LOF experiments in the mouse have been reported for all three genes encoding these proteins (Wang et al., 2002; Lyuksyutova et al., 2003; Guo et al., 2004; Zhao et al., 2005; Ranheim et al., 2005). Mice lacking *Fzd3* display aberrant A/P projections of commissural axons in the spinal cord and an absence of major fiber tracts in the developing rostral CNS, including Th-expressing fibers from the mesDA neurons (Wang et al., 2002). Interestingly, the loss of axonal fiber tracts is accompanied by increased cell death specifically in the striatum, a major target region of mesDA neurons, while other brain regions do not exhibit increased numbers of apoptotic cells. However, a loss of mesDA neurons in *Fzd3*$^{-/-}$ mice has not been observed (Wang et al., 2002). Mice lacking *Fzd6* show an abnormal macroscopic hair patterning, reminiscent of wing-hair and bristle patterning defects observed in *Drosophila frizzled* mutants (Guo et al., 2004; Vinson et al., 1989). While this suggests that Fzd6 may act via the planar cell polarity pathway in the skin, an involvement of Fzd6 in brain development and in particular in mesDA neuron generation has not been addressed. Analysis of *Fzd9*-deficient mice revealed defects in the development of the hippocampus (Zhao et al., 2005). In these mice, apoptosis was increased in the developing dentate gyrus, concomitant with a compensatory increase in proliferating cells in this region, resulting in visuospatial learning deficits and a decreased seizure threshold in adult animals. In addition, *Fzd9*$^{-/-}$ mutant mice exhibit an impairment of B-cell development (Ranheim et al., 2005). Again, the development of mesDA neurons has not been addressed in these studies.

Since the expression data presented in this work suggests a role of one or more of these three receptors in mesDA neuron development, a thorough analysis of the mesDA system in the above mentioned mutant mouse lines is necessary to address this question on a functional level *in vivo*. To account for possible redundancies between different Fzd receptors in this context, the analysis will have to include mouse lines in which two or even all three of the putative Wnt1 receptors identified in this study are inactivated. In a first approach, *Fzd3*$^{-/-}$ and

Fzd6$^{-/-}$ single and double mutant mouse lines are currently being analyzed in respect to mesDA neuron development.

A necessary prerequisite for Fzd6 to mediate the Wnt1 signal in mesDA neuron generation is the direct interaction of Wnt1 and Fzd6. Furthermore, although there are indications that the Wnt-mediated effect on mesDA neuron development may be transduced via the canonical Wnt/β-catenin pathway (Castelo-Branco et al., 2004), the Wnt1 signal transduction cascade in mesDA neurogenesis *in vivo* still remains unknown. In addition, it is still unclear whether Pitx3 could be activated directly or indirectly by a Wnt1-mediated signal in this process. To address these issues, *in vitro* experiments will be performed using the neural AHP and AHP-Wnt1 cell lines that were further characterized in this study. The finding that AHP-Wnt1 cells differentiate into DA neurons (expressing Th, *Nr4a2* and *Slc6a3*) to a larger extent than wild type AHP cells (D.-C. Lie, personal communication) further underlines the pivotal role of Wnt1 in DA neuron development. If Fzd6 functions as a specific receptor for Wnt1 in this process, the overexpression of Fzd6 in AHP-Wnt1 cells should further promote the generation of DA neurons in this assay. To test this hypothesis, AHP and AHP-Wnt1 cell lines stably expressing Fzd6 will be established and tested for DA neuron differentiation. In addition, these cell lines will provide a tool to directly examine ligand-receptor binding and may help to identify further downstream components and target genes of the Wnt signaling cascade essential for mesDA neuron development. These projects are currently the subject of a separate thesis in our group.

5. Material and methods

5.1 Laboratory equipment

Autoclave:	ASS and Aigner, Typ 667-1ST
Benchtop shakers:	Heidolph, Unimax 2010, Polymax 1040;
Benchtop thermostats:	Eppendorf, Thermomixer 5463/Comfort
Cameras:	Zeiss, AxioCam MRC, HRC; Fuji, HC2000
Centrifuges:	Sorvall, RC5C Plus (Rotors: GSA, SA600) Heraeus, Biofuge pico/fresco, Varifuge 3.0R Hettich, Universal 30F, Eba 12
Cryostat:	Microm, HM 560
Developing machine for X-ray films:	AGFA, Curix 60
Electrophoresis power supplies:	E-C Apparatus Inc., EC 250-90, EC3000-90 Consort, E443
Freezers (-20°C):	Liebherr
Freezers (-80°C):	Heraeus
Geiger counters:	Berthold, LB122
Gel documentation:	Herolab
Gel electrophoresis chambers:	MWG Biotech; PeqLab
Hybridization ovens:	ThermoHybaid; UVP, Hybridizer HB100
Hybridization tubes:	Thermo Hybaid
Incubators (bacteria):	New Brunswick, Innova 4230
Incubators (eucaryotic cells)	Heraeus
Isotope counter:	Scott - lab, Easicount 400
Laminar flows:	Nunc, Laminar Flow Workstation, Microflow Safety Cabinet
Light sources:	Leica, KL 1500; Zeiss, KL 2500 LCD
Magnetic stirrers:	IKA Labortechnik, RCT basic
Microscopes:	Leica DMIL, MZ8, MZ6, APO, M3Z Zeiss Axiovert 200M, Axioplan 2, Stemi SV 6, LSM 5 META
Microtomes:	Microm, HM 355S; Leica
Microwave oven:	Sharp
Paraffin embedding station:	Sakura, Tissue-TEK® TEC
PCR machines:	Eppendorf, Mastercycler Gradient
pH indicator:	WTW, pH 538
Photometer:	Eppendorf, Biophotometer
Pipettes (10µl - 1ml):	Gilson

Pipetting aids:	Brand, Accujet®
Precision balances:	Sartorius LC220S, LC6201S, BA210S
Refrigerators:	Liebherr
Stator disperser:	IKA Labortechnik, Ultraturrax
Thermomixers:	Eppendorf
Ultra pure water purification system:	Millipore, MilliQ
	Brand, Nutator
UV-DNA/RNA-Crosslinker :	Stratagene, UV Stratalinker ®1800
Vortexers:	Scientific Industries, Vortex Genie
Waterbaths:	Julabo U3 ; Lauda A100/E100; Leica HI 1210

5.2 Suppliers of enzymes, chemicals, kits and other consumables

The suppliers of materials and kit systems are cited with the corresponding method. Laboratory glass ware was obtained from Schott. Unless otherwise stated, all chemicals were supplied by Sigma-Aldrich. Restriction enzymes, T3, T7, SP6 RNA polymerases, RNase inhibitors and yeast tRNA were obtained from Roche Diagnostics.

Miscellaneous:

Ampuwa® water	Fresenius AG, Bad Homburg
Autoradiography films (Biomax, X-OMAT), X-ray cassettes	Amersham, Freiburg
Bacteria culture dishes, disposable pipettes	Greiner Labortechnik, Frickenhausen
Consumables for cell culture	Nunc, Wiesbaden
Developer (D-19), Fixer	Kodak, New Haven, USA
DNA standard for gel electrophoresis (Smartladder®)	Eurogentec, Köln
Embedding molds	Polysciences, Peel-A-Way
Falcon® tubes, canulas, syringes	Becton Dickinson, Europe (Schubert & Weiss, München)
Nuclear fotoemulsion (type NTB-2)	Kodak, New Haven, USA
Parafilm®	American National Can, USA
Pipette tips 0.1-10µl; 1-20µl; 1-200µl; 101-1000µl	Starlab, Ahrensburg
Safe-Lock reaction tubes (1.5/2.0ml)	Eppendorf, Hamburg
X-ray films:	RM2155

5.3 Working with deoxyribonucleic acids (DNA)

5.3.1 Cleavage of plasmid DNA by restriction endonucleases

Plasmid DNA was cleaved by commercially available restriction endonucleases (RE). The amount of enzyme per µg DNA was 1-10 units. Conditions were set up according to manufacturer's recommendations and the reaction was incubated for at least 1h.

5.3.2 Dephosphorylation of linearized plasmids

To prevent the religation of a linearized plasmid, the 5' ends are dephosphorylated. To this end, the plasmid was incubated with shrimp alkline phosphatase (USB Corporation) at 37°C for 30min. The enzyme was added directly after the restriction digest. After the reaction, the plasmid was isolated either by isopropanol precipitation (see 5.3.4.1) or by gel extraction (see 5.3.2).

5.3.3 DNA gel electrophoresis

Depending on the fragment sizes to be separated, TAE/agarose gels containing 0.8% (separation of large fragments up to 10kb) to 2% agarose (separation of small fragments 100-200bp) were used. DNA fragments were visualised by adding 1µg/ml ethidium bromide to the gel, which intercalates into the DNA and fluoresces at 312nm and 366nm of UV light.
6x sample buffer was added to the DNA samples, the samples were loaded on the gel and the fragments were separated in a 60-100V electric field.

50x TAE:
1.5M Tris base
1M acetic acid
0.05M EDTA
pH 8.5

6x sample buffer:
0.2% bromophenol blue
60% glycerol

5.3.4 DNA isolation

5.3.4.1 Isopropanol precipitation of DNA

DNA was precipitated from aqueous solutions by adding 1/10 volume of 3M sodium acetate (pH 5) and 1 volume isopropanol. After inverting the tube several times, the DNA precipitated as a filamentous pellet. The sample was centrifuged for 1min at 16000g, washed with 70% ethanol and centrifuged again for 1min at 16000g. The ethanol was removed with a pipette, DNA was air dried for 5-10min and redissolved in TE buffer or aqua dest.

TE buffer: 10mM Tris-HCl pH 7.5-8.0
1mM EDTA

5.3.4.2 Gel extraction of DNA fragments

The isolation of DNA fragments after gel electrophoresis was carried out using the QIAquick® Gel Extraction Kit (Qiagen) according to manufacturer's specifications. The DNA fragment of interest was excised from the gel and purified following the protocol of the kit.

5.3.4.3 Purification of PCR products

PCR products were isolated using the QIAquick® PCR Purification Kit (Qiagen) according to manufacturer's specifications.

5.3.5 Determination of DNA and RNA concentration

DNA and RNA concentration was measured using the BioPhotometer (Eppendorf) following manufacturer's instructions. To estimate the quality of the DNA, the ratio of absorbance at 260nm and 280nm was determined. A_{260}/A_{280} values ≥ 1.8 were obtained for purified DNA.

5.3.6 Ligation of DNA fragments

To covalently bind two DNA ends, T4 DNA ligase was used to create a new phosphodiester bond between the two ends, of which at least one has to carry a 5' phosphate group. Between 20-100ng of vector and a 3 – 5 fold molar excess of insert were applied in a ligation reaction. The Rapid DNA Ligation Kit (Roche Diagnostics) was routinely used to carry out DNA ligations.

Ligation reaction:
2µl 5x dilution buffer
xµl vector
xµl fragment
ad 10µl aqua dest.

The reaction set up was heated 5min to 70°C and cooled down on ice.

10µl 2x reaction buffer
1µl T4 DNA Ligase

were added and incubated 5-15min at RT. The resulting ligation product was used to transform chemically competent bacteria (5.5.3)

5.3.7 TOPO-TA Cloning®

TOPO TA Cloning® (Invitrogen) is designed to clone PCR fragments into a TOPO-Isomerase vector. The TOPO TA Cloning® kit (Invitrogen) was used following the manufacturer's protocol. The pCRII TOPO vector provided in the kit was used for cloning and the ligation product was transformed into One Shot® TOP 10 competent cells as described below (see 5.5.3).

5.3.8 DNA amplification by polymerase chain reaction (PCR)

Specifications of a routinely used PCR set up:

PCR reaction:	2µl	10x RedTaq® buffer (Sigma-Aldrich; contains $MgCl_2$)
	1µl	template (~50-200ng genomic DNA, 10ng plasmid DNA)
	0.5µl	dNTP (10 mM each)
	1µl	forward primer (10µM)
	1µl	reverse primer (10µM)
	0.25µl	RedTaq® DNA polymerase (5U/µl, Sigma-Aldrich)
	ad 20µl	aqua dest.

A list of primers is given in appendix 7.1. The PCR reactions were run in Eppendorf Mastercycler Gradient PCR machines. First, the samples were heated to 94°C for 2-4min to separate the DNA strands. Then a defined number of cycles were run dependent on the specific fragments that were amplified. In a routinely used PCR program cycles consisted of strand separation at 94°C for 30s, annealing of the primers for 30-60s (annealing temperature depends on the primers, ~5°C below melting temperature of the primers) and elongation of the primed DNA strands at 72°C for 30s to several minutes (dependent on the length of the fragments). A final elongation step at 72°C for 5-10min followed the cycles. At the end of the program samples were kept at 4°C.

5.3.9 DNA sequencing

DNA sequencing was carried out by the following companies:

MWG-BIOTECH AG
Anzingerstr. 7a
85560 Ebersberg
Germany

Sequiserve
Bahnhofstr. 30
85560 Vaterstetten
Germany

Entelechon GmbH
St.Veit-Weg 2
93051 Regensburg
Germany

5.3.10 Radioactive labeling of DNA probes

The random primed labeling (α-^{32}P-dCTP, Amersham) of DNA fragments was carried out using the Megaprime™ DNA-Labeling-System (Amersham). The labeled probe was purified with S300 Columns (Pharmacia Biotech) and the activity of the labeled probe was determined. Values in the range of 250-1000cpm/µl (counts per min and µl) were obtained.

5.3.11 Radioactive end labeling of oligonucleotide probes

Oligonucleotides were radioactively end-labeled with γ-^{32}P-dATP (Amersham) using the 5'-end labeling kit (Amersham), purified with the Qiaquick® Nucleotide Removal Kit (Qiagen) and the activity of the labeled probe was determined. Values in the range of 100-300cpm/µl were obtained.

5.3.12 Isolation of genomic DNA from mouse tissue

5.3.12.1 Isolation of DNA from mouse tail tips

Genomic mouse tail DNA was isolated using the Wizard® Genomic DNA Purification Kit (Promega). Approximatly 0.5-1cm of mouse tail tissue was incubated over night in 480µl nuclei lysis solution (Promega), 100µl 0.5M EDTA and 20µl Proteinase K (20mg/ml) at 56°C. 3µl RNase A (10mg/ml) were added and the reaction was incubated for 30min at 37°C. Proteins were precipitated by adding 200µl protein precipitation solution (Promega) on ice and centrifuging for 10min at 16000g. The supernatant was transferred to a new reaction tube and 600µl isopropanol were added to precipitate the DNA. The DNA was pelleted at 16000g for 1min, washed with 70% ethanol, air dried for 10-15min and dissolved in 100µl 10mM Tris, 1mM EDTA, pH 8.0.

5.3.12.2 Isolation of DNA from mouse embryonic yolk sac tissue

For genotyping mouse embryos, yolk sac tissue was collected and incubated over night at 56°C in 100µl Fast PCR Lysis buffer containing 0.25µl Proteinase K (20mg/ml). The reaction was heated to 94°C to inactivate Proteinase K and centrifuged for 5min at 16000g. For a standard genotyping PCR (see 5.3.7), 1µl was used as template DNA.

Fast PCR Lysis buffer: 0.01M Tris-HCl pH 8.0
0.05M KCl
1.5mM $MgCl_2$
0.45% NP-40
0.45% Tween-20

5.3.13 Southern blot and hybridization with a radioactively labeled DNA probe

5.3.13.1 Restriction digest of genomic DNA

Genomic DNA was digested over night at 37°C with a suitable restriction enzyme.

Standard reaction set up: 10µg genomic DNA
3µl 10x buffer
0.3µl RNaseA (10 mg/ml)
3µl restriction enzyme (high concentrated, 40 U/µl)
2µl spermidine (0.1 M)
ad 30µl aqua dest.

5.3.13.2 Gel electrophoresis and blotting of the digested DNA

The restriction reaction was separated on a 0.8% agarose/TAE gel over night at 30V. Subsequently, the gel was denatured for 30min in denaturation buffer and neutralized 2x 15 minutes in neutralization buffer.
The DNA was blotted by capillary transfer in 20x SSC to a Hybond N+ nylon membrane (Amersham). To this end, a bridge of 3MM filter paper (Whatman, Maidstone, GB) was built over a tray containing 20x SSC. The gel (bottom side facing up), hybridization membrane, 2

3MM filter papers and several layers of bleached pulp were placed on top of the bridge in this order and the set up was weighed down with appropriate weights. Blotting was carried out over night at RT.

Denaturation buffer: 0.5M NaOH
1.5M NaCl

Neutralization buffer: 1.5M NaCl
0.5M Tris-HCl pH 7.5

20x SSC: 3M NaCl
0.3M sodium citrate
pH 7.0

5.3.13.3 Hybridization with a radioactively labeled probe

The nylon membrane carrying the blotted DNA was washed in 2x SSC and the DNA was cross-linked to the membrane with UV light (1200J, 60s). The membrane was prehybridized in 10ml Rapid Hyb Buffer (Amersham) at 65°C and subsequently hybridized with 50µl of radioactively labeled probe (see 5.3.9) in the same buffer for at least 3h. The membrane was washed 2x in low stringency wash solution at RT and 1-2x in high stringency wash solution at 65°C. Using a handheld geiger counter, the membrane should show an activity of 100-300cpm after the washes. An X-ray film was exposed to the membrane over night at -80°C.

Low stringency wash solution: 2x SSC
0.2% SDS

High stringency wash solution: 0.2x SSC
0.2% SDS

5.4 Working with ribonucleic acids (RNA)

Handling of RNA was carried out wearing gloves and using baked glass ware or RNase free disposable plastic materials at all times. Aqua dest. was treated with diethylopyrocarbonate (DEPC) and autoclaved twice prior to use.

5.4.1 Isolation of total RNA

5.4.1.1 Isolation of total RNA from mouse tissue

Mouse tissue (embryos and adult brain) was homogenized in 1ml TRIZOL® reagent (Invitrogen) per 100mg of tissue using a power homogenizer (Ultraturrax) and incubated at RT for 15min. 0.2ml chloroform per ml TRIZOL® reagent was added and the sample was shaken vigorously for 15s. After an incubation of 2-3min at RT, the sample was centrifuged at 12000g for 15min at 2-8°C. Following centrifugation, the mixture separated into a lower red phenol-chloroform phase and an upper colourless aqueous phase containing the RNA. The aqueous phase was transferred to a new reaction tube and the RNA was precipitated by adding 0.5ml isopropanol per ml TRIZOL® reagent used for the initial homogenization. Samples were incubated at RT for 10min and afterwards centrifuged at 12000g for 10min at 2-8°C. The supernatant was discarded, the RNA was washed with 70% ethanol, air dried and redissolved in the appropriate amount of DEPC-treated water.

5.4.1.2 Isolation of total RNA from cultured cells

Cells grown in a confluent monolayer were directly lysed in the culture dish using 1ml TRIZOL® reagent per 10cm^2. After lysis the RNA was isolated as described under 5.4.1.1 starting by adding 0.2ml chloroform per ml TRIZOL® reagent.

5.4.2 Northern blot and hybridization with a radioactively labeled DNA probe

5.4.2.1 Gel electrophoresis of RNA

For the electrophoretic separation of RNA fragments, 1.5% agarose gels containing formaldehyde and a special running buffer were used. 20µl loading buffer were added to 5µl RNA samples (~1.5µg/µl), samples were heated to 65°C for 5min, vortexed briefly and loaded onto a 1.5% agarose gel. Gels were run at 70 – 80V for 3-5h.

10x running buffer:	200mM MOPS 50mM sodium acetate 10mM EDTA pH 7.0
1.5% gel:	1.5% agarose 10% 10x running buffer 0.025mM ethidium bromide (10mg/ml) 0.6% formaldehyde solution in DEPC-treated water
Loading buffer:	0.025% bromophenol blue 40% formamide 7.4% formaldehyde 20% 10x running buffer

5.4.2.2 Blotting of RNA to a hybridization membrane

Blotting of RNA was carried out using the same setup for capillary transfer as described in 5.3.13.2. No denaturation and neutralization of the gel was necessary. Hybond XL membranes (Amersham) were used instead of Hybond N+ membranes.

5.4.2.3 Hybridization with a radioactively labeled probe

The membrane carrying the blotted RNA was washed in 2x SSC and the RNA was cross-linked to the membrane with UV light (1200J, 60s). The membrane was prehybridized in 10ml Quick-Hyb buffer (Stratagene) at 65°C and subsequently hybridized with 50µl of

radioactively labeled probe (see 5.3.9) in the same buffer over night. The membrane was washed in high stringency wash solution (see 5.3.13.3) at 65°C. Activity was monitored every 10-20min using a handheld geiger counter. After the washes, the membrane should show an activity of 100-300cpm. An X-ray film was exposed to the membrane over night at -80°C.

5.4.3 cDNA synthesis by reverse transcription

Single stranded cDNA was synthesized from total RNA (see 5.4.1) using the Advantage™ RT-for-PCR Kit (BD Biosciences, Clontech) following the manufacturer's instructions. A standard reaction yielded a 100µl cDNA sample, of which 2-5µl were used as template in a PCR setup.

5.5 Working with *Escherichia coli*

5.5.1 Storage of bacteria

For the long term storage of bacteria, glycerol stocks were prepared containing 250µl 80% glycerol in PBS and 750µl bacterial suspension from a 100ml over night culture. The glycerol stocks were stored at -80°C.

5.5.2 Preparation of chemically competent cells

Bacteria from a glycerol stock were streaked out onto an LB agar plate and incubated over night at 37°C. 5ml of LB medium were inoculated with a single colony and incubated over night at 37°C on a shaker. 1ml of this culture was used to inoculate 100ml of LB medium, which was incubated at 37°C on a shaker until the suspension had reached an OD_{600} of 0.3-0.4. The culture was centrifuged at 2000g for 10min at 4°C and resuspended on ice in 10ml TSS. 100-200µl of competent cells were used for a standard transformation (see 5.5.3).

1x LB medium: 0.1% Bactotrypton (Difco)
0.5% Bacto-Yeast-Extract (Difco)
0.17M NaCl
pH 7.0

TSS: 50% 2x LB medium (autoclaved)
10% polyethylenglycol (PEG)
5% DMSO
0.05M $MgCl_2$ (autoclaved)

LB-Agar: 1x LB medium
1.5% agar (Bacto-Agar, Difco)

5.5.3 Chemical transformation of bacteria

100-200µl of chemo-competent cells were thawed on ice and 1ng (retransformation) - 50ng (ligation reaction) DNA were added. The cells were incubated on ice for 30min, then heat shocked for 30s at 42°C in a water bath and transferred back on ice. 500µl of RT LB medium were added and the cells were incubated for 30-60min at 37°C on a shaker. 50-200µl of the bacterial suspension were plated on LB agar plates containing an appropriate antibiotic for selection (Ampicillin (100µg/ml), Kanamycin (50µg/ml), Chloramphenicol (25µg/ml)) and the plates were incubated at 37°C over night. Single colonies were used to inoculate 2-5ml LB medium cultures, which were incubated over night at 37°C on a shaker. After isolation of the plasmid DNA (see 5.5.4), transformant clones were identified by PCR (see 5.3.8) and/or restriction digest (see 5.3.1).

5.5.4 Isolation of plasmid DNA from *E. coli*

Depending on the amount of bacterial culture, so called Mini- (3-5ml), Midi- (50-100ml) or Maxi-Preparations (200-1000ml) for the isolation of plasmid DNA were carried out using the following kits:

QIAprep® Miniprep Kit (Qiagen)
QIAGEN® Plasmid Midi Kit (Qiagen)
QIAGEN® Plasmid Maxi Kit (Qiagen)

QIAGEN® HiSpeed Maxi Kit (Qiagen)
Wizard® *Plus* Midipreps DNA Purification System (Promega)

5.5.5 Detection of recombinant colonies by colony hybridization

In cases of low ligation efficiency, the number of screened clones after transformation with a ligation product was increased by performing a so-called colony lift with subsequent hybridization. The transformation of bacteria was carried out as described in 5.5.3., but the bacteria suspension was plated on 10-20 LB agar plates in portions of 25-50µl. After incubation over night, colonies were transferred to Hybond XL membrane discs (Amersham), marking the orientation of the membrane on the plates. The membranes were denatured by placing them for 2x 5min on Whatman filter paper soaked with denaturation buffer and neutralized by placing them for 2x 5min on 3MM filter paper (Whatman) soaked with neutralization buffer (see 5.3.13.2). After washing for 5min on 2x SSC soaked 3MM filter paper (Whatman), the DNA was crosslinked to the membrane by UV light (1200J, 60s). Hybridization with a radioactively labeled probe corresponding to the insert of interest was carried out as described in 5.3.13.3. The orientation of the membranes was marked on the X-ray film and recombinant clones were identified by comparing the position of the signals on the film with the original LB agar plates.

5.6 Mouse embryonic stem (ES) cell culture

All incubation steps were carried out in incubators (Heraeus) at 37°C and a CO_2 content of 5%, unless otherwise stated. For long term storage, cells were kept in liquid nitrogen at -196°C. 96-well plates with ES cells were stored at -80°C. Medium on ES cells was changed every day.

5.6.1 Feeder cell culture

To keep mouse embryonic stem cells in an undifferentiated, pluripotent state, they have to be cultured on so-called feeder cells. These are mitotically inactive, neomycin resistant mouse

fibroblasts. The feeder cells were isolated from embryos of the transgenic mouse line C57Bl/6J-TgN (pPGK Neo bpA) 3 Ems (Jackson Laboratories, Simpson EM.O.), carrying a neomycin resistance gene. The cells were stored in 1ml aliquots in liquid nitrogen at -196°C. For the preparation of feeder cell plates, fibroblasts were thawed quickly at 37°C in a water bath, transferred into 10ml Dulbecco's Modified Eagle Medium (DMEM, Gibco) complete (see below) and centrifuged for 5min at 270g. The pellet was resuspended in 9ml DMEM complete, distributed on three 15cm Ø plates containing 22ml DMEM complete each and incubated until plates were confluent. To render the cells mitotically inactive, the medium was replaced by 25ml DMEM complete containing 150µl Mitomycin C (1mg/ml) and the cells were incubated for 2.5h. The plates were washed 2x with 10ml PBS (w/o Ca and Mg, Gibco) and then incubated with Trypsin/EDTA (Gibco) for 5min. The cell suspension was pipetted up and down 3x to obtain a single cell suspension and was transferred to a Falcon tube containing the same amount of DMEM complete as Trypsin used. The cells were pelleted for 5min at 270g and resuspended in 7.5ml DMEM complete per 15cm Ø plate. The cells were counted using a Neubauer chamber (Brand). The suspension was diluted to obtain 2 x 10^5 cells/ml and plated on appropriate culture dishes according to table 5.1.

culture dish	**medium [ml]**	**feeder cell suspension [2x10^5 cells/ml] [ml]**
10cm Ø plate	7	3
6 well plate	2	0.5
4 well plate	-/-	1 (1:10 dilution)
24 well plate	-/-	1 (1:10 dilution)
48 well plate	-/-	0.5 (1:10 dilution)
96 well plate	-/-	0.15 (1:10 dilution)

Table 2 Volumes of medium and feeder cell suspension on different culture plates.

DMEM complete: 10% Fetal Calf Serum (Gibco)
1% L-glutamine (Gibco)
1% MEM non essential amino acids (Gibco)
in DMEM (Gibco)

5.6.2 Thawing and passage of ES cells

A vial of ES cells was quickly thawed at 37°C in a water bath and transferred into 10ml ES cell medium. Cells were pelleted at 270g for 3min, resuspended in 10ml ES cell medium and distributed on two 10cm Ø feeder plates containing 5ml ES cell medium each. After 2-3 days, the cells were washed twice with PBS, incubated for 10min in 3ml Trypsin/EDTA (Gibco), after which 4ml ES cell medium were added and the cells were centrifuged for 3min at 270g. After resuspension in 12ml ES cell medium, the cells were distributed on six 10cm Ø feeder plates containing 8ml ES cell medium each.

ES cell medium:
12.5% Fetal Calf Serum (PAN Biotech)
1.5% L-glutamine (Gibco)
0.05M HEPES (Gibco)
1% MEM non essential amino acids (Gibco)
0.1mM β-mercaptoethanol
$9 \cdot 10^5$ U ESGRO® (Chemicon)

ESGRO®: leukemia inhibitory factor (LIF)

5.6.3 Electroporation of ES cells

The cells were trypsinized as described in 5.6.1.2, resuspended in 1ml PBS per 10cm Ø plate and kept on ice. The cell number was determined using a Neubauer chamber (Brand) and the cell suspension was diluted in PBS to 1.5 x 10^7 cells/ml. 800µl cell suspension were transferred to an electroporation cuvette (Bio-Rad Laboratories), 20µl (1µg/µl) linearized targeting vector was added and the cells were electroporated in a Bio-Rad gene pulser at 0.24kV, 500µF. The cuvette was incubated for 20min on ice, after which the cells were transferred carefully into 5ml ES cell medium, and the cell suspension was distributed on two 10cm Ø feeder plates containing 7.5ml ES cell medium. After 2 days, the medium was changed to selection medium containing G418/geneticin (180µg/ml, Gibco) and the next day, ganciclovir (2µM, Sigma-Aldrich) was added as additional selection marker. After 6-8 days, only drug-resistant ES cell colonies remained on the plates.

5.6.4 Picking and expansion of recombinant ES cell clones

The ES cell medium on the plates was changed to PBS and recombinant clones were picked and transferred into a 96-well plate under a laminar flow hood. The plate was centrifuged briefly (100g, 30s) and 30µl Trypsin/EDTA (Gibco) were added to each well. After incubation for 10min, 70µl ES cell selection medium were added, the suspension was pipetted up and down at least 10x and then transferred to a 96-well feeder plate containing 100µl ES cell selection medium per well.

5.6.5 Splitting of ES cells in 96-well plates

Two to three days after picking of the clones, the density of the cells in each well was determined under the microscope. The plate was washed twice with PBS, the cells were incubated in 30µl Trypsin/EDTA (Gibco) per well for 10min, then 70µl ES cell selection medium were added. After pipetting up and down at least 10x, between 0-100µl ES cell selection medium were added depending on the density of the cells in each well. Of this suspension, 50µl were transferred to 2 new 96-well feeder plates containing 150µl ES cell selection medium per well.
Two days later, the cells were splitted once more following the same protocol, only that this time 50µl of the resulting suspension were transferred to a new 96-well feeder plate and another 50µl were transferred to a gelatine coated 96-well plate. To coat a 96-well plate with gelatine, 100µl 0.1% gelatine solution in PBS were pipetted into each well and the plate was incubated for at least 15min at RT. The gelatine solution was removed directly before use.

5.6.6 Freezing of ES cells

Two to three days after the second splitting, the ES cells on feeder plates were washed twice with PBS and trypsinized as described in 5.6.1.5. After adding 70µl of ES cell medium and pipetting up and down for at least 10x, the plates were put on ice for 10min. Then 100µl ice cold freezing medium were added and the cells were mixed thoroughly by pipetting up and down. For freezing, the plates were sealed with parafilm, wrapped in paper towels and stored

in cryoboxes at -80°C. From these plates, identified homologous recombinant clones were expanded.

After another 2-3 days, the cells on gelatine plates were frozen. The cells were washed once with PBS, the PBS was drawn off thoroughly and the plates were sealed with parafilm and stored at -20°C. These plates were used for the identification of homologous recombinant clones (see 5.6.7).

2x Freezing medium: 50% Fetal Calf Serum (PAN Biotech)
30% ES cell medium
20% DMSO

5.6.7 DNA preparation from 96-well gelatine plates

50µl of lysis buffer per well were added directly to the frozen cells, the plates were sealed with aluminium foil and incubated over night at 50°C in a humid chamber. The next day, the plates were centrifuged for 2min at 4000rpm, 100µl precipitation solution were added and the cells were incubated on a shaker for 30-60min at RT. The DNA precipitated as a filamentous network and was centrifuged 2min at 4000rpm. The supernatant was discarded, excess liquid was blotted on a paper towel and the DNA was washed 3x with 150µl 70% ethanol and air dried for 30min at 37°C. 30µl of restriction digest mix was added to each well, the plates were sealed with aluminium foil and incubated over night at 37°C. The next day, 5µl DNA loading buffer were added to each well and the samples were subjected to Southern blotting (see 5.3.13.2 and 5.3.13.3).

Lysis buffer: 10mM Tris-HCl pH 7.5
10mM EDTA pH 8.0
10mM NaCl
0.5% Sarcosyl
1mg/ml Proteinase K

Precipitation solution: 75mM NaCl
in ice cold 100% ethanol

Restriction digest mix: 1.2µl 0,1 M spermidine
3µl restriction buffer (Roche)
0.3µl RNase A (10 mg/ml)
2µl restriction enzyme (10 U/ml, Roche)
23.5µl aqua dest.

5.6.8 Expansion of homologous recombinant clones for blastocyst injection

A 96-well feeder plate containing the verified homologous recombinant ES cell clones was put into a plastic bag and quickly thawed at 37°C in a water bath. The cells were centrifuged for 2min at 270g and the DMSO containing medium was replaced by 100µl ES cell medium in wells with homologous recombinant clones. The suspensions were pipetted up and down 5x and transferred to a new 96-well feeder plate containing 100µl ES cell medium. When the cells formed homogenous, compact and undifferentiated clones, they were trypsinized as described in 5.6.5 and transferred to a 24-well feeder plate. As soon as the cells were confluent, they were transferred to the next plate of suitable size until 2 confluent 10cm Ø feeder plates were obtained.

5.7 Working with proteins

5.7.1 Isolation of proteins from embryonic heads

The uterus of a pregnant mouse was opened in ice cold PBS and the embryos were collected and transferred to ice cold RIPA protein lysis buffer. The anterior neural tube was dissected out and homogenized on ice in 100µl RIPA buffer using a motor pestle (Kontes Glass Company). After determination of the total protein concentration (5.7.2), 20µg total protein of each sample were used for Western blot. Three volumes of 4x Laemmli buffer were added, the samples were cooked for 5min in a boiling water bath and subsequently centrifuged for 5min at 16000g at 4°C.

RIPA protein lysis buffer: 50mM Tris-HCl pH 7,5
150mM NaCl
1% Triton X-100
0.5% Sodium deoxycholate (DOC)
0.1% SDS
2mM EDTA
1 tablet Mini Protease Inhibitor Cocktail (Roche) per 10 ml
1:100 Phosphatase inhibitor cocktail 1 (Sigma-Aldrich)
1:100 Phosphatase inhibitor cocktail 2 (Sigma-Aldrich)

4x Laemmli buffer: 200mM Tris-HCl pH 6,8
40% glycerol
8% SDS
400mM β-mercaptoethanol
0.4% bromophenol blue

5.7.2 Determination of total protein concentration

Total protein concentration was measured using the BCA™ system (Pierce, PerBio). In this modified Bradford protocol, the biuret reaction (alkaline reduction of Cu^{2+} to Cu^{+} by protein) is combined with the colorimetric detection of a water-soluble complex formed by Cu^{+} cations with bicinchoninic acid (BCA). This purple complex exhibits a strong absorbance at 562nm, that is a nearly linear function of the amount of protein in the solution.
To create a calibration curve, a dilution series of bovine serum albumine (BSA) in RIPA buffer ranging from 25-2000µg/ml was prepared. 1ml of BCA™ reagent B was added to 49ml of BCA™ reagent A. The resulting solution was mixed and 2ml were added to 100µl of each BSA dilution. The samples were incubated for 30min at 37°C in a waterbath. Absorbance at 562nm was measured in a photometer for 10 different BSA concentrations and a calibration curve was calculated.
Protein samples were diluted in RIPA buffer 1:10 and 1:20 each, incubated in BCA™ solution as described above and absorbance at 562nm was measured. The mean of the two dilution values was calculated for each probe and protein concentration was estimated from the BSA calibration curve.

5.7.3 Polyacrylamide gel electrophoresis (PAGE) of proteins

Protein extracts were separated using polyacrylamide gel electrophoresis (PAGE). Protein samples prepared as described in 5.7.1 were loaded on precast NuPAGE® Novex Bis-Tris Gels (Invitrogen) and electrophoresis was performed in an XCell *SureLock*™ Mini Cell electrophoresis device (Invitrogen) according to manufacturer's recommendations. 5µl SeeBlue® Plus2 pre-stained coloured protein standard (Invitrogen) were used as a size standard. Running buffer was prepared by diluting 20x NuPAGE® MES SDS Running Buffer (Invitrogen) with the appropriate amount of aqua dest.

5.7.4 Western blot

Proteins were blotted onto nitrocellulose membranes (Amersham) using an XCell II™ Blot Module (Invitrogen) following manufacturer's instructions. For preparing the transfer buffer, 50ml 20x NuPAGE® Transfer Buffer (Invitrogen) were diluted by adding 850ml aqua dest., 100ml methanol and 1ml NuPAGE® Antioxidant (Invitrogen).
The membrane was blocked over night at 4°C in TBS-TM blocking buffer. Primary antibodies were diluted in TBS-T and incubated with the membranes for 1h on a shaker at RT. Membranes were washed 3x 10min in TBS-T. Secondary horseradish peroxidase (HRP)-conjugated antibodies were diluted according to manufacturer's specifications in TBS-T and incubated with membranes for 1h on a shaker at RT. After washing 3x 10min in TBS-T, luminescent detection of the proteins of interest was performed using the ECL™ Western Blotting Detection Reagent (Amersham) as recommended by the manufacturer. Membranes were incubated for 1min in ECL™ detection reagent and then a Hyperfilm® ECL film (Amersham) was exposed to the membranes for 10s - 10min.

TBS: 20mM Tris-HCl pH 7.6
137mM NaCl

TBS-T: TBS + 0.2% Tween-20

TBS-TM: TBS-T + 5% Difco™ Skim Milk (BD Biosciences)

A complete list of primary and secondary antibodies used for Western blot detection, including dilution factors, is given in appendix 7.3.

5.7.5 Stripping of nitrocellulose membranes

To remove all primary and secondary antibodies from nitrocellulose membranes, membranes were incubated in stripping solution for 1h at RT on a shaker. After 2 washes in TBS-T for 10min, membranes were ready for another round of immunodetection, starting by blocking in TBS-TM.

Stripping solution: 25mM glycine
1% SDS
adjust pH to 2.0 with 32% HCl

5.8 Animal handling

All mouse lines were kept in an isolated system according to the guidelines of the Tierschutzverordnung of the Regierung von Oberbayern. Food and water were accessible ad libitum. Temperature was kept at 22±2°C and humidity was kept at 55±5%. An automatic timer controlled the light/dark cycle, which was constantly set to 12h light followed by 12h darkness (12:12).
Mice were weaned 3-4 weeks after birth and the two genders were caged separately. Mice were identified by ear-clipping and genotyped using tail tip tissue.

5.8.1 Determination of embryonic stages

In general, embryos were staged in days post coitum (dpc) or embryonic days (E) with noon of the day of vaginal plug detection set as 0.5 dpc or E0.5. As the rate of development of embryos of the same litter can differ substantially, especially at early stages of development, embryos younger than E9.5 were also staged according to Theiler (Theiler-Stages (TS)) (Theiler, 1989).

5.8.2 Dissection of embryos

Pregnant mothers were killed by cervical dislocation. The uterus was dissected out and transferred to ice cold PBS. The embryos were dissected out of the uterus and fixed in 4% paraformaldehyde (PFA) in PBS (4h for stage E8.5, over night for stages E9.5-E18.5) at 4°C. Yolk sac or tail tissue was taken for genotyping. The next day embryos were processed either for paraffin or cryo embedding.

1x PBS:
137mM NaCl
2.7mM KCl
10mM Na_2HPO_4
2mM KH_2PO_4
pH 7.4

5.8.2.1 Paraffin embedding of embryos

For paraffin sections, embryos were dehydrated in a graded ethanol series (70%, 96%, 100%) and cleared in xylene. Times for each dehydration step varied with embryonic stage (see table 5.2). For storage, embryos were kept in 70% ethanol at RT. Incubation times in xylene may vary and had to be checked for transparence of the embryos.

embryonic stage	70% ethanol	96% ethanol	100% ethanol	xylene
E9.5	> 2h	10min	10min	5min
E10.5	> 2h	10min	10min	10min
E11.5	> 2h	15min	15min	10min
E12.5	3-4h	15min	15min	10-15min
E13.5	3-4h	20min	20min	15min
E14.5	> 4h	30min	30min	20-30min
E18.5 (brain)	over night	45min	45min	35min
adult brain	over night	1h	1h	1-2h

Table 3 Incubation times for dehydration and clearance of mouse embryos at different stages and for adult brains.

After clearing, the embryos were transferred into liquid paraffin (65°C), incubated over night at 65°C and then embedded in fresh paraffin in embedding molds.

5.8.2.2 Cryoprotection of embryos

For cryostat sections, embryos were washed in PBS for several hours after fixation over night in 4% PFA and transferred into 20% sucrose in PBS. After incubation for at least over night at 4°C, the sucrose solution was removed on clean paper towels and embryos were embedded in TissueTek® OCT medium (Sakura) at -20°C.

5.8.3 PFA perfusion of adult mice and paraffin embedding of the brain

For the proper fixation of adult brain tissue, mice were perfused intracardially with 4% PFA in PBS. Mice were killed in isoflurane or CO_2, the thorax was opened and a canula was inserted into the left ventricle of the heart. The right atrium was cut open to provide an outflow for the PFA solution. The canula was connected to a peristaltic pump with a plastic tube. First, the blood was replaced by PBS for 1-2min, then 4% PFA in PBS was perfused for 5min. The brain was dissected out and fixed over night in 4% PFA in PBS at 4°C. After fixation, it was processed for paraffin embedding as described in 5.8.2.1

5.9 Histological techniques

5.9.1 Sections of embryos and adult brain

5.9.1.1 Paraffin sections

Paraffin embedded embryos and adult brains were cut on a microtome in sections of 8µm thickness. The sections were transferred to a water bath (37°C), drawn on microscope slides (Superfrost®Plus, Menzel GmbH) and placed on a heating plate (Leica) at 37-40°C. Slides were incubated over night at 37°C and stored at 4°C.

5.9.1.2 Cryosections

Embryos embedded in TissueTek® OCT medium (Sakura) were adapted to -20°C for at least 30min in the cryostat. 16µm thick sections were cut in a cryostat and transferred to cooled microscope slides (Superfrost®Plus, Menzel GmbH), placed on a heating plate (37°C) for several minutes and precooled again for the next section. Slides were stored at -20°C.

5.9.2 Immunohistochemistry on paraffin and cryosections

5.9.2.1 Standard immunohistochemistry on paraffin sections

All incubation steps were carried out at RT unless otherwise stated. Paraffin was removed from the sections by incubation for at least 1h in Roti®-Histol (Roth) followed by dehydration in a graded series of ethanol (2x 5min in 100% ethanol, 2x 5min in 96% ethanol, 2x 5min in 70% ethanol). Slides were rinsed for 10min in aqua dest. and then incubated for 3min in 0.01M sodium citrate, pH 6.0. For antigen retrieval, slides were boiled in a microwave (900W, 5min) in 0.01M sodium citrate, cooled down for 10min at RT, boiled again in the microwave (600W, 3min) and cooled down to RT. After washing 2x 5min in PBS, slides were incubated for 5min in 0.01% H_2O_2 in PBS to inactivate endogenous peroxidases followed by washing 2x 5min in PBS. To minimize unspecific binding of the antibody, slides were incubated in blocking solution for 1h in a humid chamber. The primary antibody was diluted in blocking solution, 100µl of antibody solution were pipetted on each slide and slides were covered with a coverslip and incubated over night at 4°C in a humid chamber. A list of applied primary and secondary antibodies with dilution factors is given in appendix 7.3.
For peroxidase-stained sections, slides were washed the next day 3x 10min in PBS and then incubated with a biotin conjugated secondary antibody diluted in blocking solution for 1h at RT followed by 3 washes for 15min in PBS. To enhance signal intensity, slides were treated with the Vectastain ABC kit (Vector Laboratories) according to manufacturer's instructions. After washing 2x 5min in PBS, slides were incubated for 5min in 0.1M Tris-HCl, pH 7.4. For the peroxidase reaction, 500µl DAB solution were pipetted on each slide and incubated 1-15min in a humid chamber, depending on signal intensity and signal to background ratio. Slides were washed 2x 5min in PBS, dehydrated in a graded series of ethanol and cleared in Roti®-Histol (Roth), after which they were coverslipped Roti®-Histokitt.
For immunofluorescence, sections were incubated with Cy2- or Cy3-conjugated secondary antibodies in blocking medium. After 3 washes for 5min in PBS, slides were rinsed briefly in aqua dest. and coverslipped in ProTaqstura (Biocyc GmbH & Co. KG).

Blocking solution: 10% Fetal Calf Serum (Gibco)
0.25% Triton-100
in 1x PBS

DAB solution: 0.05mM 3,3'-diaminobenzidine (DAB) solution
0.1 M Tris-HCl, pH 7.4
0.02% H_2O_2

5.9.2.2 Standard immunohistochemistry on cryosections

Cryosections were thawed at RT for at least 30min before use. Slides were washed 2x 5min in PBS and then treated as described in 5.9.2.1 for paraffin sections, omitting the deparaffination/rehydration steps.

5.9.2.3 BrdU labeling and immunodetection

Cells undergoing DNA replication during the S phase of the cell cycle can be labeled with the thymidine analog Bromo-2'-deoxy-uridine (BrdU) which is incorporated into newly synthesized DNA instead of endogenous thymidine. To label embryos with BrdU, pregnant mice were injected intraperitoneally at the appropriate developmental stage of the embryos with BrdU reagent (1000x conc., Bromo-2'-deoxy-uridine Labeling and Detection Kit II, Roche) at 10µl/g body weight. Embryos were dissected and processed for cryosectioning as described in 5.8.2 and 5.9.1.2.
Immunohistochemistry was carried out as described in 5.9.2.2, only that the primary antibody (Bromo-2'-deoxy-uridine Labeling and Detection Kit II, Roche) was incubated for 30min at 37°C prior to over night incubation at 4°C.

5.9.2.4 Double labeling of cryosections for BrdU and Ki67

The standard immunohistochemistry protocol described in 5.9.2.2 was modified for simultaneous detection of BrdU and Ki67. After washing in PBS and incubation in 0.01M sodium citrate, slides were boiled only once in the microwave (360W, 7min) and cooled down for at least 30min. Mouse anti-BrdU and rabbit anti-Ki67 primary antibodies were applied simultaneously, incubated 30min at 37°C, then over night at 4°C.
On the following day, slides were washed 3x 10min in PBS and incubated for 1h at RT with a biotin conjugated anti-rabbit secondary antibody diluted in blocking solution. After washing 3x 10min in PBS, a Cy3 conjugated anti-mouse secondary antibody and Cy2 conjugated Streptavidin were applied simultaneously and incubated for 1h at RT. Slides were washed

again 3x 10min in PBS, rinsed in aqua dest. and coverslipped in ProTaqstura (Biocyc GmbH & Co. KG).

5.9.3 Cresyl violet staining

Paraffin sections were deparaffinated and rehydrated as described in 5.9.2.1, cryosections were washed for 1min in 50% ethanol and 70% ethanol, respectively, and then rinsed briefly in aqua dest. Sections were stained for 10-15s in cresyl violet solution, rinsed for 2min in aqua dest. and differentiated by incubation for 2x 2min in 70% ethanol, 15s in 96% ethanol containing 1% acetic acid, 2x 1min in 96% ethanol and 2x 2min in 100% ethanol. Slides were coverslipped as described in 5.9.2.1.

Cresylviolet solution:
7.8mM cresyl violet
12.5mM sodium acetate
25mM acetic acid
pH 3.5
filtrate before use

5.9.4 *In situ* hybridization on paraffin sections

For *in situ* hybridization, DEPC-treated water was used for all solutions and work was carried out wearing gloves at all times to avoid RNA degradation by RNase contamination.

5.9.4.1 Synthesis of radioactively labeled RNA probes

Radioactively labeled RNA probes (riboprobes) were synthesized by *in vitro* transcription. As templates, plasmids carrying a cDNA fragment corresponding to the designated mRNA of interest, flanked by 2 different RNA polymerase promotors, were used. The plasmids were linearized with the appropriate restriction endonuclease (see 5.3.1) either at the 5'-end (for the antisense probe) or the 3'-end (for the sense probe as control) of the cDNA fragment. The DNA was purified by isopropanol/ethanol precipitation. Probes were labeled with uridine 5'-[α-^{35}S]thiotriphosphate (^{35}S-UTP, Amersham) using the following reaction setup:

3µl 10x transcription buffer
3µl ATP/CTP/GTP ribonucleotide mix (10mM each)
1µl 0.5 M dithiothreitol (DTT)
1µl Protector RNase Inhibitor (Roche)
1.5µg linearized plasmid
3µl ^{35}S-UTP (0.1 mCi)
1µl RNA polymerase (T3, T7 or SP6)
ad 30µl aqua dest.

The reaction was incubated for 3h at 37°C, adding another microliter of RNA polymerase after 1h. To destroy the DNA template after *in vitro* transcription, 2µl of DNase I (10U/µl, Roche) were added to the reaction and incubated for 15min. Riboprobes were purified using the RNeasy MinElute Cleanup Kit (Qiagen) according to the manufacturer's protocol. 1µl of the ^{35}S-labeled riboprobe was added to 2ml scintillation liquid (Rotiszint®, Roth) and the activity of the probe was determined in a β-radiation counter (Easicount 400, Scott-Lab). Values between 0.5-2.5 x 10^6cpm were obtained. Riboprobes were stored at -20°C for up to 1 week.

5.9.4.2 Pretreatment of paraffin sections

All steps were carried out at RT, unless otherwise stated. Paraffin sections were deparaffinated by incubation for 2x 30min in Roti®-Histol (Roth), followed by 2x 5min in 100% ethanol and 5min in 70% ethanol. Slides were rinsed for 3min in aqua dest. and 3min in PBS and then incubated for 20min in 4% PFA in PBS on ice. They were washed 2x 5min in PBS, incubated for 7min in Proteinase K (20µg/ml) in Proteinase K buffer and washed again 5min in PBS. Sections were fixed again for 20min in 4% PFA in PBS on ice, washed 5min in PBS and then treated with 0.1M triethanolamine-HCl (pH 8.0) for 10min, adding dropwise 630µl acetic acid anhydrate while stirring rapidly. Subsequently, slides were washed 2x 5min in 2x SSC, dehydrated in a graded ethanol series (1min each in 60%, 70%, 96% and 100% ethanol) and air dried for 30-60min.

Proteinase K buffer: 0.5M Tris-HCl pH7.5
0.05M EDTA pH 8.0
pH to 7.8

20x SSC: 3M NaCl
300mM sodium citrate
pH to 7.4

5.9.4.3 Hybridization of pretreated slides with a riboprobe

Slides were prehybridized with hybridization mix for at least 1h at 57°C. To this end, 100µl of hybridization mix were pipetted on each slide, slides were covered with a coverslip and put into a humid chamber containing hybridization chamber fluid. For hybridization, 100µl hybridization mix per slide containing the radioactively labeled riboprobe (7 x 10^6cpm) were heated for 2min to 94°C and put on ice. Prehybridization mix was removed from the slides together with the coverslip, the hybridization mix with the riboprobe was applied and slides were covered with a new coverslip. Hybridization was carried out over night at 57°C.

Hybridization mix: 50% formamide
20mM Tris-HCl pH 8.0
300mM NaCl
5mM EDTA pH 8.0
10% dextrane sulfate
0.02% Ficoll 400
0.02% BSA
0.5mg/ml yeast tRNA
0.2mg/ml carrier DNA (salmon sperm DNA, Sigma)
200mM DTT

Chamber fluid: 50% formamide
10% 20x SSC
in aqua dest.

5.9.4.4 Stringent washes

Coverslips were removed and slides were washed 4x 5min in 4x SSC at RT. Slides were incubated for 30min in RNase A (20µg/ml in NTE buffer) at 37°C to remove excess unbound riboprobe. Slides were rinsed in decreasing concentrations of SSC buffer containing 1mM DTT (5min 2x SSC, 10min 1x SSC, 10min 0.5x SSC) at RT and then washed under high stringency conditions 2x 30min in 0.1x SSC, 1mM DTT at 64°C. After 2 washing steps for 10min in 0.1x SSC, slides were dehydrated in a graded ethanol series (1min each in 30%

ethanol/300mM NH_4OAc, 50% ethanol/300mM NH_4OAc, 70% ethanol/300mM NH_4OAc, 96% ethanol, 2x 100% ethanol) and air dried for 30-60min.

NTE buffer: 0.5M NaCl
10mM Tris-HCl pH 8.0
5mM EDTA pH 8.0

5.9.4.5 Exposure of slides to autoradiographic films and nuclear fotoemulsion

The following procedures were carried out in a dark room. To check whether the hybridization procedure was successful and to determine the intensity of the signal, an slides were exposed to an X-ray film for 2-3 days. Slides were then dipped in KODAK NTB2 emulsion (Kodak). The fotoemulsion was prewarmed in a waterbath to 42°C and diluted 1:1 with prewarmed aqua dest. Slides were inserted into plastic mounts and slowly immersed into the emulsion. Excess emulsion was blotted on a paper towel and the slides were left drying over night. Slides were then sorted into dark plastic boxes containing silica gel desiccant and exposed for 4-6 weeks at 4°C.

5.9.4.6 Development of slides

Slides were equilibrated to RT for at least 2h before proceeding with development. Slides were developed for 4min in KODAK D19 developer (Kodak), washed for 30s in tap water and fixed for 15-20min in KODAK fixer (Kodak). Slides were rinsed for 15-20min in flowing tap water. After air drying, remaining fotoemulsion was removed from the back of the slides using a razor blade. Slides were routinely stained with kresylviolet (see 5.9.3).

5.10 Microscopy and image editing

Brightfield and darkfield microscopy was carried out on a Zeiss Axioplan2 microscope (5x-100x Plan Neofluar® objectives, Zeiss) or on a Zeiss Stemi SV 6 stereomicroscope (Plan-achromat S objective, Zeiss). For fluorescence microscopy, the Zeiss Axiovert 200M and the confocal microscope Zeiss LSM 510 META were used. Images were taken with the digital cameras Zeiss AxioCam MRC/HRC and recorded using Axiovision software, versions 3.1

and 4.0. If necessary, images were edited with Adobe Photoshop software, versions 8.0 and CS.

5.10.1 Quantification of phospho-histone H3 labeled cells using the Zeiss axioplan 2 microscope

For each analyzed section, the area of the right half of the neural tube was outlined and measured using the Zeiss Axioplan 2 microscope and Neurolucida software. Subsequently, the number of cells labeled for phosphorylated histone H3 in the outlined area was determined. Means and standard deviations were calculated for each brain area in the wild type and mutant situation, respectively.

5.10.2 Quantification of BrdU/Ki67 double labeled cells using the confocal laser scanning microscope Zeiss LSM 510 META

To quantify the number of double labeled cells, sections were analyzed with the confocal laser scanning microscope Zeiss LSM 510 META. A z-stack image series in intervals of 1µm was recorded from each section comprising the entire thickness of the tissue. Channels for Cy2 (Ki67) and Cy3 (BrdU) were recorded separately and overlay images were generated using the Zeiss LSM 510 META software. Each channel was assigned a different color, red for Cy3 (BrdU) and green for Cy2 (Ki67), so that double labeled cells appeared yellow in overlay images. The number of red, green and yellow cells was determined by scrolling through the entire z-stack and counting each population separately. Means and standard deviations were calculated for the wild type and mutant situation, respectively.

6. References

Alberts, B., Johnson, A., Lewis, J., Raff, M., Roberts, K. and Walter, P. (2002). Molecular Biology of the Cell. New York: Garland Science.

Andersson, E., Jensen, J. B., Parmar, M., Guillemot, F. and Bjorklund, A. (2006a). Development of the mesencephalic dopaminergic neuron system is compromised in the absence of neurogenin 2. *Development* **133**, 507-16.

Andersson, E., Tryggvason, U., Deng, Q., Friling, S., Alekseenko, Z., Robert, B., Perlmann, T. and Ericson, J. (2006b). Identification of intrinsic determinants of midbrain dopamine neurons. *Cell* **124**, 393-405.

Basilico, C. and Moscatelli, D. (1992). The FGF family of growth factors and oncogenes. *Adv Cancer Res* **59**, 115-65.

Bauer, H. C., Bauer, H., Lametschwandtner, A., Amberger, A., Ruiz, P. and Steiner, M. (1993). Neovascularization and the appearance of morphological characteristics of the blood-brain barrier in the embryonic mouse central nervous system. *Brain Res Dev Brain Res* **75**, 269-78.

Bayer, S. A., Wills, K. V., Triarhou, L. C. and Ghetti, B. (1995). Time of neuron origin and gradients of neurogenesis in midbrain dopaminergic neurons in the mouse. *Exp Brain Res* **105**, 191-9.

Beatus, P. and Lendahl, U. (1998). Notch and neurogenesis. *J Neurosci Res* **54**, 125-36.

Bertrand, N., Castro, D. S. and Guillemot, F. (2002). Proneural genes and the specification of neural cell types. *Nat Rev Neurosci* **3**, 517-30.

Bhanot, P., Brink, M., Samos, C. H., Hsieh, J. C., Wang, Y., Macke, J. P., Andrew, D., Nathans, J. and Nusse, R. (1996). A new member of the frizzled family from Drosophila functions as a Wingless receptor. *Nature* **382**, 225-30.

Bilovocky, N. A., Romito-DiGiacomo, R. R., Murcia, C. L., Maricich, S. M. and Herrup, K. (2003). Factors in the genetic background suppress the engrailed-1 cerebellar phenotype. *J Neurosci* **23**, 5105-12.

Blak, A. A., Naserke, T., Weisenhorn, D. M., Prakash, N., Partanen, J. and Wurst, W. (2005). Expression of Fgf receptors 1, 2, and 3 in the developing mid- and hindbrain of the mouse. *Dev Dyn* **233**, 1023-30.

Bossenmeyer-Pourie, C., Chihab, R., Schroeder, H. and Daval, J. L. (1999). Transient hypoxia may lead to neuronal proliferation in the developing mammalian brain: from apoptosis to cell cycle completion. *Neuroscience* **91**, 221-31.

Boutros, M., Mihaly, J., Bouwmeester, T. and Mlodzik, M. (2000). Signaling specificity by Frizzled receptors in Drosophila. *Science* **288**, 1825-8.

Castella, P., Sawai, S., Nakao, K., Wagner, J. A. and Caudy, M. (2000). HES-1 repression of differentiation and proliferation in PC12 cells: role for the helix 3-helix 4 domain in transcription repression. *Mol Cell Biol* **20**, 6170-83.

Cau, E., Casarosa, S. and Guillemot, F. (2002). Mash1 and Ngn1 control distinct steps of determination and differentiation in the olfactory sensory neuron lineage. *Development* **129**, 1871-80.

Chenn, A. and Walsh, C. A. (2002). Regulation of cerebral cortical size by control of cell cycle exit in neural precursors. *Science* **297**, 365-9.

Ciani, L. and Salinas, P. C. (2005). WNTs in the vertebrate nervous system: from patterning to neuronal connectivity. *Nat Rev Neurosci* **6**, 351-62.

Cool, S. M., Sayer, R. E., van Heumen, W. R., Pickles, J. O. and Nurcombe, V. (2002). Temporal and spatial expression of fibroblast growth factor receptor 4 isoforms in murine tissues. *Histochem J* **34**, 291-7.

Dahlstrom, A. and Fuxe, K. (1964). Localization of monoamines in the lower brain stem. *Experientia* **20**, 398-9.

Dailey, L., Ambrosetti, D., Mansukhani, A. and Basilico, C. (2005). Mechanisms underlying differential responses to FGF signaling. *Cytokine Growth Factor Rev* **16**, 233-47.

Dailey, L., Laplantine, E., Priore, R. and Basilico, C. (2003). A network of transcriptional and signaling events is activated by FGF to induce chondrocyte growth arrest and differentiation. *J Cell Biol* **161**, 1053-66.

Dann, C. E., Hsieh, J. C., Rattner, A., Sharma, D., Nathans, J. and Leahy, D. J. (2001). Insights into Wnt binding and signalling from the structures of two Frizzled cysteine-rich domains. *Nature* **412**, 86-90.

de la Pompa, J. L., Wakeham, A., Correia, K. M., Samper, E., Brown, S., Aguilera, R. J., Nakano, T., Honjo, T., Mak, T. W., Rossant, J. et al. (1997). Conservation of the Notch signalling pathway in mammalian neurogenesis. *Development* **124**, 1139-48.

Deng, C., Wynshaw-Boris, A., Zhou, F., Kuo, A. and Leder, P. (1996). Fibroblast growth factor receptor 3 is a negative regulator of bone growth. *Cell* **84**, 911-21.

des Portes, V., Pinard, J. M., Billuart, P., Vinet, M. C., Koulakoff, A., Carrie, A., Gelot, A., Dupuis, E., Motte, J., Berwald-Netter, Y. et al. (1998). A novel CNS gene required for neuronal migration and involved in X-linked subcortical laminar heterotopia and lissencephaly syndrome. *Cell* **92**, 51-61.

Dono, R. (2003). Fibroblast growth factors as regulators of central nervous system development and function. *Am J Physiol Regul Integr Comp Physiol* **284**, R867-81.

Dymecki, S. M. (1996). Flp recombinase promotes site-specific DNA recombination in embryonic stem cells and transgenic mice. *Proc Natl Acad Sci U S A* **93**, 6191-6.

Echelard, Y., Epstein, D. J., St-Jacques, B., Shen, L., Mohler, J., McMahon, J. A. and McMahon, A. P. (1993). Sonic hedgehog, a member of a family of putative signaling molecules, is implicated in the regulation of CNS polarity. *Cell* **75**, 1417-30.

Edlund, T. and Jessell, T. M. (1999). Progression from extrinsic to intrinsic signaling in cell fate specification: a view from the nervous system. *Cell* **96**, 211-24.

Farah, M. H., Olson, J. M., Sucic, H. B., Hume, R. I., Tapscott, S. J. and Turner, D. L. (2000). Generation of neurons by transient expression of neural bHLH proteins in mammalian cells. *Development* **127**, 693-702.

Ferguson, K. L. and Slack, R. S. (2003). Growth factors: can they promote neurogenesis? *Trends Neurosci* **26**, 283-5.

Ferguson, K. L., Vanderluit, J. L., Hebert, J. M., McIntosh, W. C., Tibbo, E., MacLaurin, J. G., Park, D. S., Wallace, V. A., Vooijs, M., McConnell, S. K. et al. (2002). Telencephalon-specific Rb knockouts reveal enhanced neurogenesis, survival and abnormal cortical development. *Embo J* **21**, 3337-46.

Fode, C., Gradwohl, G., Morin, X., Dierich, A., LeMeur, M., Goridis, C. and Guillemot, F. (1998). The bHLH protein NEUROGENIN 2 is a determination factor for epibranchial placode-derived sensory neurons. *Neuron* **20**, 483-94.

Ford-Perriss, M., Abud, H. and Murphy, M. (2001). Fibroblast growth factors in the developing central nervous system. *Clin Exp Pharmacol Physiol* **28**, 493-503.

Fujita, H., Ohta, M., Kawasaki, T. and Itoh, N. (1991). The expression of two isoforms of the human fibroblast growth factor receptor (flg) is directed by alternative splicing. *Biochem Biophys Res Commun* **174**, 946-51.

Galderisi, U., Jori, F. P. and Giordano, A. (2003). Cell cycle regulation and neural differentiation. *Oncogene* **22**, 5208-19.

Geling, A., Itoh, M., Tallafuss, A., Chapouton, P., Tannhauser, B., Kuwada, J. Y., Chitnis, A. B. and Bally-Cuif, L. (2003). bHLH transcription factor Her5 links patterning to regional inhibition of neurogenesis at the midbrain-hindbrain boundary. *Development* **130**, 1591-604.

Gimeno, L., Brulet, P. and Martinez, S. (2003). Study of Fgf15 gene expression in developing mouse brain. *Gene Expr Patterns* **3**, 473-81.

Gimeno, L., Hashemi, R., Brulet, P. and Martinez, S. (2002). Analysis of Fgf15 expression pattern in the mouse neural tube. *Brain Res Bull* **57**, 297-9.

Gleeson, J. G., Allen, K. M., Fox, J. W., Lamperti, E. D., Berkovic, S., Scheffer, I., Cooper, E. C., Dobyns, W. B., Minnerath, S. R., Ross, M. E. et al. (1998). Doublecortin, a brain-specific gene mutated in human X-linked lissencephaly and double cortex syndrome, encodes a putative signaling protein. *Cell* **92**, 63-72.

Gleeson, J. G., Lin, P. T., Flanagan, L. A. and Walsh, C. A. (1999). Doublecortin is a microtubule-associated protein and is expressed widely by migrating neurons. *Neuron* **23**, 257-71.

Goodrich, D. W. and Lee, W. H. (1990). The molecular genetics of retinoblastoma. *Cancer Surv* **9**, 529-54.

Greferath, U., Bennie, A., Kourakis, A., Bartlett, P. F., Murphy, M. and Barrett, G. L. (2000). Enlarged cholinergic forebrain neurons and improved spatial learning in p75 knockout mice. *Eur J Neurosci* **12**, 885-93.

Guo, N., Hawkins, C. and Nathans, J. (2004). Frizzled6 controls hair patterning in mice. *Proc Natl Acad Sci U S A* **101**, 9277-81.

Hans, F. and Dimitrov, S. (2001). Histone H3 phosphorylation and cell division. *Oncogene* **20**, 3021-7.

Harmer, N. J., Pellegrini, L., Chirgadze, D., Fernandez-Recio, J. and Blundell, T. L. (2004). The crystal structure of fibroblast growth factor (FGF) 19 reveals novel features of the FGF family and offers a structural basis for its unusual receptor affinity. *Biochemistry* **43**, 629-40.

Hartfuss, E., Galli, R., Heins, N. and Gotz, M. (2001). Characterization of CNS precursor subtypes and radial glia. *Dev Biol* **229**, 15-30.

Hatakeyama, J., Bessho, Y., Katoh, K., Ookawara, S., Fujioka, M., Guillemot, F. and Kageyama, R. (2004). Hes genes regulate size, shape and histogenesis of the nervous system by control of the timing of neural stem cell differentiation. *Development* **131**, 5539-50.

Hirata, H., Tomita, K., Bessho, Y. and Kageyama, R. (2001). Hes1 and Hes3 regulate maintenance of the isthmic organizer and development of the mid/hindbrain. *Embo J* **20**, 4454-66.

Hsieh, M., Boerboom, D., Shimada, M., Lo, Y., Parlow, A. F., Luhmann, U. F., Berger, W. and Richards, J. S. (2005). Mice null for Frizzled4 (Fzd4-/-) are infertile and exhibit impaired corpora lutea formation and function. *Biol Reprod* **73**, 1135-46.

Huang, H. C. and Klein, P. S. (2004). The Frizzled family: receptors for multiple signal transduction pathways. *Genome Biol* **5**, 234.

Hunter, T. (1993). Braking the cycle. *Cell* **75**, 839-41.

Iavarone, A., Garg, P., Lasorella, A., Hsu, J. and Israel, M. A. (1994). The helix-loop-helix protein Id-2 enhances cell proliferation and binds to the retinoblastoma protein. *Genes Dev* **8**, 1270-84.

Ibrahimi, O. A., Zhang, F., Eliseenkova, A. V., Itoh, N., Linhardt, R. J. and Mohammadi, M. (2004). Biochemical analysis of pathogenic ligand-dependent FGFR2 mutations suggests distinct pathophysiological mechanisms for craniofacial and limb abnormalities. *Hum Mol Genet* **13**, 2313-24.

Inagaki, T., Choi, M., Moschetta, A., Peng, L., Cummins, C. L., McDonald, J. G., Luo, G., Jones, S. A., Goodwin, B., Richardson, J. A. et al. (2005). Fibroblast growth factor 15 functions as an enterohepatic signal to regulate bile acid homeostasis. *Cell Metab* **2**, 217-25.

Ishibashi, M., Ang, S. L., Shiota, K., Nakanishi, S., Kageyama, R. and Guillemot, F. (1995). Targeted disruption of mammalian hairy and Enhancer of split homolog-1 (HES-1) leads to up-regulation of neural helix-loop-helix factors, premature neurogenesis, and severe neural tube defects. *Genes Dev* **9**, 3136-48.

Ishibashi, M. and McMahon, A. P. (2002). A sonic hedgehog-dependent signaling relay regulates growth of diencephalic and mesencephalic primordia in the early mouse embryo. *Development* **129**, 4807-19.

Ishikawa, T., Tamai, Y., Zorn, A. M., Yoshida, H., Seldin, M. F., Nishikawa, S. and Taketo, M. M. (2001). Mouse Wnt receptor gene Fzd5 is essential for yolk sac and placental angiogenesis. *Development* **128**, 25-33.

Itoh, N. and Ornitz, D. M. (2004). Evolution of the Fgf and Fgfr gene families. *Trends Genet* **20**, 563-9.

Jacks, T., Fazeli, A., Schmitt, E. M., Bronson, R. T., Goodell, M. A. and Weinberg, R. A. (1992). Effects of an Rb mutation in the mouse. *Nature* **359**, 295-300.

Jarriault, S., Le Bail, O., Hirsinger, E., Pourquie, O., Logeat, F., Strong, C. F., Brou, C., Seidah, N. G. and Isra l, A. (1998). Delta-1 activation of notch-1 signaling results in HES-1 transactivation. *Mol Cell Biol* **18**, 7423-31.

Jen, Y., Manova, K. and Benezra, R. (1996). Expression patterns of Id1, Id2, and Id3 are highly related but distinct from that of Id4 during mouse embryogenesis. *Dev Dyn* **207**, 235-52.

Jen, Y., Manova, K. and Benezra, R. (1997). Each member of the Id gene family exhibits a unique expression pattern in mouse gastrulation and neurogenesis. *Dev Dyn* **208**, 92-106.

Jessell, T. M. (2000). Neuronal specification in the spinal cord: inductive signals and transcriptional codes. *Nat Rev Genet* **1**, 20-9.

Jin, K., Mao, X. O., Sun, Y., Xie, L., Jin, L., Nishi, E., Klagsbrun, M. and Greenberg, D. A. (2002). Heparin-binding epidermal growth factor-like growth factor: hypoxia-inducible expression in vitro and stimulation of neurogenesis in vitro and in vivo. *J Neurosci* **22**, 5365-73.

Kabos, P., Kabosova, A. and Neuman, T. (2002). Blocking HES1 expression initiates GABAergic differentiation and induces the expression of p21(CIP1/WAF1) in human neural stem cells. *J Biol Chem* **277**, 8763-6.

Kageyama, R., Ohtsuka, T., Hatakeyama, J. and Ohsawa, R. (2005). Roles of bHLH genes in neural stem cell differentiation. *Exp Cell Res* **306**, 343-8.

Kay, J. N., Finger-Baier, K. C., Roeser, T., Staub, W. and Baier, H. (2001). Retinal ganglion cell genesis requires lakritz, a Zebrafish atonal Homolog. *Neuron* **30**, 725-36.

Kele, J., Simplicio, N., Ferri, A. L., Mira, H., Guillemot, F., Arenas, E. and Ang, S. L. (2006). Neurogenin 2 is required for the development of ventral midbrain dopaminergic neurons. *Development* **133**, 495-505.

Kiecker, C. and Lumsden, A. (2004). Hedgehog signaling from the ZLI regulates diencephalic regional identity. *Nat Neurosci* **7**, 1242-9.

Kim, K. S., Kim, C. H., Hwang, D. Y., Seo, H., Chung, S., Hong, S. J., Lim, J. K., Anderson, T. and Isacson, O. (2003). Orphan nuclear receptor Nurr1 directly transactivates the promoter activity of the tyrosine hydroxylase gene in a cell-specific manner. *J Neurochem* **85**, 622-34.

Lang, A. E. and Lozano, A. M. (1998). Parkinson's disease. Second of two parts. *N Engl J Med* **339**, 1130-43.

Laplantine, E., Rossi, F., Sahni, M., Basilico, C. and Cobrinik, D. (2002). FGF signaling targets the pRb-related p107 and p130 proteins to induce chondrocyte growth arrest. *J Cell Biol* **158**, 741-50.

LeCouter, J. E., Kablar, B., Whyte, P. F., Ying, C. and Rudnicki, M. A. (1998). Strain-dependent embryonic lethality in mice lacking the retinoblastoma-related p130 gene. *Development* **125**, 4669-79.

Lee, E. Y., Hu, N., Yuan, S. S., Cox, L. A., Bradley, A., Lee, W. H. and Herrup, K. (1994). Dual roles of the retinoblastoma protein in cell cycle regulation and neuron differentiation. *Genes Dev* **8**, 2008-21.

Lee, M. K., Tuttle, J. B., Rebhun, L. I., Cleveland, D. W. and Frankfurter, A. (1990). The expression and posttranslational modification of a neuron-specific beta-tubulin isotype during chick embryogenesis. *Cell Motil Cytoskeleton* **17**, 118-32.

Lee, W. H., Bookstein, R., Hong, F., Young, L. J., Shew, J. Y. and Lee, E. Y. (1987). Human retinoblastoma susceptibility gene: cloning, identification, and sequence. *Science* **235**, 1394-9.

Lendahl, U., Zimmerman, L. B. and McKay, R. D. (1990). CNS stem cells express a new class of intermediate filament protein. *Cell* **60**, 585-95.

Lewis, J. (1996). Neurogenic genes and vertebrate neurogenesis. *Curr Opin Neurobiol* **6**, 3-10.

Lie, D. C., Colamarino, S. A., Song, H. J., Desire, L., Mira, H., Consiglio, A., Lein, E. S., Jessberger, S., Lansford, H., Dearie, A. R. et al. (2005). Wnt signalling regulates adult hippocampal neurogenesis. *Nature* **437**, 1370-5.

Liu, A. and Joyner, A. L. (2001). Early anterior/posterior patterning of the midbrain and cerebellum. *Annu Rev Neurosci* **24**, 869-96.

Logan, C. Y. and Nusse, R. (2004). The Wnt signaling pathway in development and disease. *Annu Rev Cell Dev Biol* **20**, 781-810.

Lyuksyutova, A. I., Lu, C. C., Milanesio, N., King, L. A., Guo, N., Wang, Y., Nathans, J., Tessier-Lavigne, M. and Zou, Y. (2003). Anterior-posterior guidance of commissural axons by Wnt-frizzled signaling. *Science* **302**, 1984-8.

Ma, Q., Chen, Z., del Barco Barrantes, I., de la Pompa, J. L. and Anderson, D. J. (1998). neurogenin1 is essential for the determination of neuronal precursors for proximal cranial sensory ganglia. *Neuron* **20**, 469-82.

MacPherson, D., Sage, J., Crowley, D., Trumpp, A., Bronson, R. T. and Jacks, T. (2003). Conditional mutation of Rb causes cell cycle defects without apoptosis in the central nervous system. *Mol Cell Biol* **23**, 1044-53.

Maldonado, R. (2003). The neurobiology of addiction. *J Neural Transm Suppl*, 1-14.

Marin, F. and Puelles, L. (1994). Patterning of the embryonic avian midbrain after experimental inversions: a polarizing activity from the isthmus. *Dev Biol* **163**, 19-37.

Martinez, S., Marin, F., Nieto, M. A. and Puelles, L. (1995). Induction of ectopic engrailed expression and fate change in avian rhombomeres: intersegmental boundaries as barriers. *Mech Dev* **51**, 289-303.

Martinez, S., Wassef, M. and Alvarado-Mallart, R. M. (1991). Induction of a mesencephalic phenotype in the 2-day-old chick prosencephalon is preceded by the early expression of the homeobox gene en. *Neuron* **6**, 971-81.

Maruoka, Y., Ohbayashi, N., Hoshikawa, M., Itoh, N., Hogan, B. L. and Furuta, Y. (1998). Comparison of the expression of three highly related genes, Fgf8, Fgf17 and Fgf18, in the mouse embryo. *Mech Dev* **74**, 175-7.

Mastick, G. S., Davis, N. M., Andrew, G. L. and Easter, S. S., Jr. (1997). Pax-6 functions in boundary formation and axon guidance in the embryonic mouse forebrain. *Development* **124**, 1985-97.

Maxwell, S. L., Ho, H. Y., Kuehner, E., Zhao, S. and Li, M. (2005). Pitx3 regulates tyrosine hydroxylase expression in the substantia nigra and identifies a subgroup of mesencephalic dopaminergic progenitor neurons during mouse development. *Dev Biol* **282**, 467-79.

McWhirter, J. R., Goulding, M., Weiner, J. A., Chun, J. and Murre, C. (1997). A novel fibroblast growth factor gene expressed in the developing nervous system is a downstream target of the chimeric homeodomain oncoprotein E2A-Pbx1. *Development* **124**, 3221-32.

Menezes, J. R. and Luskin, M. B. (1994). Expression of neuron-specific tubulin defines a novel population in the proliferative layers of the developing telencephalon. *J Neurosci* **14**, 5399-416.

Miller, J. R. (2002). The Wnts. *Genome Biol* **3**, REVIEWS3001.

Miyake, A., Nakayama, Y., Konishi, M. and Itoh, N. (2005). Fgf19 regulated by Hh signaling is required for zebrafish forebrain development. *Dev Biol* **288**, 259-75.

Murray, A. (1994). Cell cycle checkpoints. *Curr Opin Cell Biol* **6**, 872-6.

Nakamura, Y., Sakakibara, S., Miyata, T., Ogawa, M., Shimazaki, T., Weiss, S., Kageyama, R. and Okano, H. (2000). The bHLH gene hes1 as a repressor of the neuronal commitment of CNS stem cells. *J Neurosci* **20**, 283-93.

Nieoullon, A. (2002). Dopamine and the regulation of cognition and attention. *Prog Neurobiol* **67**, 53-83.

Norton, J. D. (2000). ID helix-loop-helix proteins in cell growth, differentiation and tumorigenesis. *J Cell Sci* **113 (Pt 22)**, 3897-905.

Ohnuma, S. and Harris, W. A. (2003). Neurogenesis and the cell cycle. *Neuron* **40**, 199-208.

Ohnuma, S., Hopper, S., Wang, K. C., Philpott, A. and Harris, W. A. (2002). Co-ordinating retinal histogenesis: early cell cycle exit enhances early cell fate determination in the Xenopus retina. *Development* **129**, 2435-46.

Ohtsuka, T., Ishibashi, M., Gradwohl, G., Nakanishi, S., Guillemot, F. and Kageyama, R. (1999). Hes1 and Hes5 as notch effectors in mammalian neuronal differentiation. *Embo J* **18**, 2196-207.

Ohtsuka, T., Sakamoto, M., Guillemot, F. and Kageyama, R. (2001). Roles of the basic helix-loop-helix genes Hes1 and Hes5 in expansion of neural stem cells of the developing brain. *J Biol Chem* **276**, 30467-74.

Ornitz, D. M. (2000). FGFs, heparan sulfate and FGFRs: complex interactions essential for development. *Bioessays* **22**, 108-12.

Ornitz, D. M. and Itoh, N. (2001). Fibroblast growth factors. *Genome Biol* **2**, REVIEWS3005.

Ornitz, D. M. and Marie, P. J. (2002). FGF signaling pathways in endochondral and intramembranous bone development and human genetic disease. *Genes Dev* **16**, 1446-65.

Panhuysen, M., Vogt Weisenhorn, D. M., Blanquet, V., Brodski, C., Heinzmann, U., Beisker, W. and Wurst, W. (2004). Effects of Wnt1 signaling on proliferation in the developing mid-/hindbrain region. *Mol Cell Neurosci* **26**, 101-11.

Parr, B. A., Shea, M. J., Vassileva, G. and McMahon, A. P. (1993). Mouse Wnt genes exhibit discrete domains of expression in the early embryonic CNS and limb buds. *Development* **119**, 247-61.

Patten, I. and Placzek, M. (2000). The role of Sonic hedgehog in neural tube patterning. *Cell Mol Life Sci* **57**, 1695-708.

Perlmann, T. and Wallen-Mackenzie, A. (2004). Nurr1, an orphan nuclear receptor with essential functions in developing dopamine cells. *Cell Tissue Res* **318**, 45-52.

Prakash, N., Brodski, C., Naserke, T., Puelles, E., Gogoi, R., Hall, A., Panhuysen, M., Echevarria, D., Sussel, L., Weisenhorn, D. M. et al. (2006). A Wnt1-regulated genetic network controls the identity and fate of midbrain-dopaminergic progenitors in vivo. *Development* **133**, 89-98.

Prakash, N. and Wurst, W. (2004). Specification of midbrain territory. *Cell Tissue Res* **318**, 5-14.

Prakash, N. and Wurst, W. (2006). Development of dopaminergic neurons in the mammalian brain. *Cell Mol Life Sci*.

Ranheim, E. A., Kwan, H. C., Reya, T., Wang, Y. K., Weissman, I. L. and Francke, U. (2005). Frizzled 9 knock-out mice have abnormal B-cell development. *Blood* **105**, 2487-94.

Ratineau, C., Petry, M. W., Mutoh, H. and Leiter, A. B. (2002). Cyclin D1 represses the basic helix-loop-helix transcription factor, BETA2/NeuroD. *J Biol Chem* **277**, 8847-53.

Reuss, B. and von Bohlen und Halbach, O. (2003). Fibroblast growth factors and their receptors in the central nervous system. *Cell Tissue Res* **313**, 139-57.

Ross, S. E., Greenberg, M. E. and Stiles, C. D. (2003). Basic helix-loop-helix factors in cortical development. *Neuron* **39**, 13-25.

Sadler, J. E. (1998). Biochemistry and genetics of von Willebrand factor. *Annu Rev Biochem* **67**, 395-424.

Saitsu, H., Komada, M., Suzuki, M., Nakayama, R., Motoyama, J., Shiota, K. and Ishibashi, M. (2005). Expression of the mouse Fgf15 gene is directly initiated by Sonic hedgehog signaling in the diencephalon and midbrain. *Dev Dyn* **232**, 282-92.

Sato, T., Joyner, A. L. and Nakamura, H. (2004). How does Fgf signaling from the isthmic organizer induce midbrain and cerebellum development? *Dev Growth Differ* **46**, 487-94.

Saucedo-Cardenas, O., Quintana-Hau, J. D., Le, W. D., Smidt, M. P., Cox, J. J., De Mayo, F., Burbach, J. P. and Conneely, O. M. (1998). Nurr1 is essential for the induction of the dopaminergic phenotype and the survival of ventral mesencephalic late dopaminergic precursor neurons. *Proc Natl Acad Sci U S A* **95**, 4013-8.

Schlessinger, J. (2000). Cell signaling by receptor tyrosine kinases. *Cell* **103**, 211-25.

Scholzen, T. and Gerdes, J. (2000). The Ki-67 protein: from the known and the unknown. *J Cell Physiol* **182**, 311-22.

Schoorlemmer, J. and Goldfarb, M. (2001). Fibroblast growth factor homologous factors are intracellular signaling proteins. *Curr Biol* **11**, 793-7.

Schwarz, M., Alvarez-Bolado, G., Urbanek, P., Busslinger, M. and Gruss, P. (1997). Conserved biological function between Pax-2 and Pax-5 in midbrain and cerebellum development: evidence from targeted mutations. *Proc Natl Acad Sci U S A* **94**, 14518-23.

Sherr, C. J. (1994). G1 phase progression: cycling on cue. *Cell* **79**, 551-5.

Siegenthaler, J. A. and Miller, M. W. (2005). Transforming growth factor beta1 promotes cell cycle exit through the cyclin-dependent kinase inhibitor p21 in the developing cerebral cortex. *J Neurosci* **25**, 8627-36.

Smidt, M. P., Asbreuk, C. H., Cox, J. J., Chen, H., Johnson, R. L. and Burbach, J. P. (2000). A second independent pathway for development of mesencephalic dopaminergic neurons requires Lmx1b. *Nat Neurosci* **3**, 337-41.

Smidt, M. P., Smits, S. M., Bouwmeester, H., Hamers, F. P., van der Linden, A. J., Hellemons, A. J., Graw, J. and Burbach, J. P. (2004). Early developmental failure of substantia nigra dopamine neurons in mice lacking the homeodomain gene Pitx3. *Development* **131**, 1145-55.

Smidt, M. P., van Schaick, H. S., Lanctot, C., Tremblay, J. J., Cox, J. J., van der Kleij, A. A., Wolterink, G., Drouin, J. and Burbach, J. P. (1997). A homeodomain gene Ptx3 has highly restricted brain expression in mesencephalic dopaminergic neurons. *Proc Natl Acad Sci U S A* **94**, 13305-10.

Smits, S. M., Ponnio, T., Conneely, O. M., Burbach, J. P. and Smidt, M. P. (2003). Involvement of Nurr1 in specifying the neurotransmitter identity of ventral midbrain dopaminergic neurons. *Eur J Neurosci* **18**, 1731-8.

Sternberg, N. and Hamilton, D. (1981). Bacteriophage P1 site-specific recombination. I. Recombination between loxP sites. *J Mol Biol* **150**, 467-86.

Stevens, C. F. (1998). Neuronal diversity: too many cell types for comfort? *Curr Biol* **8**, R708-10.

Suzuki-Hirano, A., Sato, T. and Nakamura, H. (2005). Regulation of isthmic Fgf8 signal by sprouty2. *Development* **132**, 257-65.

Theiler, K. (1989). The house mouse. Atlas of embryonic development. New York: Springer Verlag.

Umbhauer, M., Djiane, A., Goisset, C., Penzo-Mendez, A., Riou, J. F., Boucaut, J. C. and Shi, D. L. (2000). The C-terminal cytoplasmic Lys-thr-X-X-X-Trp motif in frizzled receptors mediates Wnt/beta-catenin signalling. *Embo J* **19**, 4944-54.

van den Munckhof, P., Luk, K. C., Ste-Marie, L., Montgomery, J., Blanchet, P. J., Sadikot, A. F. and Drouin, J. (2003). Pitx3 is required for motor activity and for survival of a subset of midbrain dopaminergic neurons. *Development* **130**, 2535-42.

Vanderluit, J. L., Ferguson, K. L., Nikoletopoulou, V., Parker, M., Ruzhynsky, V., Alexson, T., McNamara, S. M., Park, D. S., Rudnicki, M. and Slack, R. S. (2004). p107 regulates neural precursor cells in the mammalian brain. *J Cell Biol* **166**, 853-63.

Vincentz, J. W., McWhirter, J. R., Murre, C., Baldini, A. and Furuta, Y. (2005). Fgf15 is required for proper morphogenesis of the mouse cardiac outflow tract. *Genesis* **41**, 192-201.

Vinson, C. R., Conover, S. and Adler, P. N. (1989). A Drosophila tissue polarity locus encodes a protein containing seven potential transmembrane domains. *Nature* **338**, 263-4.

Wallen, A., Zetterstrom, R. H., Solomin, L., Arvidsson, M., Olson, L. and Perlmann, T. (1999). Fate of mesencephalic AHD2-expressing dopamine progenitor cells in NURR1 mutant mice. *Exp Cell Res* **253**, 737-46.

Wang, Y., Huso, D., Cahill, H., Ryugo, D. and Nathans, J. (2001). Progressive cerebellar, auditory, and esophageal dysfunction caused by targeted disruption of the frizzled-4 gene. *J Neurosci* **21**, 4761-71.

Wang, Y., Thekdi, N., Smallwood, P. M., Macke, J. P. and Nathans, J. (2002). Frizzled-3 is required for the development of major fiber tracts in the rostral CNS. *J Neurosci* **22**, 8563-73.

Wang, Y., Zhang, J., Mori, S. and Nathans, J. (2006). Axonal growth and guidance defects in Frizzled3 knock-out mice: a comparison of diffusion tensor magnetic resonance imaging, neurofilament staining, and genetically directed cell labeling. *J Neurosci* **26**, 355-64.

Warren, N. and Price, D. J. (1997). Roles of Pax-6 in murine diencephalic development. *Development* **124**, 1573-82.

Wassef, M. and Joyner, A. L. (1997). Early mesencephalon/metencephalon patterning and development of the cerebellum. *Perspect Dev Neurobiol* **5**, 3-16.

Wilson, S. W. and Houart, C. (2004). Early steps in the development of the forebrain. *Dev Cell* **6**, 167-81.

Wodarz, A. and Nusse, R. (1998). Mechanisms of Wnt signaling in development. *Annu Rev Cell Dev Biol* **14**, 59-88.

Wong, H. C., Bourdelas, A., Krauss, A., Lee, H. J., Shao, Y., Wu, D., Mlodzik, M., Shi, D. L. and Zheng, J. (2003). Direct binding of the PDZ domain of Dishevelled to a conserved internal sequence in the C-terminal region of Frizzled. *Mol Cell* **12**, 1251-60.

Wright, T. J., Hatch, E. P., Karabagli, H., Karabagli, P., Schoenwolf, G. C. and Mansour, S. L. (2003). Expression of mouse fibroblast growth factor and fibroblast growth factor receptor genes during early inner ear development. *Dev Dyn* **228**, 267-72.

Wright, T. J., Ladher, R., McWhirter, J., Murre, C., Schoenwolf, G. C. and Mansour, S. L. (2004). Mouse FGF15 is the ortholog of human and chick FGF19, but is not uniquely required for otic induction. *Dev Biol* **269**, 264-75.

Wurst, W. and Bally-Cuif, L. (2001). Neural plate patterning: upstream and downstream of the isthmic organizer. *Nat Rev Neurosci* **2**, 99-108.

Xie, M. H., Holcomb, I., Deuel, B., Dowd, P., Huang, A., Vagts, A., Foster, J., Liang, J., Brush, J., Gu, Q. et al. (1999). FGF-19, a novel fibroblast growth factor with unique specificity for FGFR4. *Cytokine* **11**, 729-35.

Yamaguchi, T. P. (2001). Heads or tails: Wnts and anterior-posterior patterning. *Curr Biol* **11**, R713-24.

Ye, W., Shimamura, K., Rubenstein, J. L., Hynes, M. A. and Rosenthal, A. (1998). FGF and Shh signals control dopaminergic and serotonergic cell fate in the anterior neural plate. *Cell* **93**, 755-66.

Zetterstrom, R. H., Solomin, L., Jansson, L., Hoffer, B. J., Olson, L. and Perlmann, T. (1997). Dopamine neuron agenesis in Nurr1-deficient mice. *Science* **276**, 248-50.

Zhao, C., Aviles, C., Abel, R. A., Almli, C. R., McQuillen, P. and Pleasure, S. J. (2005). Hippocampal and visuospatial learning defects in mice with a deletion of frizzled 9, a gene in the Williams syndrome deletion interval. *Development* **132**, 2917-27.

Zhao, S., Maxwell, S., Jimenez-Beristain, A., Vives, J., Kuehner, E., Zhao, J., O'Brien, C., de Felipe, C., Semina, E. and Li, M. (2004). Generation of embryonic stem cells and transgenic mice expressing green fluorescence protein in midbrain dopaminergic neurons. *Eur J Neurosci* **19**, 1133-40.

Zhou, Y., Sun, Z., Means, A. R., Sassone-Corsi, P. and Bernstein, K. E. (1996). cAMP-response element modulator tau is a positive regulator of testis angiotensin converting enzyme transcription. *Proc Natl Acad Sci U S A* **93**, 12262-6.

Zhu, L. L., Wu, L. Y., Yew, D. T. and Fan, M. (2005). Effects of hypoxia on the proliferation and differentiation of NSCs. *Mol Neurobiol* **31**, 231-42.

Zigmond, M. J., Bloom, F. E., Landis, S. C., Roberts, J. L. and Squire, L. R. (1999). Fundamental Neuroscience. San Diego: Academic Press.

7. Appendix

7.1 Primers for PCR

Genotyping of *Fgf15* embryos and mice

***Fgf15* P1**
5'-CGCCTTCTTGACGAGTTCTT-3'

***Fgf15* P2**
5'-CAAGGGAATATGGCTCCAGTCTG-3'

***Fgf15* P3**
5'-ATATCCACGCAGAAGCTGGCAGTG-3'

Targeting vector for the conditional inactivation of *Fgf15*

5' arm forward
5'-GCTCTGCGTGCCTTCTAGTCTCTG-3'

reverse
5'-TCCTGGTTGCTAGATGGCAGAGGA-3'

3' arm forward
5'-CTCGAGGTCTGCCTTTGACTCCTTAG-3'

reverse
5'-CTCGAGTACCCTTCAGGCCTTTGACA-3'

5' arm loxP forward
5'-AATTCTCGAGATAACTTCGTATAATGTATGCTATACGAAGTTAT-3'

5' arm loxP reverse
5'-AATTATAACTTCGTATAGCATACATTATACGAAGTTATCTCGAG-3'

Primers for RT-PCR analysis of the AHP and AHP-Wnt1 cell lines

Fzd1 (accession number: NM 021266)
forward
5'-AGAGCTGCAAGAGTTATGCCATCC-3'

reverse
5'-GTAGTCTCCCCCTGTTTGCTGTTG-3'

Fzd2 (accession number: NM 172035)
forward
5'-TCGTCATCGCCTGCTACTTCTATG-3'

reverse
5'-GGTGAGACGCGTGTAGAACTTCCT-3'

Fzd3 (accession number: NM 153474)
forward
5'-ATCAAAGAAGCAAAGCAGGGAGTG-3'

reverse
5'-TAATGTGAGTCATGGGGTTGTTGC-3'

Fzd4 (accession number: NM 022623)
forward
5'-CCAACTTAGTGGGACACGAGCTG-3'

reverse
5'-GGCAAACCCAAATTCTTTCAGGAC-3'

Fzd5 (accession number: NM 173838)

forward	**reverse**
5’-AAGTACTTCATGTGCCTGGTGGTG-3’	5’-CTATACGTGCGACAGGGACACTTG-3’

Fzd6 (accession number: XM 343230)

forward	**reverse**
5’-GAGTCTTCAGTGGCCTGTATCTTG-3’	5’-ACTCACAGGACTCTTGCAGCACTC-3’

Fzd7 (accession number: XM 237191)

forward	**reverse**
5’-GTAGGCTCCTTGGAGGAGTGTGAG-3’	5’-TGGCTGTTCTTGGTGTCCTTTACC-3’

Fzd8 **(accession number: NM 008058)**

forward	**reverse**
5’-TGTGCCTAGTAGTGGGCATCACAT-3’	5’-GGACAATGGCATTTGCTTAGGGTA-3’

Fzd9 **(accession number: NM 153305)**

forward	**reverse**
5’-TGCTCAAAATCTTCATGTCCTTGG-3’	5’-CTAGAGGTGTGTGGGGTTCTCCAG-3’

Fzd10 **(accession number: NM 175284)**

forward	**reverse**
5’-CATGGAGCAGTTCAAATTCAGGTG-3’	5’-GCTCTTCTCCACATGGTGGAACTT-3’

Tcf7 **(accession number: XM 343891)**

forward	**reverse**
5’-CCCCTCAATGCTTTCATGCTTTAC-3’	5’-CGAATGCATTTCTTTTTCCTCCTG-3’

Tcf7l1 **(accession number: NM 009332)**

forward	**reverse**
5’- TACCCCTTCCTGATGATTCCAGAC-3’	5’-GGAGAAGTGGTCGTTGCTGTAGGT-3’

Tcf7l2 **(accession number: NM 009333)**

forward	**reverse**
5’-GCATCAGGACTCCAAAAAGGAAGA-3’	5’-TTCCCATAGTTATCCCGTGCAGAC-3’

Fzd6 expression vectors

Fzd6 **cDNA forward**
5’-CGGATCCGTCTGGCAAGATGGAAAGGTC-3’

Fzd6 **cDNA without 3’UTR reverse**
5’-GGATATCTTTCTTCAAGCGTCGGAATGG-3’

Fzd6 **cDNA with 3’UTR reverse**
5’-TCCACATATGTAAACTTCAGACAC-3’

7.2 *Fzd6* cDNA fragments used for *Fzd6* expression vectors

The sequences of the cDNA fragments used for the *Fzd6* expression vectors are given below. Start codon is depicted in blue, stop codon in red, *Bam*HI restriction site in purple, *Eco*RV restriction site in green.

Fzd6 cDNA fragment without 3'UTR

```
1    CGGATCCGTC   TGGCAAGATG   GAAAGGTCCC   CGTTTCTGTT   GGCGTGCATT
51   CTTCTGCCCC   TCGTAAGAGG   ACACAGCCTT   TTCACCTGTG   AGCCAATCAC
101  CGTTCCCAGA   TGTATGAAAA   TGACTTACAA   CATGACGTTC   TTCCCTAACC
151  TGATGGGTCA   TTATGACCAG   GGGATCGCTG   CTGTGGAAAT   GGGGCACTTT
201  CTGCATCTTG   CAAATCTAGA   ATGTTCACCA   AACATTGAAA   TGTTCCTTTG
251  CCAAGCTTTT   ATACCAACCT   GCACAGAGCA   AATTCATGTA   GTTCTACCCT
301  GTCGGAAATT   GTGTGAGAAA   ATAGTTTCTG   ATTGCAAAAA   ACTAATGGAC
351  ACTTTTGGCA   TCCGATGGCC   TGAAGAACTT   GAATGTAACA   GATTGCCACA
401  CTGTGATGAC   ACTGTTCCTG   TAACTTCTCA   TCCACACACA   GAGCTTTCTG
451  GGCCACAGAA   GAAATCAGAT   CAAGTCCCAA   GAGACATTGG   ATTTTGGTGT
501  CCAAAGCACC   TTAGGACTTC   CGGGGACCAA   GGCTATAGGT   TTCTGGGAAT
551  TGAACAGTGT   GCCCCTCCGT   GCCCCAATAT   GTATTTTAAA   AGTGATGAAC
601  TAGACTTTGC   CAAAAGTTTC   ATAGGAATAG   TTTCAATATT   TTGTCTTTGT
651  GCAACTCTGT   TCACGTTCCT   TACATTTTTA   ATTGACGTTA   GACGATTCAG
701  ATACCCAGAG   AGACCAATTA   TCTATTACTC   TGTCTGCTAC   AGCATTGTCT
751  CTCTCATGTA   CTTCGTGGGG   TTTTTGCTGG   GCAATAGCAC   GGCTTGTAAT
801  AAGGCAGACG   AGAAGCTGGA   GCTCGGGGAC   ACCGTTGTCC   TAGGGTCAAA
851  GAATAAGGCT   TGCAGTGTGG   TATTTATGTT   TCTGTATTTT   TTTACAATGG
901  CTGGCACCGT   GTGGTGGGTG   ATTCTCACCA   TTACGTGGTT   CTTAGCTGCC
951  GGGAGAAAAT   GGAGTTGCGA   AGCTATTGAA   CAAAAAGCAG   TGTGGTTCCA
1001 TGCCGTTGCC   TGGGGGGCGC   CCGGGTTCCT   GACCGTCATG   CTGCTCGCTA
1051 TGAATAAGGT   TGAAGGAGAC   AACATTAGCG   GCGTTTGCTT   CGTTGGCCTG
1101 TATGACCTGG   ACGCCTCTCG   CTACTTCGTC   CTTCTGCCTC   TGTGCCTCTG
1151 CGTATTTGTT   GGGCTGTCTC   TCCTCTTAGC   CGGCATCATC   TCCTTGAATC
1201 ATGTCCGACA   AGTCATACAG   CATGATGGCC   GGAACCAAGA   GAAGCTAAAG
1251 AAATTCATGA   TTCGCATCGG   AGTCTTCAGT   GGCCTGTATC   TTGTGCCCTT
1301 AGTGACACTT   CTCGGTTGCT   ATGTCTATGA   GCTAGTGAAC   AGGATCACCT
1351 GGGAGATGAC   ATGGTTCTCT   GATCATTGTC   ACCAGTACCG   CATCCCGTGC
1401 CCTTACCAGG   CAAATCCAAA   AGCTCGACCA   GAATTGGCTT   TATTTATGAT
1451 AAAATATCTG   ATGACATTAA   TTGTTGGTAT   CTCTGCGGTC   TTCTGGGTTG
1501 GAAGCAAAAA   GACGTGCACA   GAATGGGCCG   GGTTCTTTAA   GCGAAACCGC
1551 AAGCGAGACC   CCATCAGTGA   GAGCCGCCGA   GTGCTGCAAG   AGTCCTGTGA
1601 GTTCTTCCTG   AAGCACAACT   CTAAAGTGAA   GCACAAGAAG   AAGCATGGCG
1651 CACCAGGGCC   TCATAGGCTG   AAGGTCATTT   CCAAGTCCAT   GGGAACTAGC
1701 ACAGGAGCGA   CCACAAATCA   TGGCACCTCT   GCCATGGCAA   TCGCTGACCA
1751 TGATTACTTA   GGGCAAGAAA   CTTCAACAGA   AGTCCACACC   TCCCCAGAAG
1801 CATCCGTCAA   AGAGGGACGA   GCAGACCGAG   CAAACACTCC   CAGCGCCAAA
1851 GATCGGGACT   GTGGGGAATC   TGCAGGGCCC   AGCTCCAAGC   TCTCTGGGGA
1901 CCGGAACGGC   AGGGAAAGCC   GAGCGGGCGG   CCTGAAGGAG   AGAAGCAATG
1951 GATCAGAGGG   GGCTCCAAGT   GAAGGAAGGG   TAAGTCCAAA   GAGCAGCGTT
2001 CCTGAGACTG   GCCTGATAGA   CTGCAGCACT   TCACAGGCCG   CCAGTTCTCC
2051 AGAACCAACC   AGCCTCAAGG   GCTCCACATC   TCTGCCTGTT   CACTCAGCTT
2101 CCAGAGCTAG   GAAAGAGCAG   GGTGCTGGCA   GCCATTCCGA   CGCTTGAAGA
2151 AAAGATATCC
```

Fzd6 cDNA fragment with 3'UTR

```
1    CGGATCCGTC  TGGCAAGATG  GAAAGGTCCC  CGTTTCTGTT  GGCGTGCATT
51   CTTCTGCCCC  TCGTAAGAGG  ACACAGCCTT  TTCACCTGTG  AGCCAATCAC
101  CGTTCCCAGA  TGTATGAAAA  TGACTTACAA  CATGACGTTC  TTCCCTAACC
151  TGATGGGTCA  TTATGACCAG  GGGATCGCTG  CTGTGGAAAT  GGGGCACTTT
201  CTGCATCTTG  CAAATCTAGA  ATGTTCACCA  AACATTGAAA  TGTTCCTTTG
251  CCAAGCTTTT  ATACCAACCT  GCACAGAGCA  AATTCATGTA  GTTCTACCCT
301  GTCGGAAATT  GTGTGAGAAA  ATAGTTTCTG  ATTGCAAAAA  ACTAATGGAC
351  ACTTTTGGCA  TCCGATGGCC  TGAAGAACTT  GAATGTAACA  GATTGCCACA
401  CTGTGATGAC  ACTGTTCCTG  TAACTTCTCA  TCCACACACA  GAGCTTTCTG
451  GGCCACAGAA  GAAATCAGAT  CAAGTCCCAA  GAGACATTGG  ATTTTGGTGT
501  CCAAAGCACC  TTAGGACTTC  CGGGGACCAA  GGCTATAGGT  TTCTGGGAAT
551  TGAACAGTGT  GCCCCTCCGT  GCCCCAATAT  GTATTTTAAA  AGTGATGAAC
601  TAGACTTTGC  CAAAAGTTTC  ATAGGAATAG  TTTCAATATT  TTGTCTTTGT
651  GCAACTCTGT  TCACGTTCCT  TACATTTTTA  ATTGACGTTA  GACGATTCAG
701  ATACCCAGAG  AGACCAATTA  TCTATTACTC  TGTCTGCTAC  AGCATTGTCT
751  CTCTCATGTA  CTTCGTGGGG  TTTTTGCTGG  GCAATAGCAC  GGCTTGTAAT
801  AAGGCAGACG  AGAAGCTGGA  GCTCGGGGAC  ACCGTTGTCC  TAGGGTCAAA
851  GAATAAGGCT  TGCAGTGTGG  TATTTATGTT  TCTGTATTTT  TTTACAATGG
901  CTGGCACCGT  GTGGTGGGTG  ATTCTCACCA  TTACGTGGTT  CTTAGCTGCC
951  GGGAGAAAAT  GGAGTTGCGA  AGCTATTGAA  CAAAAAGCAG  TGTGGTTCCA
1001 TGCCGTTGCC  TGGGGGGCGC  CCGGGTTCCT  GACCGTCATG  CTGCTCGCTA
1051 TGAATAAGGT  TGAAGGAGAC  AACATTAGCG  GCGTTTGCTT  CGTTGGCCTG
1101 TATGACCTGG  ACGCCTCTCG  CTACTTCGTC  CTTCTGCCTC  TGTGCCTCTG
1151 CGTATTTGTT  GGGCTGTCTC  TCCTCTTAGC  CGGCATCATC  TCCTTGAATC
1201 ATGTCCGACA  AGTCATACAG  CATGATGGCC  GGAACCAAGA  GAAGCTAAAG
1251 AAATTCATGA  TTCGCATCGG  AGTCTTCAGT  GGCCTGTATC  TTGTGCCCTT
1301 AGTGACACTT  CTCGGTTGCT  ATGTCTATGA  GCTAGTGAAC  AGGATCACCT
1351 GGGAGATGAC  ATGGTTCTCT  GATCATTGTC  ACCAGTACCG  CATCCCGTGC
1401 CCTTACCAGG  CAAATCCAAA  AGCTCGACCA  GAATTGGCTT  TATTTATGAT
1451 AAAATATCTG  ATGACATTAA  TTGTTGGTAT  CTCTGCGGTC  TTCTGGGTTG
1501 GAAGCAAAAA  GACGTGCACA  GAATGGGCCG  GGTTCTTTAA  GCGAAACCGC
1551 AAGCGAGACC  CCATCAGTGA  GAGCCGCCGA  GTGCTGCAAG  AGTCCTGTGA
1601 GTTCTTCCTG  AAGCACAACT  CTAAAGTGAA  GCACAAGAAG  AAGCATGGCG
1651 CACCAGGGCC  TCATAGGCTG  AAGGTCATTT  CCAAGTCCAT  GGGAACTAGC
1701 ACAGGAGCGA  CCACAAATCA  TGGCACCTCT  GCCATGGCAA  TCGCTGACCA
1751 TGATTACTTA  GGGCAAGAAA  CTTCAACAGA  AGTCCACACC  TCCCCAGAAG
1801 CATCCGTCAA  AGAGGGACGA  GCAGACCGAG  CAAACACTCC  CAGCGCCAAA
1851 GATCGGGACT  GTGGGGAATC  TGCAGGGCCC  AGCTCCAAGC  TCTCTGGGGA
1901 CCGGAACGGC  AGGGAAAGCC  GAGCGGGCGG  CCTGAAGGAG  AGAAGCAATG
1951 GATCAGAGGG  GGCTCCAAGT  GAAGGAAGGG  TAAGTCCAAA  GAGCAGCGTT
2001 CCTGAGACTG  GCCTGATAGA  CTGCAGCACT  TCACAGGCCG  CCAGTTCTCC
2051 AGAACCAACC  AGCCTCAAGG  GCTCCACATC  TCTGCCTGTT  CACTCAGCTT
2101 CCAGAGCTAG  GAAAGAGCAG  GGTGCTGGCA  GCCATTCCGA  CGCTTGAAGA
2151 AAACTGTCTC  GTTCCCCCAG  AAGCACATGT  ATGTTACACT  GGAGATGACC
2201 AACTGATTTG  TCTTATAAAG  GCCACTGTTG  AGCTGGGAGA  GTAGCCCAGT
2251 GGTACAGCGC  CCACCTGGAA  TACTTGAGGA  CCTGGGGTTG  TCTCCCAGCA
2301 CTGCAAAAGG  AAAATTCACT  GTTACAGTCT  TCCTTGCACT  TAAACCAGCT
2351 TTGTCTATTG  TTTTTTTGGT  TTGGCTTTTA  TTTTTGTTGC  TGTTATTTTT
2401 GTTGTTGTTT  GTTTGTTTTT  TTGTTTGTTT  GTTTGAGACA  GGGTTTCTTT
2451 GCTAGCCCTG  ACTGTCCTGA  AACTCCCTCT  GTAGACCAGG  CTGGCCTCAA
2501 ACTTACAGAG  ATCTGCCTGC  CTCAGCCTCC  CGAGTGCTGG  GAATAATGGT
2551 GTGGTCACCA  CTGCCCAGCC  TTTTGTCTGT  TTTTAAACTT  GAAAGAAACA
2601 ACAGCCCAGA  TTTCAAAAAT  AATATAATGC  ATTTATACCT  AAAAAACCAA
2651 CCAGGAGTGC  CCAGTTAATA  ACACTTTTTA  AATGTGGGGA  TGGGAAGGGC
2701 ATTAGAGGAG  TCTTCCTTCT  ATTGAAGATT  CATTAAAGTA  TTTTAAGATA
2751 TGCTCTTTCA  CTCTTTATAT  AAATCCAAGA  TTTTTCTTTG  CTGAAGTATT
2801 TAAAACTTTT  GTACCTTTAT  ATGTAGATAT  GAATTTGAAA  ATATGCTTAT
2851 GTGTATTTGA  ACTTTTGAAA  ATCCTAGAGA  ATTGAATCAA  ATATTTTTAT
2901 GATGTTTTTC  TACTATTTTA  GCTACTTTGC  GACTGTGATA  GCTGTTACAC
```

```
2951 TAGATTTTTA    AAAAACTTGT    ACAGCAGCCT    CTTTACAGTA    AAAAGAGTGG
3001 GTGTCACACT    GAAAGGTCTG    TAAGAAGTGG    TCACAGCCAC    CCCTACCTTC
3051 CCCAAAAGGA    GGAACTTGGT    GGCAGGTCCC    TCCCTGATTG    GACTGTCCCT
3101 TTCTTTCTGC    ATGTTATAAA    TCAGCAGGTA    AGATGGTAGG    TTTTTACAAG
3151 ATAGGCCGAG    CTGTCGATTC    CCCTTTTAAG    TGTTGAATTA    GGATTGAATT
3201 ATGGCCATTT    GTAGTTGCTC    GTGCCTGTCT    TTATTTTAGT    ATTTTATTTC
3251 CCGAGACAGG    AACTCACTGT    GTGGTGCTCC    TTGGCTGTCT    GGTGTTCAGT
3301 CTGTCCCAGG    CAGGTCACAG    AGATCTCCCC    CTCTGCAGCC    CACTCATCTC
3351 TCCCAAGCCA    CCACACTCAG    CTTTTATCTG    TTTTAAAAAT    TTAAACTTAA
3401 AAAAATGTTT    TTGGAATAGT    ACAAACACAT    TGTGTTGTAA    ATTTCTTTGA
3451 TGCTATGCAA    AATTCCTATC    TGCATCTAAG    CCTGCAAAAG    AAAATGTGCG
3501 AAGGGCAGAG    TCAGAGTTGG    GCAGGGAGAG    TGTAGTGCAG    CAGATGCAGC
3551 GTGAAGACAC    TGAAGGTGCT    AAGACAGCGT    CTCAGTGCTG    GTCCTCCTTA
3601 AGGATTATCT    CGCCAGCGAG    GTTTTCTTAG    ATACTTTGAT    CCCATTGGAG
3651 CTCTGTTAAA    GTTTAAAATG    AAAATTATCA    TGTACTGTAT    GGGAAATGTA
3701 AATACTAACT    TTTCCACATA    TGTAAACTTC    AGACACGATA    TCC
```

7.3 Antibodies

antigen	species	host	conjugate	application	dilution	company	cat. no.
cleaved caspase 3	mouse	rabbit polyclonal	-	IHC(P)	1:200	Cell Signalling	9661
VWF	mouse	rabbit polyclonal	-	IHC(C, P)	1:200	Chemicon	AB7356
phospho-histone 3	mouse	rabbit polyclonal	-	IHC(P)	1:1000	upstate	06-570
BrdU	-	mouse monoclonal	-	IHC(C, P)	1:10	Roche	1 299 964
Ki67	mouse	rabbit polyclonal	-	IHC(C, P)	1:100	Novocastra	NCL-Ki67-MM1
Dcx	mouse	rabbit polyclonal	-	IHC(P)	1:80	gift from O. Reiner	-
TuJ1	mouse	mouse monoclonal	-	IHC(P)	1:5000	Chemicon	MAB1637
p107	mouse	rabbit polyclonal	-	WB	1:2000	Santa Cruz	sc-318
β-actin	mouse	mouse monoclonal	-	WB	1:5000	abcam	ab6276
IgG (H+L)	mouse	goat	HRP	WB	1:10000	Jackson Immunoresearch	115-035-003
IgG (H+L)	mouse	goat	biotin-SP	IHC(C, P)	1:500	Jackson Immunoresearch	115-065-003
IgG (H+L)	mouse	donkey	Cy3	IHC(C)	1:250	Jackson Immunoresearch	715-166-151
IgG (H+L)	rabbit	goat	HRP	WB	1:10000	Jackson Immunoresearch	111-035-003
IgG (H+L)	rabbit	goat	biotin-SP	IHC(C, P)	1:500	Jackson Immunoresearch	111-065-003
Streptavidin	-	-	Cy2	IHC(C, P)	1:250	Jackson Immunoresearch	016-220-084

Table 5 List of applied antibodies with dilution factors. (H+L) heavy and light chain of the immunoglobulin molecule; IHC immunohistochemistry; (C, P) on cryosections and paraffin sections, respectively; WB Western blot; HRP horseradish peroxidase; biotin-SP biotin with long spacer (Jackson Immunoresearch); Cy2 Cyanine; Cy3 Indocarbocyanine.

7.4 Tables to figures 16 and 18

		wildtype	mutant
area [µm²/1000]	forebrain	374,4 ± 57,9	305,1 ± 49,7
	midbrain	129,7 ± 13,8	121,3 ± 15,8
	hindbrain	244,8 ± 31,1	224,5 ± 38,7
cells	forebrain	279 ± 45	265 ± 49
	midbrain	78 ± 13	88 ± 15
	hindbrain	141 ± 14	155 ± 30
cells/area [µm²/1000]	forebrain	0,77 ± 0,081	0,87 ± 0,059
	midbrain	0,60 ± 0,035	0,73 ± 0,084
	hindbrain	0,58 ± 0,023	0,70 ± 0,120

Table 6 Quantification of phospho-histone H3 positive cells in the anterior neural tube of wild type and *Fgf15-/-* embryos at E11.5. Means ± standard deviations are given. n=5 wt, 5 mut.

	Fgf15+/+	***Fgf15-/-***
BrdU+/Ki67+	16.2 ± 0.49	25.0 ± 0.79
BrdU+	107.0 ± 1.46	102.8 ± 1.74
Ki67+	31.4 ± 0.65	35.4 ± 0.78
BrdU+/Ki67+ per BrdU+	15.1 ± 0.40	24.3 ± 0.60

Table 7 Quantification of cells remaining in the cell cycle between E10.5 and E11.5 in wild type and *Fgf15-/-* embryos. BrdU+ number of cells immunopositive for BrdU. Ki67+ number of cells immunopositive for Ki67. BrdU+/Ki67+ number of double positive cells.

7.5 Abbreviations

Ø	diameter
A	absorbance
A/P	anterior-posterior
aa	amino acids
Aldh1a1	retinaldehyde dehydrogenase 1
ANR	anterior neural ridge
AP	alar plate
asc	achaete-scute
ath	athonal
BAC	bacteria artificial chromosome
BCIP	5-bromo-4-chloro-3-indolyl-phosphate
BGH	bovine growth hormone
bHLH	basic helix-loop-helix
Bmp	Bone morphogenic protein
bp	base pairs
BP	basal plate
BrdU	Bromo-2'-deoxy-uridine
BSA	bovine serum albumine
c	centi (10^{-2})
°C	degrees Celsius
Cdk	Cyclin-dependent kinase
Cdki	Cdk inhibitor
cDNA	copy-DNA
Ci	Curie
CMV	cytomegalovirus
CNS	central nervous system
CO_2	carbon dioxide
cpm	counts per minute
CRD	cysteine-rich domain
D/V	dorso-ventral
Da	Dalton
DA	dopaminergic
DAB	3,3´-diaminobenzidine
dATP	2´-deoxyadenosine-5´-triphosphate
dCTP	2´-deoxycytidine-5´-triphosphate
Dcx	Doublecortin
dGTP	2´-deoxyguanosine-5´-triphosphate
di	diencephalon
DMF	dimethyl formamide
DMSO	dimethyl sulfoxide
DNA	2´-deoxyribonucleic acid
dNTP	2´-deoxynucleoside-5´-triphosphate
Dsh	Dishevelled
dTTP	2´-deoxythymidine-5´-triphosphate
E	embryonic day
E. coli	*Escherichia coli*
e.g.	for example (latin: *exempli gratia*)
E(spl)	enhancer of split
EDTA	ethylenediamine tetraacetate
Egf	Epidermal growth factor
En	Engrailed
ES	embryonic stem
F	Farad
F	filial generation
Fgf	Fibroblast growth factor
Fgfr	Fgf receptor
Fhf	Fgf homologous factor
Fig.	figure
Flp	Flipase
FP	floor plate
Fzd	Frizzled
g	gravity constant
g	gram
GOF	gain-of-function
Gsk	Glycogen synthase kinase
h	hours
hb	hindbrain
HEPES	N-2-hydroxyethylpiperazine-N´-2-ethane sulfonic acid
Hes	Hairy and enhancer of split
Her	Hairy and enhancer of split related
HLH	helix-loop-helix
HR	homologous recombination
HRP	horseradish peroxidase
H_2O_2	hydrogen peroxide
i.e.	that is (latin: *id est*)
Id	Inhibitor of differentiation
INT	2-[4-Iodophenyl]-3-[4-nitrophenyl]-5-phenyl-tetrazolium chloride
J	Joule
k	kilo (10^{3})
kb	kilobases
KCl	potassium chloride
kDa	kilo Dalton
KH_2PO_4	potassium dihydrogen phosphate
l	liter
lab	labyrinth
Lef	Lymphoid enhancer binding factor
Lmx	LIM homeobox transcription factor
LOF	loss-of-function
µ	micro (10^{-6})
m	meter
m	milli (10^{-3})
M	molar
Mash	Mammalian achaete-scute homolog
Math	Mammalian athonal homolog
mb	midbrain
md	maternal decidua
MES	2-(N-morpholino)ethane sulfonic acid
mes	mesencephalon
mesDA	mesencephalic dopaminergic
met	metencephalon
$MgCl_2$	magnesium chloride
MHB	mid-/hindbrain boundary
min	minutes
MOPS	3-(N-morpholino)propane sulfonic acid
mRNA	messenger-RNA
Msx	Msh like
mut	mutant
myel	myelencephalon
MZ	mantle zone

n	nano (10^{-9})
NaCl	sodium chloride
Na_2HPO_4	sodium hydrogen phosphate
NBT	4-Nitro-blue tetrazolium chloride
NCBI	National Center for Biotechnology Information
Neo	Neomycin
NeuroD	Neurogenic differentiation
Ngn	Neurogenin
NH_4OAc	ammonium acetate
NICD	intracellular domain of Notch
Nkx	NK transcription factor related
NP-40	Nonidet-P 40
Nr4a2	Nuclear receptor subfamily 4, group A, member 2
NSC	neural stem cell
NTP	nucleoside-5´-triphosphate
OD	optical density
Otx	Orthodenticle homolog
P	postnatal day
pA	polyadenylation signal
PAGE	polyacrylamide gel electrophoresis
Pax	Paired box gene
PBS	phosphate buffered saline
Pbx	Pre B-cell leukemia transcription factor
PCR	polymerase chain reaction
Pdgf	Platelet-derived growth factor
PFA	paraformaldehyde
PGK	Phosphoglycerate kinase
Pitx	Pituitary homeodomain transcription factor
PNS	peripheral nervous system
PVP	perineural vascular plexus
Rb	Retinoblastoma
RNA	ribonucleic acid
RP	roof plate
RT	room temperature
RT-PCR	reverse transcriptase PCR
s	seconds
SDS	sodium dodecylsulfate
Shh	Sonic hedgehog
Slc	Solute carrier family
sp	spongiotrophoblast
SV	simian virus
SVZ	subventricular zone
tACE	testis-specific angiotensin-converting enzyme
Tcf	T-cell specific transcription factor
tel	telencephalon
Tgf	Transforming growth factor
Th	Tyrosine hydroxylase
Tk	Thymidine kinase
Tris	tris(hydroxymethyl)aminomethan
tRNA	transfer-RNA
TuJ1	class III β-tubulin
U	unit
UTR	untranslated region
UV	ultra violet
V	Volt
Vegfr	Vascular endothelial growth factor receptor
VWF	von-Willebrand-factor
VZ	ventricular zone
W	Watt
WB	Western blot
Wnt	Wingless-related MMTV integration site
wt	wild type
ZLI	zona limithans intrathalamica

Hiermit versichere ich, dass ich mich zu keiner Zeit anderweitig um die Erlangung des Doktorgrades beworben habe.

Ferner versichere ich, dass ich die vorliegende Arbeit selbständig und ohne fremde Hilfe verfasst habe und keine anderen als die hier angegebenen Quellen und Hilfsmittel benutzt und die den verwendeten Werken wörtlich oder inhaltlich entnommenen Stellen als solche kenntlich gemacht habe.

Neuherberg, den 22.02.2006

Thomas Fischer